Dissertation zur Erlangung des Doktorgrades
der Fakultät für Biologie
der Ludwig-Maximilians-Universität München

Identification and Characterization of Two Novel Primate-specific Histone H3 Variants, H3.X and H3.Y

Sonja M. Wiedemann
aus München

September 2010

Eingereicht am 30. September 2010

Mündliche Prüfung am 20. Dezember 2010

1. Gutachter: Prof. Dr. Peter Becker
2. Gutachter: Prof. Dr. Stefan Jentsch
3. Gutachter: Prof. Dr. Heinrich Leonhardt
4. Gutachter: Prof. Dr. Thomas Cremer
5. SV: Dr. Sandra Hake

Ehrenwörtliche Versicherung

Ich versichere hiermit ehrenwörtlich, dass die vorgelegte Dissertation von mir selbständig und ohne unerlaubte Hilfe angefertigt wurde.

München, den ....

(Sonja Wiedemann)

Acknowledgements

First of all I want to thank Dr. Sandra Hake for giving me the opportunity to work on this very exciting project, for always finding time for discussions, even in busy times, for giving useful scientific input, never running out of ideas when the project was stuck and for letting me find my own way. Thank you for being a boss when I needed a boss and a friend when I needed a friend. You are doing a great job!

I am grateful to Prof. Dr. Peter Becker for always having time for me, for his advice and constant support and for providing not only a scientifically motivating environment but also a perfect lab atmosphere.

I also want to express my gratitude to the other members of my thesis advisory committee, Prof. Gunnar Schotta and Prof. Stefan Jentsch, for their time and helpful comments.

Heartfelt thanks go to all members of the Hake group for creating the perfect mixture between science and fun in the lab. Thank you for endless discussions about scientific problems, for always taking over when help was needed, for constantly emptying the candy drawer ("I was running this morning") and for simply being my friends!

I also would like to thank all past and present members of the molecular biology department for creating a scientifically motivating environment, help whenever needed, discussions and criticism and of course for the fun.

I would like to acknowledge my collaborators for their excellent experimental contribution and scientific interest, especially Silke Mildner, Clemens Bönisch, Sarah Matheisl, Lars Israel, Tobias Straub, Lothar Schermelleh, Heinrich Leonhardt, Elisabeth Kremmer und Rainer Merkl.

For technical help, reagents and cell lines, I want to thank Christiane Simon, Sandra Vengadasalam, Mariacristina Chioda, Ignasi Forné, Martin Heidemann, Corinna Hintermair, Robert Löwe, Stefan Müller and Marion Cremer.

My special thanks go to my husband Thomas, thank you for always being there for me.

Contents

Summary **1**

Zusammenfassung **3**

1 Introduction **5**
1.1 Chromatin . . . 5
1.2 Epigenetic regulation . . . 7
1.3 Histone variants . . . 9
1.3.1 H1 variants . . . 10
1.3.2 H2A variants . . . 12
1.3.3 H2B variants . . . 15
1.3.4 H3 variants . . . 17
1.3.5 Targeted chromatin incorporation of histone variants . . . 19
1.3.6 Evolution of histone variants . . . 20
1.4 Objective . . . 21

2 Materials and Methods **22**
2.1 Materials . . . 22
2.1.1 Technical devices . . . 22
2.1.2 Chemicals and consumables . . . 23
2.1.3 Kits, enzymes and markers . . . 25
2.1.4 Antibodies . . . 26
2.1.4.1 Primary antibodies . . . 26
2.1.4.2 Secondary antibodies . . . 26
2.1.5 Plasmids . . . 27
2.1.6 Oligonucleotides . . . 27
2.1.7 Bacterial strains and cell lines . . . 27
2.1.7.1 *E. coli* strains . . . 27
2.1.7.2 Mammalian cell lines . . . 28
2.1.8 Software . . . 29
2.2 Buffers and solutions . . . 29
2.3 Cell biological methods . . . 31
2.3.1 Cultivation and manipulation of mammalian cells . . . 31
2.3.1.1 Cultivation of mammalian cells . . . 31
2.3.1.2 Cultivation of U2OS cells under different stress conditions . . . 32
2.3.1.3 Establishment of stably transfected human cell lines . . . 32
2.3.1.4 mRNA knockdown using small interfering RNAs (siRNAs) . . . 33
2.3.2 Proliferation analysis of adherent human cells . . . 33

2.3.3 Antibody generation and specificity testing . . . 34
2.3.4 Immunofluorescence (IF) microscopy . . . 34
2.3.5 Metaphase chromosome spreads . . . 35
2.3.6 Fluorescence recovery after photobleaching (FRAP) . . . 35
2.3.7 Immunohistochemistry (IH) microscopy . . . 36
2.4 Molecular biological methods . . . 36
2.4.1 Agarose gel electrophoresis . . . 36
2.4.2 RNA extraction of mammalian cells . . . 37
2.4.3 RNA expression profiling . . . 37
2.4.4 cDNA synthesis . . . 37
2.4.5 Quantification of mRNA levels with quantitative PCR (qPCR) . . . 38
2.4.6 Cloning of mammalian H3 variants . . . 39
2.4.7 Site directed mutagenesis of H3.Y . . . 39
2.4.8 Expression of human histone proteins in *E. coli* . . . 39
2.5 Biochemical methods . . . 40
2.5.1 Histone extraction from mammalian cells . . . 40
2.5.2 Reversed phase-high performance liquid chromatography (RP-HPLC) of mammalian histones . . . 40
2.5.3 Mass spectrometrical analysis of HPLC-purified mammalian histones . 40
2.5.4 Mononucleosome immunoprecipitation (IP) . . . 40
2.5.5 SDS polyacrylamide gel electrophoresis (SDS-PAGE) . . . 41
2.5.6 Coomassie staining of polyacrylamide gels . . . 41
2.5.7 Silver staining of polyacrylamide gels . . . 41
2.5.8 Western blotting . . . 42
2.6 Bioinformatics . . . 42
2.6.1 Phylogenetic analysis of histone variants . . . 42
2.6.2 *In silico* modeling of novel histone variants . . . 43

3 Results **44**
3.1 Identification of novel histone H3 variant genes . . . 44
3.2 Endogenous *H3.X* and *H3.Y* expression in human cell lines and tissues . . . 46
3.3 Localization, nucleosome structure and chromatin incorporation of novel tagged H3 variants . . . 48
3.4 Expression and sub-nuclear localization of endogenous H3.X/Y proteins . . . 53
3.5 Induction of endogenous H3.X/Y expression in U2OS cells . . . 55
3.5.1 Increase in H3.X/Y expressing U2OS cells through nutritional and proliferative stress . . . 55
3.5.2 Increase of endogenous H3.Y protein expression in U2OS cells after SO treatment . . . 58
3.6 Effects of H3.Y on gene expression . . . 61
3.6.1 De-regulation of genes mainly implicated in growth control, survival or differentiation pathways in HeLa HA-H3.Y cells . . . 61
3.6.2 Impairment of cell proliferation in U2OS cells after knockdown of H3.Y or H3.X+Y . . . 64
3.7 Expression of endogenous H3.X/Y protein in human brain . . . 67
3.8 Epression of endogenous H3.X/Y protein in different primate species . . . 69

4 Discussion **71**
4.1 *H3.X* and *H3.Y* are novel primate-specific histone genes 71
4.2 Structure and behavior of H3.X and H3.Y proteins is similar to other H3 variants 71
4.3 H3.X and H3.Y mRNA, but only H3.Y protein is expressed in human cells . . 72
4.4 A putative H3.X/Y protein is associated with nuclear pores 73
4.5 The number of H3.Y-expressing U2OS cells is increased by specific stress stimuli 73
4.6 H3.Y influences gene expression and cell growth 74
4.7 Outlook 75
4.7.1 Expression of endogenous H3.X and H3.Y 75
4.7.1.1 Trigger of H3.X and H3.Y expression in U2OS cells 75
4.7.1.2 H3.X and H3.Y promoter activity and regulation 75
4.7.1.3 H3.X and H3.Y expression in human tissues 76
4.7.1.4 H3.X and H3.Y expression during cell differentiation 76
4.7.2 *In vivo* function(s) of H3.X and H3.Y 77
4.7.2.1 Determination of H3.X/Y protein localization 77
4.7.2.2 Identification of H3.X and H3.Y chaperone(s) 77
4.7.2.3 Replacement of *S. cerevisiae* H3 with H3.X and H3.Y 77
4.7.2.4 Effects of H3.X and H3.Y on cell cycle progression 78
4.7.3 *In vitro* characterization of H3.X and H3.Y 78

Abbreviations **80**

Bibliography **92**

Appendix **I**

Curriculum vitae **X**

Summary

Chromatin is the packaged form of DNA in the eukaryotic nucleus, with the nucleosome as its basic unit. The nucleosome consists of DNA, wrapped around a histone octamer which is comprised of two copies of each of the four core histones H2A, H2B, H3 and H4. To allow DNA-related processes to occur, access to the DNA has to be regulated. One regulatory mechanism is the exchange of the canonical core histones by one of their replacement variants. Thus far, five members of the histone H3 family have been described: H3.1, H3.2, H3.3, testis-specific tH3 and centromere-specific CENP-A. Searching the database, we have recently identified two novel histone H3 variant genes on human chromosome 5, now termed *H3.X* and *H3.Y*. In my PhD thesis, I have analyzed their expression patterns, characterized their mRNA as well as their protein products and investigated their potential function(s).

H3.X and *H3.Y* constitute primate-specific genes which have been found, in addition to humans, also in the chimpanzee and the macaque, but not in other mammals or even lower eukaryotes. H3.X and especially H3.Y mRNA is expressed at low but significant levels in the human osteosarcoma cell line U2OS and in some human bone, breast, lung and ovary tumor tissues, as well as in testis and certain areas of the brain. Tagged H3.X and H3.Y proteins behave similar to H3.1, H3.2 and H3.3 in their nuclear localization and stable incorporation into chromatin. However, in contrast to H3.1 and H3.3, novel H3 variants primarily form heterotypic nucleosomes. Endogenous H3.Y protein is expressed in a small number of U2OS cells (<0.1 %), localizes to the nucleus and constitutes a stable chromatin component. The number of H3.Y-expressing U2OS cells can be increased by specific stress conditions, such as nutritional stress paired with high cell density. Matching its expression pattern in U2OS cells, H3.X and/or H3.Y protein(s) have also been observed in a small subpopulation of neurons in the human hippocampus. H3.Y has an influence on the expression of certain genes, most of them being implicated in regulating the cell cycle and chromatin structure. In line with this finding, knockdown of H3.X and H3.Y impairs cell growth.

In conclusion, the results of this work show that H3.Y (and maybe H3.X) are novel primate-specific histone H3 variants which play a role in cell cycle regulation. Their expression is induced by certain stress stimuli and their presence in brain and testis suggests a potential role in primate-specific brain functions and speciation.

Zusammenfassung

Chromatin ist die Verpackungsform der DNS im eukaryontischen Zellkern, mit dem Nukleosom als kleinster Einheit. Das Nukleosom besteht aus DNS, die um ein Histon-Oktamer, bestehend aus je zwei Kopien der vier Kernhistone H2A, H2B, H3 and H4, gewickelt ist. Um DNS-basierte Prozesse zu ermöglichen, muss der Zugang zur DNS reguliert werden. Ein Mechanismus dafür ist der Austausch der kanonischen Histone durch eine ihrer Varianten. Bislang wurden fünf Mitglieder der Histon H3 Familie beschrieben: H3.1, H3.2, H3.3, tH3, das nur im männlichen Reproduktionsorgan vorkommt und CENP-A, das an den Zentromeren der Chromosomen zu finden ist. Durch eine Datenbanksuche, konnten wir vor Kurzem im Humangenom zwei neue Histon H3 Variantengene auf Chromosom 5 identifizieren, die jetzt als *H3.X* and *H3.Y* bezeichnet werden. Während meiner Doktorarbeit habe ich ihre Expressionsmuster analysiert, die von ihnen kodierte mRNA, sowie das zugehörige Protein charakterisiert und ihre potentielle(n) Funktion(en) untersucht.

H3.X and *H3.Y* sind primaten-spezifische Gene, die, außer im Menschen, auch im Schimpansen und im Rhesusaffen, jedoch nicht in anderen Säugetieren oder niedrigeren Eukaryonten gefunden wurden. H3.X- und insbesondere H3.Y-mRNA wird in geringen aber dennoch signifikanten Mengen in der humanen Osteosarkoma Zelllinie U2OS und in einigen humanen Knochen-, Brust-, Lungen- und Eierstock-Tumorgeweben, sowie im Hoden und bestimmten Hirnarealen exprimiert. Epitop-markierte H3.X- und H3.Y-Proteine verhalten sich ähnlich wie H3.1, H3.2 und H3.3 bezüglich ihrer Lokalisierung im Zellkern und ihrem stabilen Einbau ins Chromatin. Im Gegensatz zu H3.1 und H3.3, bilden die neuen H3 Varianten jedoch vorzugsweise heterotypische Nukleosomen. Endogenes H3.Y-Protein wird in einer kleinen Anzahl von U2OS-Zellen (<0.1 %) exprimiert, es befindet sich im Zellkern und stellt einen stabilen Bestandteil des Chromatins dar. Die Anzahl H3.Y-exprimierender U2OS-Zellen kann durch spezifische Stress-Stimuli erhöht werden, beispielsweise durch Nahrungsmangel gepaart mit hoher Zelldichte. Vergleichbar mit dem Expressionsmuster in U2OS-Zellen, konnten H3.X und/oder H3.Y-Protein(e) auch in einer kleinen neuronalen Subpopulation im humanen Hippocampus detektiert werden. H3.Y beeinflusst die Expression bestimmter Gene, von denen die meisten an der Regulation des Zellzyklus sowie der Struktur des Chromatins beteiligt sind. In Übereinstimmung mit diesem Befund, ist das Wachstum von Zellen mit verminderten Mengen H3.X und H3.Y beeinträchtigt.

Zusammengenommen zeigen diese Ergebnisse dass H3.Y (und vielleicht auch H3.X) neue primaten-spezifische Histon H3 Varianten sind, die an der Zellzyklus-Regulation beteiligt sind. Ihre Expression wird durch bestimmte Stress-Stimuli induziert und ihr Vorkommen in Gehirn- und Hodengewebe spricht für eine potentielle Rolle in primaten-spezifischen Hirnfunktionen sowie der Artenbildung.

1 Introduction

1.1 Chromatin

Chromatin is the packaged form of DNA in the eukaryotic nucleus (van Holde, 1988). On the first level of compaction, DNA is wrapped around an octamer consisting of two copies of each of the four core histones H2A, H2B, H3 and H4. This structure, the nucleosome, organizes 146 bp of DNA in 1.65 turns, forming a flat, left-handed superhelix (Fig. 1.1A). The four core histones have an unstructured N-terminal tail, which is enriched in basic amino acids, a globular domain and a short C-terminus. Their globular or histone-fold domains (HFDs) share a highly similar structure consisting of three α-helices (α1 - α3) connected by two loops (L1 and L2). These domains fold together in antiparallel pairs: H3 with H4, and H2A with H2B. The assembly of the nucleosome is thought to start with an $(H3\text{-}H4)_2$ tetramer, held together by a strong four helix bundle (4HB) between the two H3 molecules, (H3 and H3' in Fig. 1.1B) and is completed by the addition of two H2A-H2B dimers. The interaction

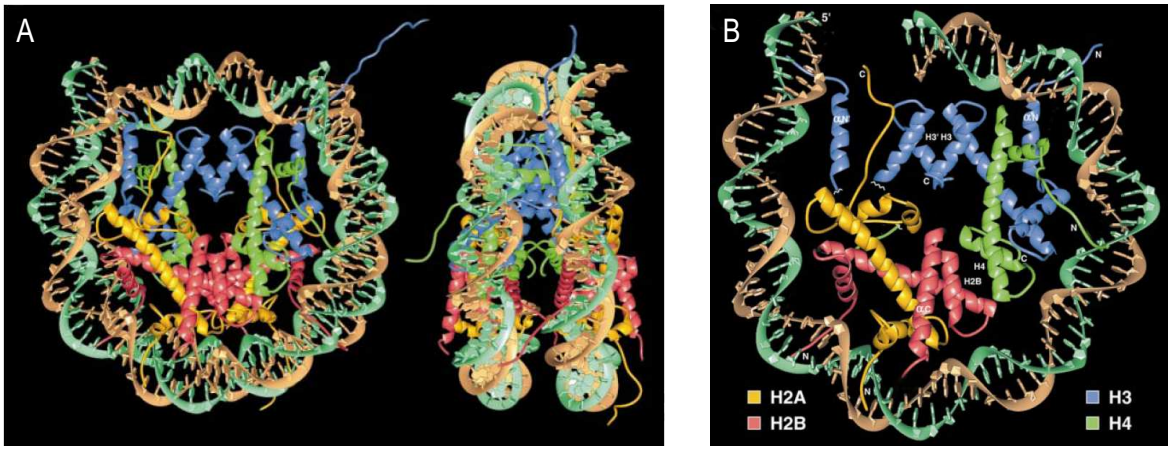

Figure 1.1. Crystal structure of the nucleosome.
Depicted are ribbon traces of the 146 bp DNA molecules (brown and turquoise) and the core histones H2A (yellow), H2B (red), H3 (blue) and H4 (green). (A) The complete nucleosome core particle is shown with the view down the DNA superhelix axis (left) and perpendicular to it (right). In both cases the pseudo-twofold axis is aligned vertically with the DNA center at the top. (B) The 73-bp half of the nucleosome core particle is shown with the view down the superhelix axis and the pseudodyad axis aligned vertically. Histone proteins primarily associated with the 73-bp superhelix half are depicted (without interparticle tail regions). The two copies of each histone pair are distinguished as unprimed and primed (e.g. H3 and H3'). 4HBs are labeled as H3' H3 and H2B H4; HFD extensions of H3 and H2B are labeled as αN', αN and αC, respectively; N- and C-terminal tail regions as N or C. Images adapted from Luger et al., 1997 (modified).

between H2A-H2B dimers and the $(H3\text{-}H4)_2$ tetramer is mediated by weak 4HBs between the $\alpha 2$ and $\alpha 3$ helices of H2B and H4 (Fig. 1.1B) (Luger et al., 1997). To achieve higher levels of compaction, the nucleosome core particle is bound by one molecule of the linker histone H1, forming a chromatosome (Fig. 1.2) and organizing additional 15 to 20 bp of DNA (Simpson, 1978). H1 has a different structure than the core histones, consisting of a conserved globular domain with long N- and C-terminal tails. Its C-terminus is enriched in lysines and strongly interacts with DNA. It is well accepted that H1 binds the nucleosome at the DNA entry/exit site at or near the dyad axis, however, its precise binding site is still controversial (Happel and Doenecke, 2009; Woodcock and Ghosh, 2010). Although more than 80 % of the nucleosomes have H1 bound at a given time, H1 is highly mobile, binding nucleosomes only transiently and translocating from one to the other every few minutes (Bustin et al., 2005; Happel and Doenecke, 2009). The next level of chromatin compaction is the formation of the 30 nm fiber (Fig. 1.2), a conformation which is transcriptionally inactive. Albeit investigated in numerous studies, the structure of this fiber remains elusive. The two major models currently being discussed are a solenoid structure, where the order of the nucleosomes follows their sequence along the DNA, or a zigzag structure, where odd and even numbered nucleosomes build separate stacks (Staynov, 2008). Even less is known about higher order chromatin structures, finally leading to a 10000- to 20000-fold higher DNA compaction in metaphase chromosomes (Fig. 1.2) (Woodcock and Ghosh, 2010).

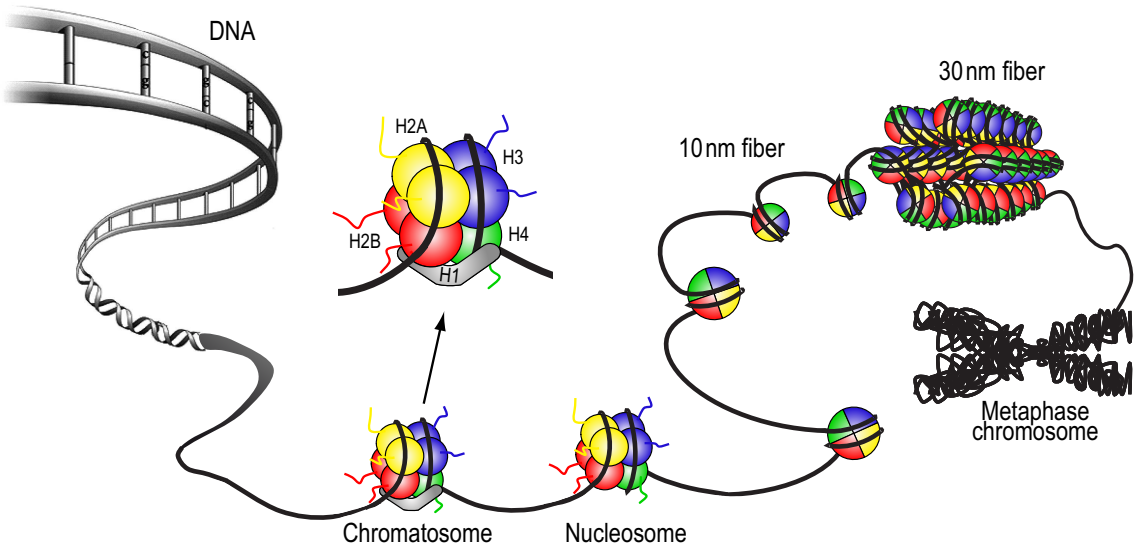

Figure 1.2. Chromatin - composition and compaction.
The basic unit of chromatin is the nucleosome, consisting of DNA, wrapped around an octamer of two copies of each of the four core histones H2A (yellow), H2B (red), H3 (blue) and H4 (green). For further compaction, one molecule of the linker histone H1 (gray) can be bound, resulting in a chromatosome. Nucleosomes with linker DNA constitute the 10 nm fiber, which can be further compacted by stacking of nucleosomes, leading to the 30 nm fiber. Little is known about higher-order chromatin structures finally leading to a condensation of the genetic material to the level of metaphase chromosomes. Image adapted from Qiu, 2006 (modified).

1.2 Epigenetic regulation

Except for short stretches of DNA, the genetic information in eukaryotes is associated with histones and packed more or less tightly in higher order structures (see section 1.1). Regions with a more open chromatin structure constitute euchromatin, whereas tightly packed regions are known as constitutive or facultative heterochromatin. Constitutive heterochromatin, such as pericentric heterochromatin, is always silenced. In contrast, facultative heterochromatin is only silenced in certain contexts, for example as part of the inactive X chromosome (Xi) in female mammals. For all DNA-related process, such as transcription or replication, chromatin structure and DNA accessibility have to be regulated. To meet this need, several epigenetic mechanisms have evolved, the major ones being DNA methylation, posttranslational modification (PTM) of histones, incorporation (or replacement) of histone variants, nucleosome-remodeling, non-coding RNAs (ncRNAs) and the position within the nucleus (nuclear architecture) (Fig. 1.3) (Bönisch et al., 2008). The term epigenetics has been coined by Conrad Waddington in 1942 for "the branch of biology which studies the causal interactions between genes and their products, which bring the phenotype into being" (Waddington, 1942; Goldberg et al., 2007). Today, epigenetics is usually defined as heritable changes in genome function that occur without changes in the DNA sequence (Probst et al., 2009). DNA methylation, which denotes the addition of a methyl group to the C-5 position of cytosines, is implicated in long-term silencing. Methylated DNA is therefore often found in heterochromatic regions. During early development, after all methyl marks have been erased, methylation patterns are established *de novo*, marking different sites in the maternal and the paternal genome (imprinting). In somatic mammalian cells, methylation occurs symmetrically at CpG dinucleotides, enabling the maintenance DNA methyltransferase Dnmt1 to copy the marks after replication, thereby maintaining the silenced state of the underlying DNA sequence (Bönisch et al., 2008; Espada and Esteller, 2010).

Histones can be posttranslationally modified, primarily on their N-terminal tails. So far, acetylation, methylation, phosphorylation, ubiquitination, SUMOylation and ADP ribosylation have been described as major marks (Cosgrove, 2007). PTMs are transferred by "writer" and removed by "eraser" enzymes (Fig. 1.3). They act by either changing the charge of a residue, thereby influencing its affinity for the DNA or adjacent nucleosomes, or they establish high-affinity sites for specific "reader" molecules (Fig. 1.3). While acetylation has been generally linked to gene activiation, the function of methylation marks depends on the actual residue. Methylated H3 lysine (K) 4 and H3K36, for example, are found in euchromatic regions whereas methylated H3K9, H3K27 and H4K20 constitute heterochromatic marks (Fuchs et al., 2006). Moreover, histones can carry several different PTMs at the same time, estab-

lishing a possible histone-code (Strahl and Allis, 2000; Turner, 2000), which has a different readout than each modification alone. This combinatorial action of histone PTMs also explains how for instance the phosphorylation of H3S10 can promote such different processes as the induction of immediate-early genes (Clayton and Mahadevan, 2003) and the condensation of chromosomes during cell division (Wei et al., 1999; Hendzel et al., 1997). Adding another level of complexity, histones cannot only be modified but also exchanged with one of their replacement variants. These proteins can on the one hand influence the structure and stability of the nucleosome and offer on the other hand alternative modification sites due to sequence differences. The four core histones and the linker histone H1 show variation to different extents. For a more detailed overview see section 1.3.

To move nucleosomes and allow access to nucleosomal DNA, several ATP-dependent nucleosome remodeling complexes have evolved, each containing an ATPase of the SWI/SNF-family. Depending on the ATPase subtype and the factors associated with it, these complexes catalyze the partial or complete dissasembly of nucleosomes (histone eviction) or the repositioning of

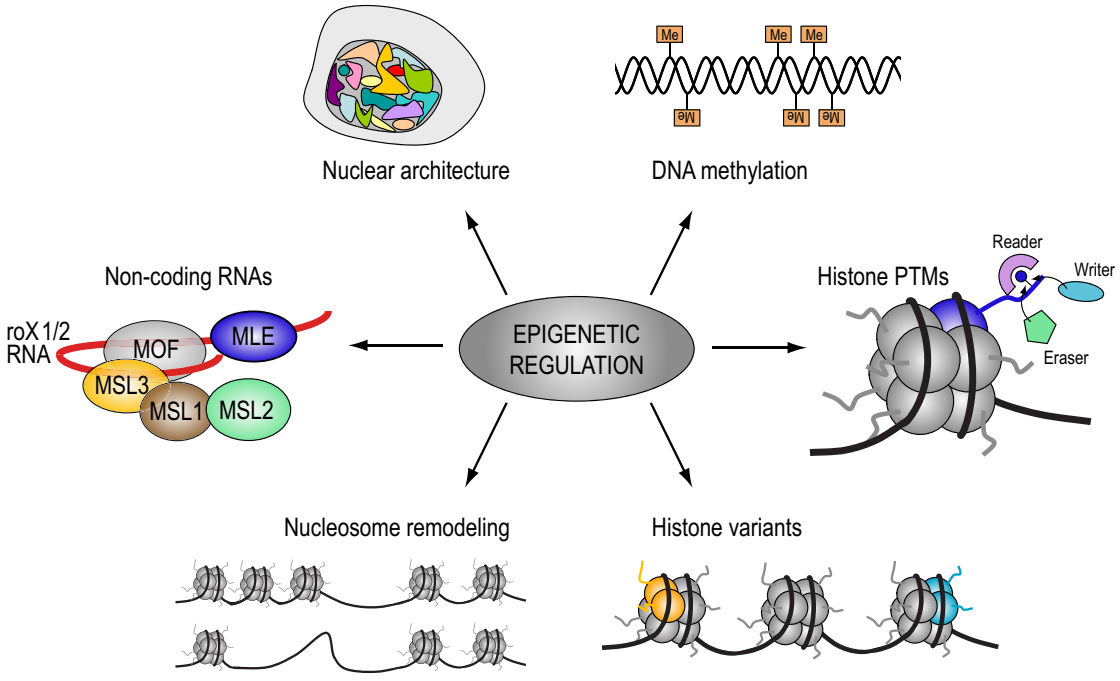

Figure 1.3. Epigenetic regulation.
Schematic overview depicting major epigenetic regulatory processes which act on different levels. DNA is methylated on specific cytosines. Histones, organizing DNA in nucleosomes, can be posttranslationally modified by "writer" enzymes, thereby changing the charge and/or the binding site for specific "reader" molecules. PTMs can also be removed by "eraser" enzymes. In addition, histones can be exchanged by histone variants with different sequences, resulting in a change of structural properties and PTM sites. Accessibility of chromatinized DNA can be regulated by ATP-dependent nucleosome remodeling, for example shifting or evicting nucleosomes. NcRNAs are implicated in diverse processes. Examples are the roX1/2 RNAs in the *Drosophila* dosage compensation complex and Xist RNA, implicated in X chromosome inactivation in mammals. Not only the packaging of DNA is important for DNA-related processes, but also the localization within the nucleus. Histone gene clusters for instance, localize to nuclear Cajal bodies where specific histone mRNA processing factors are concentrated. All of these processes do not act alone but are interconnected. See text for details.

nucleosomes along the DNA (nucleosome sliding) (Fig. 1.3) (Becker and Hörz, 2002; Saha et al., 2006). Nucleosomes, which have histone H1 bound, can also be remodeled, but only by some of the complexes (Maier et al., 2008). It is important to mention that remodelers do not just increase the accessibility of the DNA but can also establish repressive chromatin states (Becker and Hörz, 2002; Saha et al., 2006).

NcRNAs are a diverse class of molecules, differing in size, structure and function. They can influence gene expression levels, either acting post-transcriptionally or directly influencing transcription. One example for the latter is the RNA-induced initiation of transcriptional gene silencing (RITS) complex in *Schizosaccharomyces pombe*, which is targeted to homologous sequences by small ncRNAs and mediates the formation of heterochromatin (Bernstein and Allis, 2005). In addition, long ncRNAs, such as Xist, which is implicated in X chromosome inactivation in female mammals (Bernstein and Allis, 2005), HOTAIR, which silences certain *HOX* genes in humans (Rinn et al., 2007) and roX 1/2, components of the dosage compensation complex in flies, mediating the two-fold activation of the single male X chromosome (Fig. 1.3) (Bernstein and Allis, 2005), have been described. Taking into account that most of the genome is actually transcribed (Gerstein et al., 2007), future studies will certainly reveal more regulatory ncRNAs, maybe also acting by completely different mechanisms.

Within the nucleus, sub-structures can be observed, which lack a demarcating membrane and are instead defined by the presence of a certain set of proteins (e.g. Cajal or PML bodies). Moreover, in interphase cells, chromosomes adopt distinct territories, the position of which seems to be dependent on chromosome size, gene density and morphology. Despite some recent studies showing on the one hand that in human cells localization of genes to the nuclear periphery influences their expression and explaining on the other hand some long-range interactions of specific loci in detail, the general mechanisms how nuclear architecture influences gene expression are still unknown (Schneider and Grosschedl, 2007; Nunez et al., 2009).

Although all of these mechanisms can function independently, in most cases several of them act together to establish and maintain a certain chromatin state (Bönisch et al., 2008). One prominent example illustrating this complexity, is the X inactivation in female mammals, where one X chromosome is silenced through the concerted action of DNA methylation, histone PTMs, histone variants and ncRNAs.

1.3 Histone variants

The core histones H2A, H2B, H3 and H4 and the linker histone H1 show variation to a different extent. Since this variation is not only dependent on the protein but also on the species, this overview focuses on mammalian and in particular human histone variants.

Histone variants fall into two groups, canonical histones and replacement variants. The genes encoding canonical histone proteins are intron-free, replication-dependently expressed, organized in multi-copy clusters and their mRNAs have a conserved stem-loop structure at the 3' end instead of a poly(A) tail. This unique 3' structure, together with the stem loop binding protein (SLBP), is responsible for the processing, translation and degradation of canonical histone mRNAs. They thereby ensure high expression levels throughout S-phase, when large amounts of histones are needed for replication, followed by a rapid degradation at the end. Histone gene clusters typically contain multiple copies of each of the genes encoding for the five different histone proteins. A possible reason for this organization is that it allows them to be brought together in a domain enriched in factors required for their expression, the Cajal bodies in mammals. In contrast, replacement variants are encoded by solitary genes (or have only a few copies) outside of histone gene clusters. They usually contain introns, their mRNA is polyadenylated and they are expressed throughout the whole cell cycle (Marzluff et al., 2008).
For H4, no variants have been identified in mammals up to now (Table 1.1 and Fig. 1.4D). The reason for this lack of variation is presumably that H4 interacts with all other histones in the octamer, leaving little room for structural changes (Luger et al., 1997). In the following sections, the four other histone families are introduced and the diverse functions of their members described. For a summary of the data presented about core histone variants, see Table 1.1.

1.3.1 H1 variants

The linker histone H1 family shows high variability but the number of H1 variants differs extremely between species. In mammals for example, 11 H1 variants have been identified, while *Drosophila melanogaster* has only one. Focusing on human H1 variants, differences in temporal and spatial expression (Izzo et al., 2008), ability to bind and condense chromatin (Clausell et al., 2009), as well as localization to eu- or heterochromatic areas (Th'ng et al., 2005) have been reported. *H1.1-H1.5* and *H1t* are replication-dependently expressed and part of histone gene clusters whereas genes encoding replacement variants such as H1.0 are found outside of these clusters and are expressed independent of replication (Happel and Doenecke, 2009; Izzo et al., 2008). H1.2-H1.5 are present in all somatic cells with H1.2 and H1.4 being the predominant forms in most of the cells. In contrast, H1.0 is mainly expressed in terminally differentiated cells and H1.1 expression has so far only been reported for certain tissues (Meergans et al., 1997). H1x is currently the least well characterized of the human H1 variants and its expression has only been analyzed in a limited number of cell types (Happel

et al., 2005). The four remaining variants constitute a set of germ cell-specific proteins with H1oo being expressed in oocytes and H1t, H1T2 and HILS1 in testis (Happel and Doenecke, 2009; Izzo et al., 2008). Regarding H1.0-H1.5, it could be shown that they differ in their sub-cellular localization and that this localization is dependent on their C-terminal domain. H1.4, for instance, is associated with heterochromatin in most of the cells, whereas H1.2 and H1.3 are mainly found in euchromatic areas (Th'ng et al., 2005). Using native-like chromatin in form of minichromosomes, Clausell and coworkers analyzed the ability of human somatic H1 variants to condensate chromatin, classifying them as weak (H1.1 and H1.2), intermediate (H1.3) and strong condensers (H1.0, H1.4, H1.5 and H1x) (Clausell et al., 2009). To assess the biological role of individual variants, knockout studies in mice have been conducted. Knockout of one of the H1 variants H1.2, H1.3 and H1.4 alone or together with H1.0 did not show any obvious phenotype. Under these conditions, the remaining subtypes are up-regulated, compensating and maintaining a normal H1/core nucleosome ratio (Sirotkin et al., 1995; Fan et al., 2001). However, careful anaylsis of these knockout mice revealed specific effects in many cases. For H1.0, for instance, it could be shown that it is essential for the terminal differentiation of dendritic cells (Gabrilovich et al., 2002). Interestingly, triple-null mice, lacking H1.2, H1.3 and H1.4, die by mid-gestation with a broad range of defects. The ratio of H1 to nucleosomes is reduced by 50 % and the spacing between nucleosomes is shortened globally (Fan et al., 2003). In embryonic stem (ES) cells derived from these mice, albeit chromatin structure is changed dramatically, suprisingly the expression of only a small number of genes is affected. Many of these genes are usually regulated by DNA methylation, arguing for a role of (some) H1 variants in the establishment or maintenance of specific DNA methylation patterns (Fan et al., 2005). Depletion of each of the variants H1.0 and H1.2-H1.5 in human breast cancer cells, leads to alterations in a different subset of genes and different effects on cell cycle. Decreased levels of H1.2 induce G1 arrest in T47D and MCF10A breast epithelial cell lines and apoptosis in the breast cancer cell line MCF7. Moreover, depletion of H1.4 causes cell death in T47D cells, providing the first evidence for a crucial role of an H1 subtype for the survival of human cells (Sancho et al., 2008). In line with these results, studies in the last couple of years have revealed specific effects of certain H1 variants in other biological processes. Human 1.2, for example, has been shown to dissociate from chromatin after occurance of DNA double strand breaks (DSB). It accumulates in the cytoplasm where it triggers the release of cytochrome c from mitochondria, thereby transmitting apoptotic signals from the nucleus (Konishi et al., 2003). Further examples for specific roles of H1 variants in different organisms are summarized in Izzo et al., 2008.

Taken together, these data propose two distinct roles for linker histone variants: On the one hand, H1 variants are redundant in their ability to mediate global chromatin compaction

and to stabilize higher order chromatin structures. In knockout cells, the loss of a particular variant can therefore be compensated by the up-regulation of other H1 subtypes. On the other hand, each variant regulates a subset of specific genes, a role which cannot be compensated by other variant proteins (Izzo et al., 2008).

Table 1.1. Human core histone variants.
Distribution over species (Distribution), cell cycle expression profile (Expr.), sub-cellular localization (Localization), functional profile (Function) and specific chaperone (Chaperone) are summarized for all human core histone variants known to date. See text for details. Table, based on Bernstein and Hake (2006) and Talbert and Henikoff (2010), has been amended and updated with recent findings.

	Variant	Distribution	Expr.	Localization	Function	Chaperone
H2A	H2A	Widespread	RD	TG	Genome packaging	NAP1?
	H2A.X	Universal	RI	TG*	DNA repair, genome integrity	FACT
	H2A.Z-1	Universal**	RI	TG	Gene activation, silencing, chromosome segregation	HIRIP3?
	H2A.Z-2	Universal**	RI	TG	Gene activation, silencing, chromosome segregation	HIRIP3?
	H2A.Bbd.1	Mammals	ND	Xi exclusion	Spermatogenesis, Gene activation?	ND
	H2A.Bbd.2	Mammals	ND	Xi exclusion	Spermatogenesis, Gene activation?	ND
	MacroH2A1.1	Animals	ND	Xi	X chr. inactivation, gene silencing?	ND
	MacroH2A1.2	Animals	ND	Xi	X chr. inactivation, gene silencing?	ND
	MacroH2A2	Animals	ND	Xi	X chr. inactivation, gene silencing?	ND
H2B	H2B	Widespread	RD	TG	Genome packaging	NAP1?
	spH2B	Human	ND	Telomeres	ND	ND
	H2BFWT	Primates	ND	Telomeres?	Testis-specific, sperm cell number and vitality?	ND
	hTSH2B	Mammals	ND	basal part of the nucleus	Testis-specific, pronuclei formation? activation of paternal genes?	ND
H3	H3.1	Mammals	RD	ND	Genome packaging	CAF-1
	H3.2	Widespread	RD	ND	Genome packaging	ND
	H3.3	Universal	RI	Genes, TFBS, telomeres	Gene activation	HIRA, Daxx, DEK
	tH3	Mammals	RD?	ND	Testis-specific, ND	NAP2
	CENP-A	Universal	RI	Centromeres	Chromosome segregation	HJURP
H4	H4	Universal	RD	TG	Genome packaging	H3 chaperones

ND = not determined, RD = replication dependent, RI = replication independent, TG = throughout genome, Xi = inactive X chromosome, ? = hypothesized, TFBS = transcription factor binding sites. *) γ-H2A.X (= H2A.XS139ph) localizes to DNA DSBs and a population of small nuclear foci. **) H2.Z is a universal variant but only vertebrates have two genes giving rise to two different H2A.Z proteins.

1.3.2 H2A variants

The most variable core histone is H2A, for which four major variants are known to date: H2A.X, H2A.Z, macroH2A and H2A.Bbd (Barr-body deficient). These proteins show - in addition to sequence variations - also different lengths compared to canonical H2A.

The universal variant H2A.X is highly similar to H2A but is distinguished by its conserved C-terminal SQ-motif (Fig. 1.4A). Its unique S139 is phosphorylated at sites of DNA damage (Rogakou et al., 1998, 1999) by the DNA damage signaling kinases ATM (ataxia telangectasia mutated), ATR (ATM- and Rad3-related) and DNA-Pk (DNA-dependent protein kinase)

(Burma et al., 2001; Stiff et al., 2004). The phosphorylated form, termed γ-H2A.X, is present at sites of DSBs during DSB repair, meiotic recombination (Mahadevaiah et al., 2001), apoptotic digestion (Rogakou et al., 2000), V (D) J splicing (Chen et al., 2000), and class switch recombination (Petersen et al., 2001). These data suggest γ-H2A.X to be a universal cellular response to DSBs, functioning in the maintenance of genome stability. Emerging evidence proposes that γ-H2A.X also plays a role outside DSBs, for example in the replication of fac-

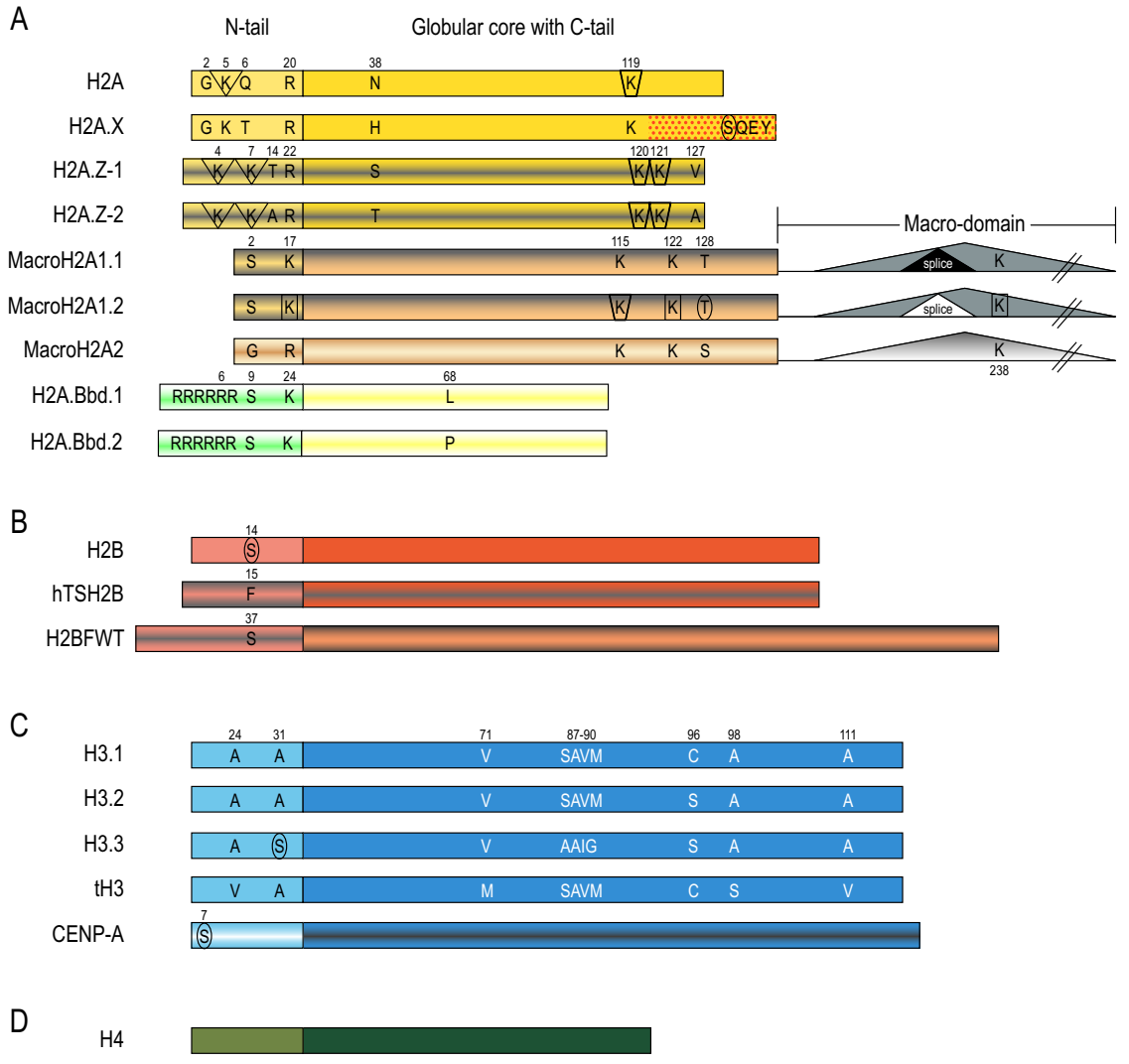

Figure 1.4. Protein sequences of human core histone variants.
Schematic representation of human core histone variants. Proteins are divided in N-terminal tail and globular domain with C-terminal tail. Human (A) H2A (yellow), (B) H2B (red), (C) H3 (blue) and (D) H4 (green) variants are depicted. Highly divergent protein sequences are visualized by different color shades without highlighting sequence differences. Amino acid differences are indicated when variants differ only in few key residues (for example H3 variants) or when variant-specific amino acids are posttranslationally modified (for example the SQEY-motif in H2A.X). PTM sites are marked as follows: ellipse = phosphorylation, square = methylation, triangle = acetylation, trapezoid = ubiquitination. The macrodomains of macroH2A histones are not drawn to scale. Their triangular shape indicates non-histone-like sequences. MacroH2A1.1 and macroH2A1.2 are splice variants (differentially spliced exon 6), denoted by an internalized white or black triangle in their macrodomain. Note that spH2B, another H2B variant, is not depicted because its protein sequence has not been identified yet. See text for details. Image adapted from Bernstein and Hake, 2006, amended with recent findings.

ultative heterochromatin on the Xi. However, these functions are less well understood and subject of current research (Ismail and Hendzel, 2008).

The second universal H2A variant is H2A.Z, which shows ∼60 % sequence identity to canonical H2A. H2A.Z plays a role in such diverse processes as gene activation, chromosome segregation, heterochromatin silencing, and progression through the cell cycle (Zlatanova and Thakar, 2008). Aiming to explain how H2A.Z can fulfill its contrasting functions, several modes of regulation have been identified. In humans, H2A.Z has been found to be enriched in promoter regions up- and downstream of transcription start sites with binding levels matching gene expression (Zlatanova and Thakar, 2008). Furthermore, posttranslational modifications seem to regulate H2A.Z function as H2A.Z acetylation levels are higher in euchromatic compared to heterochromatic regions and mono-ubiquitinated H2A.Z, which is found on the Xi, seems to be important for transcriptional repression (Talbert and Henikoff, 2010). Further variability is observed in vertebrates, where two isoforms, H2A.Z-1 and H2A.Z-2, that differ in three amino acids (Fig. 1.4A), are encoded by two different genes (Coon et al., 2005; Dryhurst et al., 2009; Matsuda et al., 2010). H2A.Z-1 knockout is lethal in mice (Faast et al., 2001) and separate knockdown of both isoforms results in distinct alterations in cell growth and gene expression (Matsuda et al., 2010). Moreover, H2A.Z-1 and H2A.Z-2 are differentially expressed in some tissues and show similar but not identical distributions in chromatin (Dryhurst et al., 2009). Taken together, these data suggest that H2A.Z-1 and H2A.Z-2 have non-redundant functions and differential effects on nucleosome stability and chromatin structure.

In 1992, the first of the macroH2A variants was identified, later named macroH2A1.1. Its N-terminal third is 64 % identical to H2A and its C-terminal part (∼30 kDa) constitutes a macrodomain (Pehrson and Fried, 1992). Its isoform macroH2A1.2, differing in a short stretch of amino acids in the non-histone domain, originates from the same gene by alternative splicing (Rasmussen et al., 1999). MacroH2A2, which is 80 % identical to macroH2A1.2, is encoded by a second gene (Fig. 1.4A) (Chadwick and Willard, 2001a). MacroH2A1.2 and macroH2A2 have different nuclear localization patterns but are both enriched on the Xi (Costanzi and Pehrson, 1998, 2001; Chadwick and Willard, 2001a), suggesting a role in X inactivation and, as they are expressed at similar levels also in males (Rasmussen et al., 1999), maybe as general repressors of transcription. However, several studies could show that macroH2A is not necessary for X inactivation, thereby also questioning macroH2A's role as general repressor (Gamble and Kraus, 2010). Two studies, mapping macroH2A localization by ChIP-chip, could recently show association of macroH2A with a large number of autosomal genes. MacroH2A-associated genes are enriched for H3K27me3, a mark for facultative heterochromatin (Buschbeck et al., 2009; Gamble et al., 2010), and consistent with this finding, most of these genes are transcriptionally silent. However, roughly 20 % of macroH2A1-bound

genes are expressed and, surprisingly, macroH2A1 positively affects about 75 % of its target genes (Gamble et al., 2010). In addition to its role in transcriptional regulation, macroH2A also seems to play a role in development as all three variants are differentially expressed in a tissue- and development-dependent manner (Pehrson et al., 1997; Costanzi and Pehrson, 2001). Furthermore, macroH2A may also be implicated in cell proliferation as its association with the Xi is cell cycle dependent and disrupted by the phosphorylation of S137, which is dramatically up-regulated during mitosis (Bernstein et al., 2008). Additionally, macroH2A becomes re-distributed when cells exit the cell cycle (Gamble et al., 2010).
Regarding sequence differences, the most variable H2A variant is the mammalian H2A.Bbd, which is only 48 % identical to H2A. In humans, it is encoded by three intronless genes on the X chromosome giving rise to two proteins that differ in only one amino acid (Fig. 1.4A) (Chadwick and Willard, 2001b). H2A.Bbd lacks the H2A C-terminus containing an acidic patch that directly contacts histone H4 (Luger et al., 1997). None of the PTM-carrying residues in H2A is present in H2A.Bbd, instead, the protein has a stretch of six arginines in its N-terminal tail (Fig. 1.4A). Tagged H2A.Bbd is co-localizing with acetylated histone H4 and excluded from the Xi, suggesting an association with transcriptionally active chromatin (Chadwick and Willard, 2001b). Reconstituted nucleosomes containing H2A.Bbd have a more relaxed conformation (Bao et al., 2004; Gautier et al., 2004; Montel et al., 2007) and organize only 120 - 130 bp of DNA (Bao et al., 2004; Doyen et al., 2006). H2A.Bbd has been proposed to constitute an acetylation independent device for the local unfolding of chromatin, thereby promoting transcription (Eirín-López et al., 2008). In addition, H2A.Bbd is involved in spermatogenesis where it probably facilitates the exchange of histones with protamines by destabilizing the nucleosome and is retained at some sites in sperm cells (Ishibashi et al., 2010).

1.3.3 H2B variants

In the nucleosome, the H3-H4 tetramer interacts with the H2A-H2B dimer through contacts made by H2B with H4 (Luger et al., 1997). This important structural role of H2B is most likely the cause for the presence of just three human H2B variants which, in addition, are restricted to the male germinal cell lineage (Fig. 1.4B and Table 1.1). Although little is known about all of these variants, maybe the most enigmatic is the human-specific spH2B, which was discovered as part of a telomere-binding complex. spH2B shows higher electrophoretic mobility than canonical H2B, binds telomeric DNA *in vitro* and shows a punctuate localization in sperm nuclei, partially coinciding with telomeric DNA (Gineitis et al., 2000).
The most conserved of the human H2B variants is the testis/sperm-specific variant hTSH2B, an ortholog of the rodent TH2B, which shows 85 % similarity to canonical H2B (van Roijen

et al., 1998; Zalensky et al., 2002). hTSH2B is only expressed in a sub-population of sperm cells ($\sim 30\,\%$) where it localizes specifically to the basal part of the nucleus, adjacent to the sperm tail attachment point. Distinct foci in cells expressing lower hTSH2B levels, propose a possible association with specific chromatin domains (Singleton et al., 2007; Zalensky et al., 2002). Expression of hTSH2B promotes a more rapid and comprehensive chromatin decondensation, suggesting a potential role in pronuclei formation and the activation of paternal genes following fertilization and during early embryonic development (Singleton et al., 2007). On the molecular level, it could be shown that although hTSH2B has a destabilizing effect on histone octamers, nucleosomes containing this novel variant are structurally and dynamically indistinguishable from their canonical counterpart (Li et al., 2005). The most pronounced sequence differences between somatic H2B and hTSH2B are found at the N-terminus (Zalensky et al., 2002), a region which in H2B is involved in interactions with DNA and important for mitotic and apoptotic condensation of chromosomes (de la Barre et al., 2001; Cheung et al., 2003). Residues, known to be phosphorylated, are missing or re-positioned and novel potential phosphorylation sites have been introduced (Kimmins and Sassone-Corsi, 2005). Interestingly, S14, phosphorylated in H2B by Mst1 kinase during apoptosis (Cheung et al., 2003), is replaced by a phenylalanine in hTSH2B (Fig. 1.4B), raising the question whether hTSH2B has the potential to prevent sperm cells from undergoing apoptosis (Bernstein and Hake, 2006).

In 2004, a primate- and testis-specific H2B variant, termed H2BFWT (H2B family member W, testis-specific), has been identified. The *H2BFWT* gene is located on the X chromosome and encodes a highly divergent H2B variant with only 45 % amino acid sequence identity with somatic H2B. Interestingly, the syntenic region on the mouse X chromosome is considerably shorter, suggesting that H2BFWT and its paralogs (three to five genes, clustered tightly on the X chromosome) have either evolved recently in the primate lineage or have been lost in rodents (Churikov et al., 2004). In a nucleosomal context, H2BFWT behaves similar to canonical H2B as shown by equal mobilization and remodeling efficiencies using SWI/SNF on *in vitro* reconstituted chromatin. This can be explained by the fact that H2BFWT sequence mainly differs in the N-terminal tail, whereas the core region, which determines the nucleosome structure, is more conserved. Although it does not influence overall nucleosome structure, the altered N-terminus has an effect on H2BFWT behavior as it leaves the protein unable to recruit chromosome condensation factors and to assist in the assembly of mitotic chromosomes (Boulard et al., 2006). Regarding the function of this novel variant, initial experiments have shown that H2BFWT partially localizes to the interstitial telomeric blocks, suggesting a telomere-associated function (Churikov et al., 2004). More recent results link H2BFWT to male infertility: A single nucleotide polymorphism in the 5' UTR of H2BFWT

has been identified, which severly reduces translation of H2BFWT, causing reduced sperm count and vitality (Lee et al., 2009).
Recently, two novel testis-specific H2B variants (H2BL1 and H2BL2), involved in pericentric heterochromatin reprogramming during mouse spermatogenesis, have been identified. H2BL1 and H2BL2 are not homologous to any of the described human H2B variants, underlining the high diversity of testis-specific histone variants (Govin et al., 2007).

1.3.4 H3 variants

In mammals, five histone H3 variants have been described to date: H3.1, H3.2, H3.3, H3.1t (tH3, testis-specific) and CENP-A (centromere-specific). Except for CENP-A, sequence differences are quite subtle among H3 proteins (Fig. 1.4C). H3.1 and H3.2 are distinguished by a single amino acid exchange at position 96, with H3.1 carrying a cysteine and H3.2 a serine. Both are replication-dependently expressed, but H3.1 is only found in mammals, whereas H3.2 is present in all eukaryotes except for budding yeast (Bernstein and Hake, 2006). Due to their high similarity, they are often treated as one protein. However, quantitative mass spectrometry analyses have revealed that expression levels and PTM patterns of these variants vary between different mammalian cell lines and tissues, arguing for distinct protein species (Hake et al., 2006; Garcia et al., 2008). H3.2 is enriched in di- and trimethylated K27, modifications associated with transcriptional silencing and marks of facultative heterochromatin. In contrast, H3.1 shows enrichment in K9 dimethylation, K64 monomethylation and K14 acetylation. K9 dimethylation is found in areas of constitutive heterochromatin (Hake et al., 2006). An interesting hypothesis, aiming to explain the different functions and modes of action of these H3 variants, is the implication of the unique C96 in H3.1 in intermolecular disulfide bonds. In this model, H3.1 promotes higher order chromatin structures and silencing of certain chromatin regions by forming disulfide bonds with neighboring nucleosomes, lamin B receptor (to retain certain loci at the nuclear periphery) or other yet to be identified factors (Hake and Allis, 2006).
The universal H3 variant H3.3 shows four amino acids difference compared to H3.2. It is expressed and incorporated into chromatin throughout the cell cycle and has been found to be enriched in PTMs associated with active transcription (Bernstein and Hake, 2006). In line with these findings, many studies in different organisms have mapped H3.3 to the complete coding region of transcribed genes and to highly enriched foci in promoter regions, establishing its reputation as activating variant. However, H3.3 also marks inactive genes (maybe accounting for a "poised" state of these genes) and genic as well as intergenic regulatory regions (Elsaesser et al., 2010). In addition, H3.3 has been shown to localize to telomeres (Wong

et al., 2009; Goldberg et al., 2010), is implicated in the establishment of heterochromatin in the mouse embryo (Santenard et al., 2010) and found associated with pericentromeric heterochromatin when its unique serine 31 (Fig. 1.4C) is phosporylated during mitosis (Hake et al., 2005). Taken together, these data suggest that H3.3 does not simply promote gene transcription but rather has very distinct functions which depend largely on its incorporation at specific loci and its interaction partners (see also section 1.3.5).

The mammalian testis-specific H3 variant tH3 differs in four amino acids from H3.1 (Fig. 1.4C) (Witt et al., 1996). Two of these changes (M71 and V111) have recently been identified to cause the significantly lower stability of tH3-containing nucleosomes which may be important for the replacement of histones with protamines during spermatogenesis (Tachiwana et al., 2010). Although tH3 is primarily expressed in testis, low amounts have also been detected in HeLa cells (Andersen et al., 2005), mouse embryos and adult mouse brain and spleen (Govin et al., 2007). The function of this somatic tH3 fraction remains to be determined.

The most divergent of the mammalian H3 variants is CENP-A, which shows only ∼60 % homology to H3 in its histone-fold domain and has a highly variable N-terminus (Sullivan, 2001). CENP-A localizes to the centromere of eukaryotic chromosomes and is essential for the assembly of the kinetochore, the attachment point of spindle microtubules during cell division. Although it is still unclear what exactly defines centromere position, several lines of evidence now suggest that it is determined by epigenetic marks, maybe the most crucial being the replacement of canonical H3 by CENP-A (Mehta et al., 2010). CENP-A is essential as its knockout in mice is lethal early in development with embryos showing severe mitotic problems, chromatin fragmentation and hypercondensation (Howman et al., 2000). In human cells, where depletion of CENP-A causes cell death accompanied by severe mitotic defects, a complete rescue can be achieved by replacement with histone H3 carrying the centromere-targeting domain (CATD) of CENP-A (Black et al., 2007). The CATD is necessary and sufficient for nucleosome assembly at centromeres and it is responsible for the unique conformational rigidity of CENP-A-containing nucleosomes (Black et al., 2004, 2007). Several studies have shown that nucleosomes containing centromere-specific histone H3 (CenH3) have an unusual structure. In *Drosophila*, for example, they seem to consist of a heterotetramer of H2A, H2B, CenH3 and H4, rather than an octamer. In addition, it has been proposed that centromeric nucleosomes organize DNA in a right-handed wrap (Talbert and Henikoff, 2010). However, the recently solved crystal structure of the CENP-A-H4 tetramer suggests that CENP-A-containing nucleosomes are octameric with conventional left-handed DNA wrapping (Sekulic et al., 2010). In summary, CENP-A seems to be the essential epigenetic factor that marks centromere location by restructuring the nucleosome from within its globular domain, mediated by the CATD.

1.3.5 Targeted chromatin incorporation of histone variants

With the growing knowledge about histone variants that partly show very distinct localization patterns, the question arose, how they are targeted and incorporated at such specific chromatin sites. For proteins playing a role in these processes, the term "histone chaperone" has been coined (Koning et al., 2007). In the last 30 years, multiple histone chaperones, implicated in the storage, transport or deposition of a certain variant or a group of histone proteins, have been described (Koning et al., 2007; Eitoku et al., 2008).

The targeted incorporation of H2A-H2B variant dimers is mediated by several different proteins. NAP1 functions as a shuttle for H2A-H2B from the cytoplasm to the nucleus (Loyola and Almouzni, 2004). In addition, it was shown to assemble nucleosomes *in vitro* (Ishimi et al., 1987, 1984) and to interact with H2A-H2B *in vitro* and *in vivo* (Chang et al., 1997; Ishimi et al., 1987; Ito et al., 1996), suggesting it to be a H2A-H2B-specific chaperone. However, biochemical studies indicate that NAP1 preferentially binds H3-H4 when all core histones are present (McBryant et al., 2003; Mazurkiewicz et al., 2006; Eckey et al., 2007), questioning the specificity of this chaperone for the H2A-H2B dimer. In budding yeast, it has been shown that Htz (H2A.Z) is deposited by Chz1 together with the SWR1 complex (Luk et al., 2007; Korber and Hörz, 2004). The conserved CHZ motif confering this function, is also found in human HIRA-interacting protein 3 (HIRIP3), a factor shown to interact with core histones (Lorain et al., 1998). In addition, p400/Domino and SRCAP, homologs of the SWR1 complex, have been identified which are able to exchange H2A-H2B with H2A.Z-H2B dimers (Gévry et al., 2007; Ruhl et al., 2006). It is tempting to speculate that HIRIP3 constitutes the human H2A.Z-specific chaperone, which together with p400/Domino or SRCAP is responsible for the site-specific incorporation of H2A.Z. H2A.X deposition could be shown to be mediated by the FACT complex. Chromatin incorporation is promoted by phosphorylation of H2A.X, whereas poly-ADP-ribosylation of the FACT subunit Spt16 reduces H2A.X exchange activity (Heo et al., 2008). For the other known H2A variants, macroH2A and H2A.Bbd, so far, no specific chaperone has been identified.

In the last couple of years, chaperones for most of the mammalian H3 variants have been found. H3.1 is deposited by the CAF-1 complex (Tagami et al., 2004) in a DNA-synthesis-coupled manner. Through the interaction with PCNA, CAF-1 is targeted to the replication fork (Shibahara and Stillman, 1999; Krude, 1995) and to sites of damaged DNA in UV-treated cells (Green and Almouzni, 2003; Polo et al., 2006). For H3.2, no specific chaperone has been described so far, but as it differs in only one amino acid from H3.1 (Fig. 1.4C), it seems likely that it is also deposited by CAF-1. For several years, it has been clear that the replication-independent deposition of H3.3 is mediated by HIRA (Tagami et al., 2004). However, several

recent publications have now shown that the picture is much more complex: HIRA is required for the incorporation of H3.3 at active and repressed genes, but it is dispensible for deposition at telomeres and many transcription factor binding sites (Goldberg et al., 2010). Instead, H3.3 incorporation at telomeres and the repression of telomeric RNA is mediated by the novel histone chaperone Daxx together with ATRX (Drané et al., 2010; Lewis et al., 2010; Goldberg et al., 2010; Wong et al., 2010). Moreover, phosphorylated DEK, associating with casein kinase 2, acts as a H3.3 chaperone in flies and humans. In flies, DEK has been shown to be a co-activator of the nuclear ecdysone receptor. Interestingly, in humans the deposition of H3.3 is impaired in acute myeloid leukemia patients carrying a chromosomal translocation fusing DEK to CAN (Sawatsubashi et al., 2010). For the testis-specific variant tH3, nothing is known about its deposition *in vivo*. However, *in vitro*, NAP2, a paralog of NAP1, efficiently incorporates tH3 into nucleosomes (Tachiwana et al., 2008). Only recently, the Holliday junction-recognizing protein (HJURP) has been identified as the chaperone specifically depositing the centromere-specific H3 protein CENP-A (Dunleavy et al., 2009; Foltz et al., 2009). Surprisingly, while centromeric DNA is replicated during S-phase, recruitment of new CENP-A by HJURP in human cells is restricted to a short time window at late telophase/early G1, leaving the cell with only 50 % of the maximal CENP-A nucleosome complement during G2 and mitosis (Jansen et al., 2007; Hemmerich et al., 2008; Dunleavy et al., 2009; Foltz et al., 2009). Whether H3 is incorporated instead or these sites remain unoccupied, is currently unclear, although it is known that H3.1 nucleosomes can be assembled with alpha-satellite DNA and that they can be found interspersed with CENP-A nucleosomes (Blower et al., 2002).

Despite the fact that the precise targeted chromatin incorporation mechanisms are still not known for a lot of histone variants, the so far identified complex processes and multitude of chaperones lead to the speculation that there might be one or several special histone chaperones for the deposition of each variant.

1.3.6 Evolution of histone variants

Histones, especially H3 and H4, are among the most conserved proteins in the eukaryotic genome. Nevertheless, a whole range of variants with quite specific functions have evolved. Two different models for the evolution of multigene families have been described: concerted evolution and the birth-and-death model of evolution. In concerted evolution, for example acting on rRNA genes, the members of the gene family are homogenized by interlocus gene recombination or gene conversion. In contrast, evolution by the birth-and-death model assumes, that new genes are created by repeated gene duplication and that some of these genes remain

in the genome for a long time whereas others are deleted or become nonfunctional. This mode of evolution applies for instance to the family of immunoglobulins (Nei and Rooney, 2005). Histone genes have long been thought to evolve through concerted evolution, however, this would mean that synonymous (silent) and nonsynonymous mutations should occur at almost the same frequency in these genes. In several studies, investigating the linker histone H1 (Eirín-López et al., 2004) as well as all four core histone families (Piontkivska et al., 2002; Rooney et al., 2002; González-Romero et al., 2008, 2010), it has now been shown that the frequency of synonymous substitutions is much higher than that of nonsynonymous. This observation speaks for an evolution of histone gene families driven by the birth-and-death mechanism combined with a strong purifying selection on the protein level.
Regarding the diversification into multiple variants, the first idea would certainly be that the respective non-specialized variant constitutes the ancestral form. However, two aspects speak against this hypothesis: First, some of the specialized variants, such as H2A.X and H3.3, are, in contrast to their canonical forms, universally expressed (Table 1.1). Second, it is difficult to imagine that something like the conserved S-Q-E/D-Φ-motif of H2A.X (Φ = hydrophobic residue, Fig. 1.4A) has appeared independently multiple times in evolution. Therefore, it seems likely that these specialized but universal proteins constitute the ancestral histones (Talbert and Henikoff, 2010).

1.4 Objective

Over the last 20 years, several novel histone variants of the mammalian H1, H2A and H2B family (e.g. macroH2A (Pehrson and Fried, 1992) or H2BFWT (Churikov et al., 2004)) have been described, but regarding H3, it was thought that with the identification of CENP-A (Palmer et al., 1987) and tH3 (Trostle-Weige et al., 1984) the set of this particular histone family was complete. However, searching the histone database (http://research.nhgri.nih.gov/histones/), several putative histone H3 variant genes were listed, opening up the fascinating possibility of a whole range of additional H3 proteins with unique functions. In my PhD thesis I was aiming to characterize the most interesting candidate(s) of this list in terms of (A) expression levels in different cell lines and tissues, (B) sub-cellular localization and (C) biological function.

2 Materials and Methods

2.1 Materials

2.1.1 Technical devices

Description	Supplier
-20 °C Freezer	Bosch, Liebherr
-80 °C Freezer	GFL
4 °C Fridge	Siemens, Liebherr
37 °C Incubator (bacteria)	Memmert
37 °C Incubator (mammalian cells)	Heraeus
Agarose gel chamber	Repair shop of Adolf-Butenandt-Institute
Autoclave (Varioklav)	H+P
2100 Bioanalyzer	Agilent
Cell counter	Casy Cell Counter, Innovatis
Centrifuges	Heraeus Megafuge 2.0 Haereus Biofuge pico Thermo/Heraeus Pico 17 Thermo Shandon Cytospin 4 Eppendorf Centrifuge 5810R Hettich Rotina 46
Concentrator plus	Eppendorf
Developer machine Curix 60	Agfa
Ettan microLC (HPLC)	Amersham Pharmacia Biotech
Gel documentation system	Peqlab
Hood	CleanAir
HPLC C4 column (250 x 4.6 mm Jupiter 10 µm 300 Å)	Phenomenex
Imaging system	LI-COR
Incubation shaker (Multitron)	Infors
LightCycler®) 480 II	Roche
LC Ultimate 3000	Dionex
LTQ Orbitrap XL	Thermo
Microscopes	DMIL LED (Leica) Axiovert 200M (Zeiss) LSM 510 META confocal (Zeiss) LSM 710 confocal (Zeiss) personalDV widefield epifluorescence (Applied Precision) UltraVIEW VoX spinning disc (PerkinElmer)

Description	Supplier
Microscopes	OMX DeltaVision prototype (Applied Precision)
Microwave	LG
MilliQ-water	Millipore
Odyssey® imaging system	LI-COR
pH-meter	inoLab pH 720
Pipetboy	Integra Biosciences
Pipettes	Gilson
Power supply	BioRad
Proteingel chamber (Novex Mini Cell)	Invitrogen
REPETMAN® multistep pipet	Gilson
Rotating wheel	Neolab, VWR
RTCA DP Analyzer	Roche
Scales	Sartorius
Shaker	Roth
Spectrophotometer	Nanodrop ND1000, Peqlab
ThermalCycler 2720	Applied Biosystems
Thermomixer 5436	Eppendorf
Trans Blot® SD Semi-dry transfer cell	BioRad
UV Stratalinker 1800	Stratagene
Vortex Genie 2®	Bachofer
Water bath	Memmert

2.1.2 Chemicals and consumables

Unless otherwise stated, all common chemicals are purchased in analytical grade from Merck.

Description	Supplier
1.5 ml and 2 ml reaction tubes	Greiner, Sarstedt
15 ml and 50ml tubes	Sarstedt
96-well plates	Peqlab
Acetonitrile	Roth
Agarose SeaKem®	ME Biozym
Ampicillin	Roth
Aqua-Poly/Mount	Polysciences
Bacto Agar	BD
Bacto Tryptone	BD
Cling film	Saran
BSA 98%	Sigma
Cellculture plates	Sarstedt
Cellophan	Roth
Combitips plus	Eppendorf
Complete Protease Inhibitor Cocktail Tablets	Roche
Coomassie Brilliant Blue R	Sigma

Description	Supplier
Cover slips	Roth
Cryovials	Roth
DAPI	Invitrogen
Developer	Agfa
DMSO	Sigma
DNA oligonucleotides	Sigma
dNTP mix	NEB
DTT	Roth
Dulbecco's Modified Eagle Medium (DMEM)	Invitrogen (low glucose + GlutaMAX) PAA (high glucose + L-glutamine)
Dynabeads® M-280 Sheep anti-Mouse IgG	Invitrogen
ECL™ Western Blotting Detection Reagents	Amersham
EDTA	Sigma
EGTA	Sigma
Ethidium bromide	Sigma
FCS dialyzed	Sigma
Filter paper	Whatman 3MM Whatman
Filter tips	Sarstedt, Molecular BioProducts
Filter unit Nalgene	0.2 µm filter holes
Fixer	Agfa
FuGENE HD Transfection Reagent	Roche
G418-sulfate (TC)	PAA
Glass pipettes 5 ml and 10 ml	Hirschmann®
Glassware	Schott
Human Gene 1.0 ST Arrays	Affymetrix
Human tissue sections (frozen)	Biochain
IPTG	Roth
Krebs-Ringer Bicarbonate Buffer	Sigma
Laboratory film	Parafilm®
Lab-Tek chamber slides	Nunc
LightCycler® 480 Multiwell Plate 384, white	Roche
LightCycler® 480 Sealing Foil	Roche
MaXtract™ High Density column	Qiagen
β-Mercaptoethanol	Sigma
McCoy's 5A Medium	Invitrogen
Microscope slides SuperFrost®	Roth
Multiply®-µStripPro with 8 0.2ml tubes	Sarstedt
Nocodazole	Sigma
NP-40	Sigma
Oligofectamine® Transfection Reagent	Invitrogen
Omnifix®-F syringes	Braun
Opti-MEM® I Reduced-Serum Medium	Invitrogen
PAP pen	Kisker
Pasteur pipettes	Brand

Description	Supplier
Penicillin / Streptomycin	PAA
Peptides	Proteomics Resource Center of The Rockefeller University Peptide Specialty Laboratories GmbH
Petridishes	Greiner
Pipette tips	Brand, Sarstedt
PMSF	Sigma
Ponceau S solution	Sigma
Propidium iodide	Sigma
Protein gel cassettes (disposable)	Invitrogen
Protran® Nitrocellulose Transfer Membrane	Whatman
PVDF Transfer Membrane Hybond™-P	Amersham
Rotiphorese Acrylamide/bisacrylamide mix	Roth
RPMI Medium 1640	Invitrogen
RTCA E-Plate 16	Roche
SDS	Serva
siRNAs	Eurofins MWG Operon
Sterican® needles	Braun
TEMED	Roth
TFA	Roth
To-Pro3	Invitrogen
Total RNA from human tissues	Applied Biosystems (normal lung and breast, tumor lung, breast and ovary) Biochain (tumor lung, breast, thyroid and bone, normal testis and brain)
Tris	Invitrogen
Triton X-100	Sigma
Trypsin/EDTA (TC)	PAA
Tween 20	Sigma
VECTASHIELD® Mounting Medium	Vector Laboratories
Water, PCR-grade	Roche
X-ray films	Fujifilm
Xylene cyanol	Sigma

2.1.3 Kits, enzymes and markers

Description	Supplier
100bp DNA marker	NEB
1kb DNA marker	NEB
DNA 1000 Kit	Agilent
Gel extraction Kit	Qiagen
LightCycler® 480 SYBR Green I Master	Roche
Maxi- and Midiprep Kit	Qiagen, Promega
Micrococcal nuclease	Sigma

Description	Supplier
PCR-purification Kit	Qiagen
peqGOLD Protein Marker IV, V	Peqlab
Phusion® DNA Polymerase	Finnzymes
Pfu Turbo DNA Polymerase	Stratagene/Agilent
ProLong® Antifade Kit	Invitrogen
ProtoScript® First Strand cDNA Synthesis Kit	NEB
ProtoScript® M-MuLV Taq RT-PCR Kit	NEB
Restriction endocucleases	NEB
RNA 6000 Nano Kit	Agilent
RNase-Free DNase Set	Qiagen
RNeasy Kit	Qiagen
RNeasy MinElute Cleanup Kit	Qiagen
Taq DNA Polymerase	NEB

2.1.4 Antibodies

2.1.4.1 Primary antibodies

Name	Supplier	Application	Dilution
rat αH3.X/Y (clone 8H6-2111)	E. Kremmer	WB	1:50
		IF	1:20
mouse αHA (clone 12CA5)	Roche	WB	1:1000
		IF	1:500
rabbit αH3S10ph	Millipore	IF	1:200
rabbit αH3 (C-terminus)	Abcam	WB	1:5000
mouse αNeuN	Millipore	IH	1:500
rabbit αGFAP	Dako Cytomation	IH	1:1000

2.1.4.2 Secondary antibodies

Name	Supplier	Application	Dilution
αrat HRP	Amersham	WB	1:5000
αrabbit HRP	Amersham	WB	1:5000
αmouse IRDye700DX	Rockland	Licor	1:10000
αrabbit IRDye800DX	Rockland	Licor	1:10000
αrat Alexa 488	Invitrogen	IF	1:2000
αmouse Alexa 488	Invitrogen	IF	1:2000
αrabbit Rhodamine red X	Dianova	IF	1:1000
αrabbit Cy5	Dianova	IH	1:250
αrat biotin	Vector Laboratories	IH	1:100
streptavidin Alexa 555	Dianova	IH	1:500

2.1.5 Plasmids

Name	Source	Description	Marker
pT7Blue-3	Novagen	used for subcloning	Amp, Kan
pIRESneo3 HA	Holger Dormann	expression of N-terminally HA-tagged proteins in mammalian cells	Amp, Neo
pIRESneo3 HA-H3.1	Clemens Bönisch		
pIRESneo3 HA-H3.2	Clemens Bönisch		
pIRESneo3 HA-H3.3	Clemens Bönisch		
pIRESneo3 HA-H3.X	Clemens Bönisch		
pIRESneo3 HA-H3.Y	this study		
pEGFP-C1	Clontech	expression of N-terminally GFP-tagged proteins in mammalian cells	Kan, Neo
pEGFP-C1 H3.1	this study		
pEGFP-C1 H3.2	this study		
pEGFP-C1 H3.3	this study		
pEGFP-C1 H3.X	this study		
pEGFP-C1 H3.Y	this study		
pET-21a(+)	Novagen	expression of un-tagged proteins in *E. coli*	Kan, Neo
pET-21a(+) H3.X	this study		
pET-21a(+) H3.Y	this study		

2.1.6 Oligonucleotides

For simplicity, oligonucleotides are listed in the appendix in Tables A.1 (Oligonucleotides for qPCR), A.2 (Oligonucleotides for cloning) and A.3 (Oligonucleotides for RNAi).

2.1.7 Bacterial strains and cell lines

2.1.7.1 *E. coli* strains

Strain	Genotype	Supplier
DH5α	F$^-$ Φ80d*lac*ZΔM15 Δ(*lac*ZYA-*arg*F)$_{U169}$ *rec*A1 *end*A1 *hsd*R17 (r_K^-, m_K^+) *pho*A *sup*E44 λ$^-$ thi-1 *gyr*A96 *rel*A1 (Hanahan, 1985)	Genentech
XL1 Blue	*rec*A1 *end*A1 *gyr*A96 *thi-1 hsd*R17 *sup*E44 *rel*A1 *lac* [F'*pro*AB *lacI*^{q}ZΔ*M15* Tn*10* (Tet^r)]	Stratagene
BL21-CodonPlus (DE3)-RIL	B F$^-$ *ompT* hsdS(r_B^-, m_B^-) *dcm*+ Tet^r gal λ (DE3) *endA* Hte [*argU ileY leuW* Cam^r]	Stratagene

2.1.7.2 Mammalian cell lines

Table 2.8. Mammalian cell lines

Cell line	Organism	Origin	Source	Medium
HeLa	*Homo sapiens*	cervical cancer	ATCC (CCL-2)	
HeLa Kyoto	*Homo sapiens*	cervical cancer	Heinrich Leonhardt	
U2OS	*Homo sapiens*	osteosarcoma	ATCC (HTB-96)	
MG63	*Homo sapiens*	osteosarcoma	ATCC (CRL-1427)	DMEM + 10 % FCS + 1 % P/S
HEK293	*Homo sapiens*	transformed embryonic kidney cells	ATCC (CRL-1573)	
Rat Nb	*Rattus norvegicus*	neuroblastoma	Marion Cremer	
NIH3T3	*Mus musculus*	fibroblasts	ATCC (CRL-1658)	
SAOS-2	*Homo sapiens*	osteosarcoma	ATCC (HTB-85)	McCoy's + 15 % FCS + 1 % P/S
Raji	*Homo sapiens*	B-cell	ATCC (CCL-86)	RPMI + 10 % FCS + 1 % P/S
Primary fibroblasts	*Homo sapiens*	skin derived	Marion Cremer	
Primary fibroblasts	*Pan paniscus*	skin derived	Stefan Müller	
Primary fibroblasts	*Macaca nemestrina*	skin derived	Stefan Müller	DMEM 20 % FCS + 1 % P/S
Primary fibroblasts	*Callithrix jacchus*	skin derived	Stefan Müller	
Primary fibroblasts	*Eulemur fulvus*	skin derived	Stefan Müller	

Table 2.9. Stably transfected mammalian cell lines

Cell line	Organism	Plasmid	Source	Medium
HeLa empty vector	*Homo sapiens*	empty pIRESneo3 HA	this study	
HeLa HA-H3.1	*Homo sapiens*	pIRESneo3 HA-H3.1	Clemens Bönisch	
HeLa HA-H3.3	*Homo sapiens*	pIRESneo3 HA-H3.3	Clemens Bönisch	
HeLa HA-H3.X	*Homo sapiens*	pIRESneo3 HA-H3.X	this study	DMEM + 10 % FCS + 1 % P/S
HeLa HA-H3.Y	*Homo sapiens*	pIRESneo3 HA-H3.Y	this study	+ 400 µg/ml G418-sulfate
U2OS empty vector	*Homo sapiens*	empty pIRESneo3 HA	this study	
U2OS HA-H3.X	*Homo sapiens*	pIRESneo3 HA-H3.X	this study	
U2OS HA-H3.Y	*Homo sapiens*	pIRESneo3 HA-H3.Y	this study	

Fetal calf serum (FCS) was inactivated by incubation for 20 min at 56 °C in a water bath. Unless stated otherwise, DMEM from PAA was used.

2.1.8 Software

Device/Application	Software
Licor	Odyssey 2.1 (LI-COR)
Image processing	Adobe Photoshop
	AxioVision (Zeiss)
	Image J
	LSM 510 META (Zeiss)
	Zen 2009 (Zeiss)
In silico modeling	I-Tasser server
Microarray data analysis	R/Bioconductor (www.bioconductor.org)
Orbitrap	Mascot (Matrix Science)
Phylogeny analysis	MacVector
Primer design	Primer3 0.4.0 (Rozen and Skaletsky, 2000)
qPCR	LightCycler® 480 SW 1.5 (Roche)
RP-HPLC	Unicorn 5.11 (GE)
RTCA DP Analyzer	RTCA Software 1.2.0.0909
Visualization of protein structures	Swiss-Pdb-Viewer
	(Guex and Peitsch, 1997)
	PyMOL (DeLano Scientific LLC)
Sequence alignments	MacVector 10.0.2

2.2 Buffers and solutions

Ampicillin stock solution	100 mg/ml	Ampicillin (1000x)
Buffer A (Mononucleosomes)	10 mM	HEPES (pH 7.9)
	10 mM	KCl
	1.5 mM	$MgCl_2$
	0.34 M	Sucrose
	10 %	Glycerol (v/v)
	1 mM	DTT
	Complete Protease Inhibitor Cocktail	
Buffer C (Mononucleosomes)	20 mM	HEPES (pH 7.9)
	20 %	Glycerol (v/v)
	0.2 mM	EDTA
	0.2 %	Triton X-100 (v/v)
	300 mM	KCl
	Complete Protease Inhibitor Cocktail	
Chloramphenicol stock solution	34 mg/ml	Chloramphenicol in ethanol (2000x)
Coomassie destaining solution	10 %	Glacial acetic acid (v/v)
	30 %	Methanol (v/v)
Coomassie staining solution	10 %	Glacial acetic acid (v/v)
	50 %	Methanol (v/v)
	0.1 %	Coomassie Brilliant Blue R (w/v)

6x DNA loading buffer	0.25 %	Bromophenol blue (w/v)
	0.25 %	Xylene Cyanol (w/v)
	30 %	Glycerol (v/v)
Ethidium bromide stock solution	10 mg/ml	Ethidium bromide (20000x)
Hypotonic lysis buffer	10 mM	Tris (pH 8.0)
	1 mM	KCl
	1.5 mM	$MgCl_2$
	Complete Protease Inhibitor Cocktail	
	1 mM	DTT
	0.4 mM	PMSF
Kanamycin stock solution	10 mg/ml	Kanamycin (1000x)
10x KCM buffer	1.2 M	KCl
	200 mM	NaCl
	100 mM	Tris (pH 8.0)
	5 mM	EDTA
5x Laemmli loading buffer	314 mM	Tris
	50 %	Glycerol (v/v)
	5 %	SDS (v/v)
	5 %	β-Mercaptoethanol (v/v)
	0.01 %	Bromophenol blue (w/v)
	adjust pH to 6.8 with HCl, store aliquots at -20 °C	
Laemmli running buffer	25 mM	Tris
	192 mM	Glycine
	0.1 %	SDS (w/v)
LB agar plates		LB medium
	1.5 %	Bacto agar (w/v)
LB medium	1.0 %	Tryptone (w/v)
	0.5 %	Yeast extract (w/v)
	1.0 %	NaCl (w/v)
Low-HEPES buffer	4 mM	HEPES (pH 7.9)
	10 mM	NaCl
No-salt buffer	3 mM	EDTA
	0.2 mM	EGTA
PBS buffer	140 mM	NaCl
	2.7 mM	KCl
	10 mM	Na_2HPO_4
	1.8 mM	KH_2PO_4
RBS buffer	10 mM	Tris (pH 7.5)
	10 mM	NaCl
	5 mM	$MgCl_2$
Separating gel	15 %	Acrylamide
	0.4 %	Bis-acrylamide
	363 mM	Tris (pH 8.8)
	0.1 %	SDS (w/v)
	0.1 %	TEMED (v/v)
	0.1 %	Ammonium persulfate (w/v)
Solvent A (HPLC)	0.1 %	TFA (v/v)

Solvent B (HPLC)	99.92 %	Acetonitrile (v/v)
	0.08 %	TFA (v/v)
Stacking gel	4 %	Acrylamide
	0.1 %	Bis-acrylamide
	125 mM	Tris (pH 6.6)
	0.1 %	SDS (w/v)
	0.1 %	TEMED (v/v)
	0.1 %	Ammonium persulfate (w/v)
TBE buffer	45 mM	Tris
	45 mM	Boric acid
	1 mM	EDTA
TBS buffer	32 mM	NaCl
	10 mM	Tris (pH 7.5)
Transfer buffer	48 mM	Tris
	39 mM	Glycine
	0.0375 %	SDS (w/v)
	20 %	Methanol (v/v)
Wash buffer (mononucleosomes)	20 mM	HEPES (pH 7.9)
	20 %	Glycerol (v/v)
	0.2 mM	EDTA
	0.2 %	Triton X-100
	300 mM	KCl
	Complete Protease Inhibitor Cocktail	

2.3 Cell biological methods

2.3.1 Cultivation and manipulation of mammalian cells

2.3.1.1 Cultivation of mammalian cells

All mammalian cell lines used in this work (see Tables 2.8 and 2.9) were kept in their respective media in a 37 °C incubator with a humidified atmosphere of 5 % CO_2. For details regarding media composition see Tables 2.8 and 2.9.

Cells were split every 2 to 3 days in a ratio between 1:2 and 1:8 depending on the doubling time of the cell line. Suspension cells (Raji): Cell suspension was partially discarded and replaced by fresh medium. Semi-adherent cells (HEK293): Cells were washed from the plate with the medium covering the cells, cell suspension was partially discarded and replaced by fresh medium. Adherent cells (fibroblasts, HeLa, osteosarcoma and neuroblastoma cells): Medium was removed, cells were washed once with sterile PBS and trypsin/EDTA-solution (1:8-diluted in sterile PBS) was added. Detached cells were resuspended in fresh growth medium, cell suspension partially discarded and replaced by fresh medium.

When harvesting cells for further experiments, cells were counted using a Casy cell counter, pelleted by gentle centrifugation (310 g, 10 min) and washed once with PBS.

For storage, cells were resuspended in FCS + 10 % DMSO, transferred to cryo vials and frozen at -80 °C. For long term storage, frozen vials were kept in liquid nitrogen. Cells in culture were replaced every 2 to 3 months. A fresh vial was thawed quickly in a 37 °C water bath, cells were pelleted by gentle centrifugation, DMSO containing FCS was removed and cells were cultured as usual.

2.3.1.2 Cultivation of U2OS cells under different stress conditions

In order to identify the factor and/or condition that triggers H3.X/Y expression in U2OS cells, different stress treatments were tested.

Starvation and Overgrowth (SO): $1 \cdot 10^6$ cells were seeded in a 10 cm plate with 7 ml medium. Cells were incubated over 8 days without splitting or replacement of medium.

Overgrowth: Cells were seeded identical to SO treatment and incubated over 8 days without splitting but with replacement of medium every day.

Starvation: $1.5 \cdot 10^6$ cells were seeded in a 15 cm plate with 12 ml medium. Cells were kept at 40-60 % confluency by splitting, however, old medium was added back to the cells afterwards.

UV-treatment: Normally grown cells were treated with 25000 µJ/cm^2, 50000 µJ/cm^2 or 100000 µJ/cm^2 UV light using a Stratalinker 1800 followed by 3 h incubation at 37 °C.

Amino acid depletion: Normally grown cells were incubated for up to 9 h in Krebs-Ringer Bicarbonate Buffer, a medium lacking amino acids.

Serum depletion: Normally grown cells were incubated for up to 12 h in DMEM containing 0.1 %, 0.5 %, 1 %, 1.5 %, 2 % or 10 % FCS.

2.3.1.3 Establishment of stably transfected human cell lines

Cells were seeded in 6-well plates 24 h prior to transfection to reach a confluency of 80-90 %. 1 µg plasmid DNA was diluted with Opti-MEM to a final volume of 100 µl, 3 µl FuGENE HD reagent were added and the transfection complex was allowed to form over 15 min at room temperature (RT). The complex was added drop-wise to the cells while shaking the plate. After 24 h incubation at 37 °C, medium was exchanged by selection medium (DMEM + 10% FCS + 1% P/S + 600 µg/ml G418-sulfate) to select for stable cell lines. Selection was carried out until cells in non-transfected control wells had died. Stable cell lines were grown in medium supplemented with 400 µg/ml G418-sulfate.

2.3.1.4 mRNA knockdown using small interfering RNAs (siRNAs)

HeLa, HeLa HA-H3.X, HeLa HA-H3.Y and U2OS cells were transfected with siRNAs to specifically reduce H3.X and/or H3.Y mRNA levels (for siRNA sequences see Table A.3). Transfections were performed using Oligofectamine transfection reagent according to the manufacturer's instructions. In brief: Cells were seeded 24 h prior to transfection for a confluency of 30 %. Plate size was chosen depending on the number of cells needed for subsequent analyses (for volumes used for different plates, see table below). For solution (A), Oligofectamine was diluted in Opti-MEM. For solution (B), siRNA stock solution (100 µM in 1x Universal Buffer) was first diluted 1:5 in sterile MilliQ-water and then further 1:8.5 in Opti-MEM. After 5 min incubation at RT, solutions (A) and (B) were mixed and the transfection complex was allowed to form over another 20 min period at RT. Cells were washed twice with sterile PBS, growth medium was replaced by DMEM (Invitrogen) not supplemented with serum or antibiotics and the transfection complex was added. After 5 h incubation at 37 °C, DMEM (Invitrogen) supplemented with 30 % FCS but without antibiotics was added. The next day, medium was replaced with normal growth medium (Invitrogen). Cells were harvested 4 days after transfection. As U2OS cells are difficult to transfect, a double-knockdown on two consecutive days was performed. Cells were harvested 4 days after the first transfection.

	Solution (A)		**Solution (B)**		**Medium**	
Plate	Oligofectamine	Opti-MEM	siRNA(20 µM)	Opti-MEM	DMEM	DMEM + 30 % FCS
12-well	3 µl	7 µl	5 µl	85 µl	400 µl	250 µl
6-well	4 µl	11 µl	10 µl	75 µl	800 µl	500 µl
10 cm	20 µl	55 µl	50 µl	375 µl	5 ml	2.5 ml

2.3.2 Proliferation analysis of adherent human cells

Proliferation capacity of adherent human cells was analyzed using two different methods: **CASY Counter:** $2 \cdot 10^5$ cells were seeded in 6-well plates (3 wells per cell line and condition) and either transfected with siRNAs the following day or used directly for analysis of proliferation capacity. Cells were trypsinized and counted every day using the CASY Counter, cell number was adjusted to keep a confluency of 50-70 % and mean of cell count in 3 wells was plotted.

RTCA DP Analyzer equipped with 16-well E-plates: Baseline was set using 100 µl medium (Invitrogen) per well, 4500 cells in 50 µl medium were added (4 wells for each cell line and experimental condition) and measurement was started after 30 min incubation at RT during which cells sink to the bottom of the well and start to adhere. Impedance was measured every 15 min over 96 h, providing quantitative information about the biological status of the

cells, including cell number, viability, and morphology. Growth medium was replaced every day. If siRNA-treated cells were analyzed, cells were seeded one day after the last siRNA transfection.

2.3.3 Antibody generation and specificity testing

The antibody against H3.X and H3.Y (αH3.X/Y) was generated by our collaborator Elisabeth Kremmer using a peptide spanning amino acids 9 to 20 of histone H3.X and H3.Y (KATAWQAPRKLP, Peptide Specialty Laboratories GmbH). The peptide was coupled to BSA and ovalbumin (OVA), respectively, and rats were immunized subcutaneously and intraperitoneally with a mixture of 50 µg peptide-OVA, 5 nmol CPG oligonucleotide (Tib Molbiol), 500 µl PBS and 500 µl *incomplete Freund's* adjuvant. Six weeks later, a boost without adjuvant was given. Fusion was performed according to standard procedures (Köhler and Milstein, 1975). Supernatants were tested by differential enzyme-linked immunosorbent assay (ELISA) with the histone peptide and an irrelevant peptide, both coupled to BSA. Monoclonal antibodies reacting specifically with the peptide were further analysed in Western blot and immunofluorescence (IF) microscopy. αH3.X/Y clone 8H6-2111 of rat IgG2a subclass was deployed in this study.
αH3.X/Y specificity was analyzed by peptide competition assay with subsequent IF analysis (see section 2.3.4). Prior addition to the cells, the antibody (diluted in blocking solution) was incubated for 4 h at 4 °C with the following peptides (1 µg/ml): biotin-coupled H3.3 unmodified (aa 22 - 41) and H3.X/Y unmodified (aa 9 - 20). Samples were analyzed on an Axiovert 200M microscope.

2.3.4 Immunofluorescence (IF) microscopy

Adherent mammalian cells were grown and stained on 12 mm cover slips in 24-well plates. In brief, cells were washed with PBS, fixed for 15 min in 1 % formaldehyde-PBS, permeabilized in PBS-T (PBS + 0.1 % Triton X-100) and blocked for 20 min in PBS-T + 1 % BSA. Samples were incubated stepwise with primary and secondary antibody (diluted in blocking solution) for 30 min with three consecutive 5 min PBS-T washes. For details about antibodies and dilutions see sections 2.1.4.1 and 2.1.4.2. DNA was stained for 5 min with 10 ng/ml 4',6-diamidino-2-phenylindole (DAPI) in PBS and mounted with ProLong Antifade Kit. Samples were analyzed using an Axiovert 200M microscope.
To determine percentage of cells with general nuclear αH3.X/Y staining, positive cells were

counted and representative pictures of the sample, showing the cell density on the cover slip, were taken. Percentage of positive cells was calculated by dividing the number of positive cells by the average cell number per picture multiplied with the number of pictures per cover slip.
For analysis on a LSM 510 META confocal microscope, DNA was counter stained using To-Pro3 and samples were mounted using Vectashield mounting medium.
Samples for 3D-SIM analysis were prepared on precision cover glass #1.5 (0.170±0.005 mm thick; Roth) and embedded in Vectashield mounting medium. Sample preparation and analysis on an OMX DeltaVision prototype was performed by our collaborator Lothar Schermelleh (Advanced Cell Imaging Unit, LMU Munich).

2.3.5 Metaphase chromosome spreads

Metaphase chromosome spreads of adherent human cells were generated as previously described (Hake et al., 2005). In short, cells were arrested in mitosis by a 15-16 h treatment with nocodazole (transfected HeLa cells: 200 ng/ml; U2OS cells: 1 µg/ml), harvested by mitotic shake-off, lysed by incubation in RBS buffer and spread on microscope slides by centrifugation in a Shandon Cytospin 4. Cells were fixed in 2 % formaldehyde in PBS and washed with KCM-Tween (1xKCM + 0.1 % Tween 20). Chromosomes were extracted with KCM-Tween + 0.1 % Triton X-100, washed with KCM-Tween and KCM-Tween-BSA (KCM-Tween + 0.25 % BSA), blocked in KCM-Tween + 2.5 % BSA and incubated with primary antibody in blocking solution overnight (ON) at 4°C. After washing with KCM-Tween-BSA, chromosomes were incubated with secondary antibody in blocking solution for 1-2 h at RT and washed with KCM-Tween and PBS + 0.1 % Tween 20. DNA was stained with 10 ng/ml DAPI for 5 min, samples were washed with PBS and mounted with Vectashield mounting medium. Except for washes, microscope slides were incubated in an opaque wet chamber. Analysis was carried out with a personalDV widefield epifluorescence microscope followed by a deconvolution procedure.

2.3.6 Fluorescence recovery after photobleaching (FRAP)

FRAP analyses were performed by our collaborator Lothar Schermelleh (Advanced Cell Imaging Unit, LMU Munich). HeLa Kyoto cells were transiently transfected with GFP-tagged histone H3 constructs (see section 2.1.5). After 24 h, cells were seeded in Lab-Tek chamber slides and incubated several hours or ON before performing FRAP experiments. FRAP rates

were determined using an UltraVIEW VoX spinning disc microscope with integrated FRAP PhotoKinesis accessory assembled to an Axio Observer D1 inverted stand (Zeiss). The microscope's heated environmental chamber was set to 37 °C and 5 % CO_2 perfusion. Several square bleach regions with a size of 5 x 5 µm were positioned on selected cell nuclei within the field of view. Photobleaching was performed using two iterations with the Acousto Optic Tunable Filter (AOTF) of the 488 nm and the 514 nm laser line set to 100 % transmission. To determine long-term recovery kinetics, 3D image stacks of 8 µm height and a z-distance between image planes of 1 µm were recorded with an initial speed of 1 f/min for the first 10 frames, followed by intervals of 10 min. Using ImageJ, raw data were corrected for lateral and rotational movements of the nucleus, differences in background and gain or loss of total fluorescence during postbleach acquisition, potentially caused by newly synthesized GFP-histones, bleaching-by-acquisition and flux of residual fluorescence from above and below the recorded optical plane. To correct for cell-to-cell differences in bleaching depth, the data were normalized to zero by subtracting the first postbleach value from all mean fluorescence values.

2.3.7 Immunohistochemistry (IH) microscopy

Commercially available human tissue sections were stained in an opaque wet chamber at RT unless stated otherwise. Frozen sections were thawed and blocked in PBS + 0.5 % Triton X-100 + 0.5 % BSA for 30 min. Samples were incubated with primary antibody in blocking solution ON at 4 °C followed by three 10 min PBS-washes. Incubation with secondary antibody in blocking solution was carried out for 2h followed by three 10 min PBS-washes. To enhance H3.X/Y signals, biotin-coupled secondary αrat antibody was used followed by a 2 h incubation with streptavidin coupled to an Alexa 555 fluorophor diluted in PBS. DNA was counter stained for 5 min with 1 µg/ml DAPI in PBS and samples were mounted using Aqua-Poly/Mount. Analysis was carried out on a LSM 710 confocal microscope.

2.4 Molecular biological methods

2.4.1 Agarose gel electrophoresis

DNA fragments were separated using 1 % agarose gels prepared with TBE buffer. To visualize DNA fragments, ethidium bromide was added to the gel at a final concentration of 0.5 µg/ml.

2.4.2 RNA extraction of mammalian cells

Total RNA from 1-2 $\cdot 10^6$ cells was extracted using the RNeasy Kit following the manufacturer's instructions, including removal of genomic DNA contaminations. RNA concentration and purity was determined using a Nanodrop ND1000 spectrophotometer, RNA was stored at -80 °C.

2.4.3 RNA expression profiling

Microarry hybridization was performed by Dietmar Martin and Kerstin Maier of the Gene Center Affymetrix Microarray Platform (Cramer Laboratory, LMU Munich). Bioinformatical analysis was carried out by Tobias Straub (Becker Laboratory, LMU Munich). Concentration and quality of total RNA preparations (see section 2.4.2) were evaluated using the RNA 6000 Nano Kit and the 2100 Bioanalyzer. 100 ng of RNA were further purified with the RNeasy MinElute Cleanup Kit and RNA amplification, labeling and hybridization to Human Gene 1.0 ST Arrays were performed according to the manufacturer's instructions. Raw microarray data were processed in R/Bioconductor as follows: gene-based expression values were calculated using the Robust Multichip Average (RMA) method as part of the 'oligo' package. For downstream analyses, genes with a log2 expression value of at least 4 in at least one of the treatment conditions were used. Differential expression estimation was based on a moderated t statistic ('limma' package) with subsequent calculation of the local false discovery rate (lfdr, 'locfdr' package). Genes were classified as responders by a lfdr cutoff of 0.2. Gene ontology enrichment analysis was performed using a hypergeometric distribution test and subsequent Bonferroni correction as supplied by the GOHyperGALL script (http://faculty.ucr.edu/~tgirke/Documents/R_BioCond/My_R_Scripts/GOHyperGAll.txt). Term redundancy was reduced by applying the GOHyperGAll_Simplfy function with a p-value cutoff of 0.001. The microarray data for siRNA transfected U2OS cells has been deposited at GEO (www.ncbi.nlm.nih.gov/geo) under the accession number GSE22415.

2.4.4 cDNA synthesis

cDNA was first synthesized using the ProtoScript First Strand cDNA Synthesis Kit and later the ProtoScript M-MuLV Taq RT-PCR Kit due to discontinuation of the first product. cDNA was transcribed from 1 µg of total RNA (see section 2.4.2) per reaction, following the instructions given in the protocol using random primers. Samples without reverse transcriptase (no

RevT) were processed in parallel to control for genomic DNA contamination. PCR amplification of a GAPDH-mRNA fragment with Taq polymerase and subsequent analysis on an agarose gel was taken as a readout for successful cDNA synthesis (for primer sequences see Table A.1).

2.4.5 Quantification of mRNA levels with quantitative PCR (qPCR)

mRNA levels of genes of interest were quantified relative to mRNA levels of stably expressed reference genes with qPCR using a LightCycler 480 II equipped with a 384-well block. Primer pairs were designed using Primer3 software (Rozen and Skaletsky, 2000), qPCR primers are listed in Table A.1. Samples were analyzed in technical triplicates for each primer pair with a total volume of 15 µl per well. For each reaction 0.75 µl cDNA (see section 2.4.4) were diluted to 5 µl with PCR-grade water and distributed to different wells using a multistep pipet and 0.1 ml combitips. In a second step 7.5 µl LightCycler 480 SYBR Green I Master mix (2x) were mixed with primers and PCR-grade water to a volume of 10 µl with each primer in a concentration of 0.44 µM. SYBR/primer mix was distributed to different wells using a multistep pipet and 0.2 ml combitips. Plate was sealed with adhesive foil, centrifuged for 2 min at 3000 g and qPCR was performed with temperature profile summarized below. Experiments were analyzed using the advanced relative quantification tool of LightCycler 480 SW 1.5 software, factoring in differences in primer efficiency (see below) and calculating mRNA levels relative to a combination of two reference genes (*HPRT1* and *HMBS*). Samples with no RevT cDNA (see section 2.4.4) were used to quantify background levels caused by genomic DNA contamination.

Primer pairs were tested for specificity and efficiency by using non template controls, melting curves and dilution series of cDNA. To calculate primer efficiencies and determine primer specific detection threshold, a dilution series of cDNA, generated from a mix of HeLa HA-H3.X and -H3.Y cells, was used. Standard curves were analyzed using the advanced absolute quantification tool of LightCycler 480 SW 1.5 software.

	Pre-Incubation	5 min	95 °C
45x	Amplification	10 s	95 °C
		10 s	60 °C
		10 s	72 °C
	Melting Curve	5 s	95 °C
		1 min	65 °C
		2.5 °C/min	97 °C

2.4.6 Cloning of mammalian H3 variants

Histone H3 variants were amplified from human cDNA (see section 2.4.4) using gene specific primers flanked by restriction endonuclease recognition sites (for primer sequences see Table A.2) and Phusion DNA polymerase. PCR-products were subcloned with EcoRV in pT7Blue-3 vector, leading to a disruption of the *LacZ* gene, thereby enabling selection of positive clones over blue/white screening. Subcloning reaction was transformed in chemically competent *E. coli* (XL1 Blue or DH5α) with a heat shock of 45 s at 42 °C. After 1 h incubation in LB medium at 37 °C, cells were plated on LB agar plates containing the respective antibiotic (ampicillin 100 µg/ml or kanamycin 10 µg/ml). Plasmid DNA was isolated using a miniprep kit. H3 variant cDNA was excised with the respective restriction endonucleases, fragments were gel purified using a gel extraction kit and ligated with the vector backbone which has been cut and purified in the same way. Ligation reaction was transformed in chemically competent XL1 Blue or DH5α as described above. Cloning success was verified by sequencing (Eurofins MWG Operon) of isolated and purified plasmids.

2.4.7 Site directed mutagenesis of H3.Y

To perform RNAi rescue experiments, siRNA target regions in H3.Y (as part of pIRESneo3 HA) were mutated without changing the amino acid sequence. Mutagenesis was performed using Pfu DNA polymerase, following the manual for the Stratagene (Agilent) site-directed mutagenesis kit. Briefly, pIRESneo3 HA-H3.Y was amplified using primers carrying the desired mutation (see Table A.2), template plasmid was digested with DpnI and PCR-reaction was transformed in chemically competent *E. coli*. Plasmid DNA was isolated with a miniprep kit, sequenced and used to establish stable cell lines (see section 2.3.1.3).

2.4.8 Expression of human histone proteins in *E. coli*

E. coli expression strain BL21-CodonPlus (DE3)-RIL was transformed with pET-21a(+) H3.X and H3.Y plasmids as descibed in section 2.4.6. Transformed *E. coli* were grown in LB medium supplemented with kanamycin (10 µg/ml) and chloramphenicol (17 µg/ml). Expression was induced in an exponentially growing culture for 3 h at 37 °C by adding IPTG to a final concentration of 0.1 mM. Cells were harvested and boiled for 10 min at 95 °C in 1x Laemmli loading buffer. Cell debris was removed by centrifugation and supernatant was used for Western blot analysis.

2.5 Biochemical methods

2.5.1 Histone extraction from mammalian cells

Histones were acid extracted as previously described (Shechter et al., 2007). In short, nuclei were isolated using hypotonic lysis buffer and extracted with 0.4 M sulfuric acid. Histones were precipitated with 100 % trichloroacetic acid and resuspended in water.

2.5.2 Reversed phase-high performance liquid chromatography (RP-HPLC) of mammalian histones

Acid extracted histones (see section 2.5.1) from U2OS, HEK293 and NIH3T3 were separated on an Ettan microLC over a C4 column (250 x 4.6 mm Jupiter 10 µm 300 Å) using a linear gradient from 35 % to 53 % solvent B with a flow of 1.0 ml/min over 30 min. Fractions of 200 µl were collected, vacuum dried and stored at -20 °C. Fractions containing H3.X and/or H3.Y protein were identified using Western blotting (see section 2.5.8) and analyzed using mass spectrometry (see section 2.5.3).

2.5.3 Mass spectrometrical analysis of HPLC-purified mammalian histones

Mass spectrometrical analysis was performed by our collaborator Lars Israel (LMU Munich, Protein Analysis Unit). In brief, RP-HPLC fractions containing H3.X and/or H3.Y (see section 2.5.2) were resolved in 0.1 M ammonium bicarbonate and treated with propionic anhydride to convert free amino groups of lysine residues to propionic amides, thereby preventing digestion after lysines. Proteolytic digestion with sequencing grade trypsin (Promega) was carried out ON at 37 °C and samples were directly loaded onto a nano-ESI-LC-MS/MS for protein identification. The resulting data where analyzed via Mascot software using a home-made database containing the diverse H3 sequences. Fragment spectra were also interpreted manually.

2.5.4 Mononucleosome immunoprecipitation (IP)

Mononucleosome IP was performed by Clemens Bönisch, PhD student in the Hake group. Mononucleosomes were generated, with some changes, as previously described (Wysocka et al., 2001). All centrifugation steps prior to Micrococcal Nuclease (MNase) treament were performed at 3200 g at 4 °C. Briefly, aliquots of $2 \cdot 10^7$ cells were lysed in buffer A + 0.1 % NP-40,

washed with buffer A and and incubated in buffer B. Mononucleosomes were generated by digestion of chromatin with 0.25 U MNase for 15 min at 37 °C in buffer A + 1 mM $CaCl_2$ and stopped by addition of EGTA (final concentration 2 mM). Un-digested material was removed by centrifugation (20000 g for 20 min), supernatants of five MNase digests were combined and salt concentration was adjusted to 150 mM KCl. Monoclonal mouse αHA was immobilized on magnetic beads (sheep αmouse IgG) and IP was performed ON. Beads were washed four times with buffer C and bound mononucleosomes were eluted with 100 mM glycine (pH 2.8). One part of these beads was used to isolate DNA with phenol/chloroform extraction using MaXtract High Density columns followed by sodium acetate/ethanol precipitation. DNA size and quality was evaluated using the DNA 1000 kit with the 2100 Bioanalyzer. From the rest of the beads, bound proteins were eluted by boiling in SDS sample buffer and subsequently analyzed by Western blotting using Licor detection (see section 2.5.8) and silver staining (see section 2.5.7).

2.5.5 SDS polyacrylamide gel electrophoresis (SDS-PAGE)

Proteins were separated using 15 % separating polyacrylamide gels covered by stacking gels using disposable cassettes and 10-, 12- or 15-well combs. Gels were run at 100 V until prestained size marker (peqGOLD Protein Marker IV or V) started to separate. Run was continued at 180 V until loading dye reached end of the gel. Subsequently, gels were stained with Coomassie Blue (see section 2.5.6) or silver nitrate (see section 2.5.7) or used for Western blotting (see section 2.5.8).

2.5.6 Coomassie staining of polyacrylamide gels

Polyacrylamide gels (see section 2.5.5) were incubated for 1 h in Coomassie staining solution, followed by incubation in Coomassie destaining solution until background staining was reduced enough for protein bands to become visible.

2.5.7 Silver staining of polyacrylamide gels

Polyacrylamide gels (see section 2.5.5) were fixed in 40 % ethanol (v/v) + 10 % glacial acid (v/v) ON or used directly after Coomassie staining (see section 2.5.6). Gels were washed in 50 % methanol and water for 10 min, respectively, followed by a 1 min incubation in 0.02 % sodium thiosulfate (w/v) and two 1 min washing steps in water. To stain protein bands,

gels were incubated in 0.1 % silver nitrate (w/v) for 20 min, rinsed twice with water (1 min each) and developed in 0.04 % formaldehyde (v/v) in 2 % sodium carbonate (w/v) with vigorous shaking. To terminate development when protein bands become visible, formaldehyde / sodium carbonate solution was discarded and replaced by 1 % acetic acid.

2.5.8 Western blotting

Polyacrylamide gels were blotted on PVDF (ECL detection) or nitrcellulose (Licor detection) membranes using a semi-dry blotting machine. Gel and membrane were equilibrated for 10 min in transfer buffer (PVDF membrane was activated in methanol for 30 s prior to equilibration) and blot was assembled by stacking two 3 mm Whatman papers soaked in transfer buffer, membrane, gel, and two more soaked 3 mm Whatman papers. Air bubbles were removed and proteins were transferred to the membrane over 1 h with 200 mA. Membrane was stained with Ponceau S solution and scanned to monitor protein loading. Membrane was blocked for 1 h in TBS + 0.1 % Tween 20 (TBS-T) + 5 % milk powder (TBS-T milk, ECL detection) or TBS + 5 % milk powder (Licor detection) and incubated ON at 4 °C with primary antibody diluted in TBS-T milk (for dilutions see section 2.1.4.1). Membrane was washed three times with TBS-T, incubated for 1 h at RT (Licor detection: light protected) with secondary antibody diluted in TBS-T milk (for dilutions see section 2.1.4.2) and washed again three times with TBS-T. Membrane was either covered with ECL detection reagent, followed by film exposure and development or scanned with the Licor machine.

2.6 Bioinformatics

2.6.1 Phylogenetic analysis of histone variants

The phylogenetic tree depicted in Fig. 3.2 was generated using coding nucleotide sequences of different histone variants from human (Hs), chimpanzee (Pt) and macaque (Mm). Sequences were aligned using ClustalW Alignment (MacVector 10.0.2) and evolutionary relationships were determined using the neighborjoining tree-building method based on Kimura 2-parameter with Gamma correction off.
Changes in program parameters and/or inclusion of 3' UTRs as well as analysis of 3' UTRs alone led to virtually the same result. The only difference was that H3.X and H3.Y were either closer to H3.3A or H3.3B.

2.6.2 *In silico* modeling of novel histone variants

To generate homology models for H3.X and H3.Y proteins, the I-TASSER server (Zhang, 2008) was used. It provides a combination of threading, assembly and refinement to generate 3D-models. As template, the server automatically chose for both novel variants chain A (histone H3.2) of pdb-file 1kx5. This structure resembles a nucleosome consisting of 147 bp of *Homo sapiens* DNA wrapped around *Xenopus laevis* histones (Davey et al., 2002). The model for H3.X had a C-score of 0.07, the model for H3.Y a C-score of 1.50. In both cases, C-score for the second best model was considerably lower. Data-sets of the models were downloaded and visualized using Swiss-Pdb-Viewer and PyMOL.

3 Results

3.1 Identification of novel histone H3 variant genes

Searching the NCBI database with the nucleotide sequence of human histone *H3.1f* (HIST1H3I; NM_003533), two putative histone H3 variant genes have been found, now termed *H3.X* (LOC340096) and *H3.Y* (LOC391769) (Fig. A.1, Appendix). Both genes were initially annotated as pseudogenes, are located on human chromosome 5 (5p15.1) and do not contain introns. Their sequence around the translation initiation start site matches the consensus for vertebrates (GCCGCCACC**AUG**GCG) (Kozak, 1991; Nakagawa et al., 2008), and depending on the search program used (polyadq or PolyA_SVM program), *H3.X* and *H3.Y* 3'-genomic sequences are predicted to include a conserved poly(A) site (Cheng et al., 2006; Tabaska and Zhang, 1999).

H3.X and *H3.Y* genes are predicted to encode for highly similar proteins of 146 and 135 amino acids, respectively, with only four amino acids difference in their overlapping region (89.7% identity) (Fig. 3.1). H3.X has an additional unusual C-terminal tail with no sequence homology to other proteins. Both putative proteins display interesting sequence differences compared to H3.1, H3.2 and H3.3, thereby generating potential new PTM sites or eliminating amino acids known to be posttranslationally modified. One example is the replacement of serine 10 and 28, phosphorylated during mitosis (Hendzel et al., 1997) and immediate-early gene induction (Clayton and Mahadevan, 2003), by alanine and arginine, respectively. In addition to these single amino acid changes, also complete stretches appear to be altered. The most prominently changed regions include the sequence surrounding lysine 14, usually acetylated and found in actively transcribed genes (Yan and Boyd, 2006), and the region around lysine 79, which is found to be methylated in transcriptionally active regions (Im et al., 2003) and upon DNA damage (Huyen et al., 2004) (Fig. 3.1). The sequence from amino acid 87 to 90 is important for the chaperone-dependent chromatin incorporation of histone variants (Ahmad and Henikoff, 2002). CAF-1 deposits H3.1, whereas HIRA and the Daxx-ATRX complex catalyze the incorporation of H3.3 (Tagami et al., 2004; Drané et al., 2010; Lewis et al., 2010). H3.X and H3.Y amino acids in this region are identical to H3.3 (Fig. 3.1), leading

to the hypothesis that these putative novel variants might be incorporated by HIRA and/or Daxx-ATRX in a replication-independent manner.

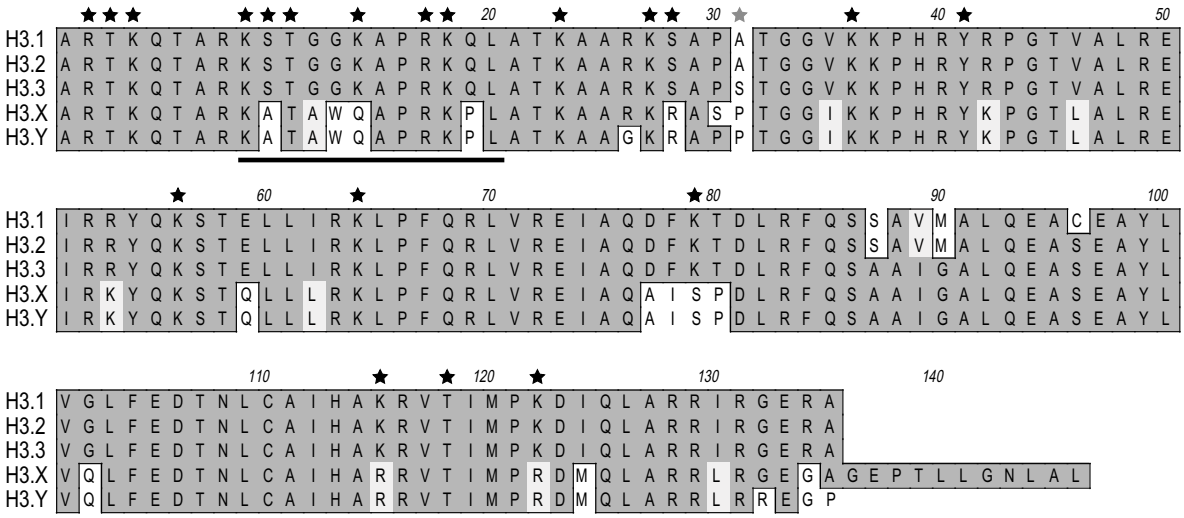

Figure 3.1. Amino acid sequence alignment of human histone H3 variants.
Protein sequences of known human histone variants H3.1, H3.2 and H3.3 are aligned with those of novel histone variants H3.X and H3.Y. Sequence similarity is encoded by background color: identical aa = dark gray, similar aa = light gray, different aa = white. Black stars indicate described PTMs on known H3 variants, gray star indicates H3.3 variant specific PTM. Black bar marks peptide sequence used for generation of αH3.X/Y antibody.

To shed light on the evolutionary origin of these novel variants, further database searches with H3.X and H3.Y protein sequences were performed, leading to the identification of highly similar genes in the chimpanzee (*Pan troglodytes:* LOC471464 (*H3.X*) and LOC471473 (*H3.Y*)) and the macaque (*Macaca mulatta:* LOC718189 (*H3.X*) and LOC718280 (*H3.Y*)) but not in any other mammalian genome. Predicted H3.X and H3.Y protein sequences of different primates are almost identical with only few single amino acid changes (Fig. A.2, Appendix). The most striking difference is the premature stop codon in the macaque H3.X, resulting in a truncated protein with the size of H3.Y. Interestingly, following nucleotides would code for the unique H3.X C-terminus.

H3.X and *H3.Y* genes are located on different chromosomes in the primates analyzed (*Pan troglodytes*: chromosome 5, *Macaca mulatta*: chromosome 6), but the region containing both loci is in all cases flanked by the *CDH18* and the *BASP1* gene. These two genes can also be found on one chromosome in the mouse and rat genome, however, the distance between them is much shorter. Together, these data give rise to the hypothesis that *H3.X* and *H3.Y* loci originate from gene duplications in evolutionary younger terms and constitute primate-specific histone variants. To determine which gene was the origin of this duplication, the phylogenetic tree for the coding nucleotide sequences of human, chimpanzee and macaque *H3.X* and *H3.Y*

together with a variety of other human histone variants was calculated (Fig. 3.2). Clearly visible in this analysis, *H3.X* and *H3.Y* most likely originate from a gene duplication of one of the *H3.3* genes. However, whether the source was *H3.3A* or *H3.3B* cannot be answered with certainty as depending on the sequence used for generating the tree (including or excluding 3'UTR, coding or non-coding sequences), *H3.X* and *H3.Y* appear to be closer to the one or the other (data not shown). In contrast to the human and chimpanzee sequences, macaque *H3.X* and *H3.Y* sequences are more similar to each other than to the respective gene in other species, which might be due to the premature stop-codon in the macaque *H3.X* sequence (Fig. 3.2 and Fig. A.2, Appendix).
In summary, two novel histone H3 variant genes could be identified, termed *H3.X* and *H3.Y*, which seem to be specific for the primate lineage.

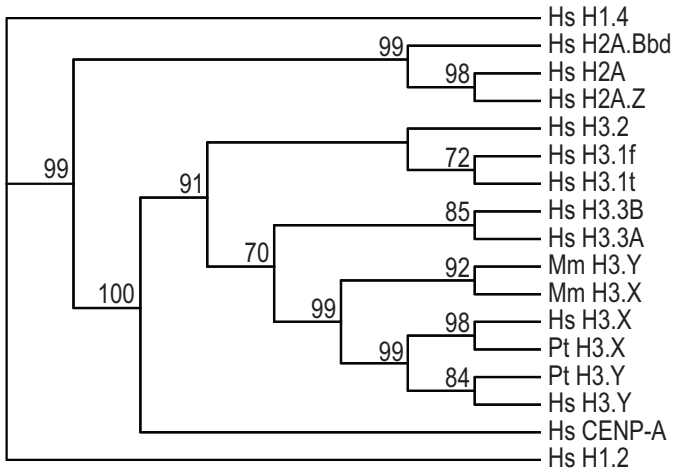

Figure 3.2. Phylogenetic tree of H3.X and H3.Y from different species.
Comparison of coding nucleotide sequences of H3.X and H3.Y from different primates with other human histone variants, reveals greater similarity of both variants to H3.3 than to any other variant. Hs = *Homo sapiens*, Pt = *Pan troglodytes*, Mm = *Macaca mulatta*; numbers indicate bootstrap probabilities.

3.2 Endogenous *H3.X* and *H3.Y* expression in human cell lines and tissues

To asses if *H3.X* and *H3.Y* are pseudogenes or indeed novel H3 variants, the first step was to analyze their mRNA expression levels in different human cell lines by quantitative PCR (qPCR). One primer pair detecting both variants and one primer pair specifically targeting the unique 3' sequence of H3.X was chosen because of the high sequence similarity between *H3.X* and *H3.Y* (Fig. A.1, Appendix). Both variants are transcribed at low levels in the human osteosarcoma cell line U2OS (Fig. 3.3A). Minimal amounts of H3.Y could be detected

in HEK293 cells, whereas no expression was observed in HeLa cells. As negative control, mouse NIH3T3 cells were used, showing no expression of H3.X or H3.Y (Fig. 3.3A). In U2OS cells, H3.Y is stronger expressed than H3.X but absolute expression levels are still very low, namely ∼16-fold lower than CENP-A (Fig. 3.3B). These data suggest that *H3.X* and *H3.Y* genes are transcribed in some human cell lines, albeit at low total levels.

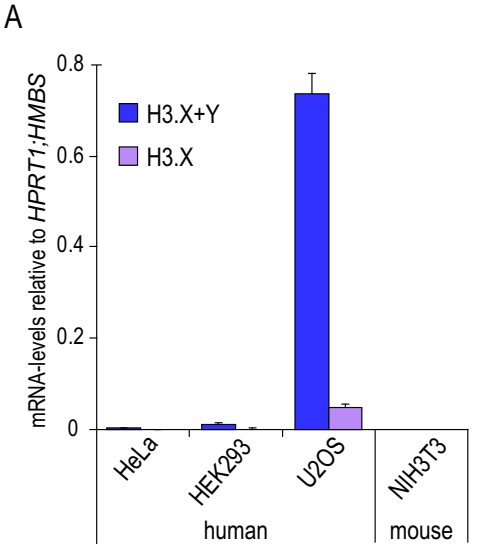

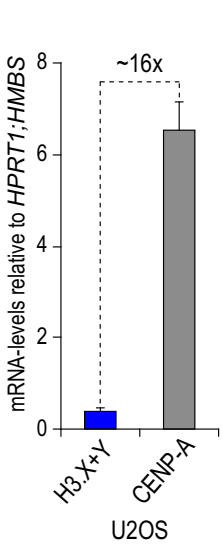

C

Tissue	No. of samples	expression of H3.X+Y	expression of H3.X
Bone tumor	1	+	-
Breast normal	1	-	-
Breast tumor	2	+ (1/2)	-
Lung normal	1	-	-
Lung tumor	2	+ (2/2)	-
Ovary tumor	1	+	-
Thyroid tumor	1	-	-
Testis normal	1	+	+
Total fetal brain	1	+	+
Cerebral cortex	1	+	+
Cerebellum	1	+	+
Thalamus	1	-	-
Hippocampus	1	+	+

Figure 3.3. H3.X/Y mRNA levels in different cell lines and human tissues.
(A) qPCR analysis of endogenous H3.X/Y levels with cDNA from different human and mouse cell lines shows expression of H3.Y and to a lesser extent H3.X in U2OS cells. Primer pairs amplifying H3.X and H3.Y (H3.X+Y, blue) or H3.X alone (purple) were used, levels are depicted relative to HPRT1 and HMBS. Error bars represent SEM of two independent biological experiments. Mouse NIH3T3 cells were used as negative control showing no H3.X/Y expression. (B) qPCR comparison of endogenous H3.X/Y and CENP-A levels with cDNA from U2OS cells, reveals approximately 16-fold higher expression of the latter. Primer pairs amplifying H3.X and H3.Y (H3.X+Y, blue) or CENP-A (gray) were used, levels are depicted relative to HPRT1 and HMBS. Error bars represent SEM of two independent biological experiments. (C) cDNA prepared from commercially available total RNA from different normal and malignant human tissues was analyzed by qPCR for H3.X/Y expression. Tissues positive for H3.X+Y- and H3.X-expression are marked with a "+", numbers of positive samples are indicated in brackets. Controls generated without reverse transcription were used to assess amplification threshold.

Encouraged by the finding that *H3.X* and *H3.Y* are expressed in U2OS cells, the next step was to analyze primary cells as part of human tissues by qPCR. The initial idea was to take malignant tissues as U2OS cells are derived from a moderately differentiated sarcoma of the tibia. In addition, normal tissues for comparison and samples from different brain regions as well as testis were chosen because of the primate-specific appearance of H3.X and H3.Y. H3.X/Y levels were quantified with cDNA, synthesized using commercially available total RNA from the tissues listed (Fig. 3.3C). Interestingly, low but significant expression of H3.X/Y mRNA could be detected in some bone, breast, lung and ovary tumors. In RNA from human brain areas and testis, H3.X/Y expression was observed in all samples except

for the thalamus. In contrast to all other tissues tested, also H3.X mRNA was present in these brain and testis samples (Fig. 3.3C). In conclusion, mRNAs of novel primate-specific H3 variants H3.X and H3.Y are not only present in human cell lines, but are also in primary cells from different human organs.

3.3 Localization, nucleosome structure and chromatin incorporation of novel tagged H3 variants

To gain insight into the structural features and *in vivo* behavior of H3.X and H3.Y proteins, the coding sequences of H3.X and H3.Y were cloned from human cDNA and HeLa cells, constitutively expressing these with an N-terminal HA-tag, were established. For comparison, HeLa cells, constitutively expressing HA-tagged versions of H3.1, H3.2 and H3.3 (here referred to as "known H3 variants") were used. Confocal imaging of these cells shows solely nuclear localization of all histone H3 variants (Fig. 3.4A). Detection of HA signals in mitotic cells, co-localizing with mitotic chromosomes, points towards chromatin incorporation of all tagged H3 variants analyzed. To further address this point, the same cell lines were used to prepare metaphase chromosome spreads. Immunofluorescence (IF) microscopic analysis of αHA and DAPI stained spreads shows stable chromatin association of all tagged H3 variants and a distinct localization pattern of individual variants (Fig. 3.4B).
Since H3.X and H3.Y seem to behave like the known H3 variants regarding their localization and chromatin association, we were wondering if the sequence differences between novel and known H3 variants have any influence on protein structure, finally leading to an altered nucleosome structure and stability. In collaboration with Rainer Merkl from the University of Regensburg, homology models based on the crystal structure of *Xenopus laevis* H3.2 (Davey et al., 2002) have been calculated. Overlays of predicted H3.X and H3.Y structures with H3.2 crystal structure show no major changes in secondary or tertiary structure elements (Fig. 3.5A). Interestingly, the extra C-terminus of H3.X is proposed to fold into an additional α-helix. Exchange of both H3.2 chains in the crystal structure of the nucleosome by H3.X or H3.Y homology models does not result in any sterical clashes with the other histone chains. Surprisingly, the additional α-helix of the H3.X protein would fit perfectly in the free space in the middle of the nucleosome, close to the acidic patch of H2A (Fig. 3.5B).
In order to distinguish, whether tagged H3.X and H3.Y are only associated with chromatin or constitute stable core nucleosomal components, the protein composition of mononucleosomes in HeLa cells, expressing HA-tagged H3 variants, was analyzed. Clemens Bönisch, another PhD student in the Hake group, digested isolated chromatin with micrococcal nuclease to

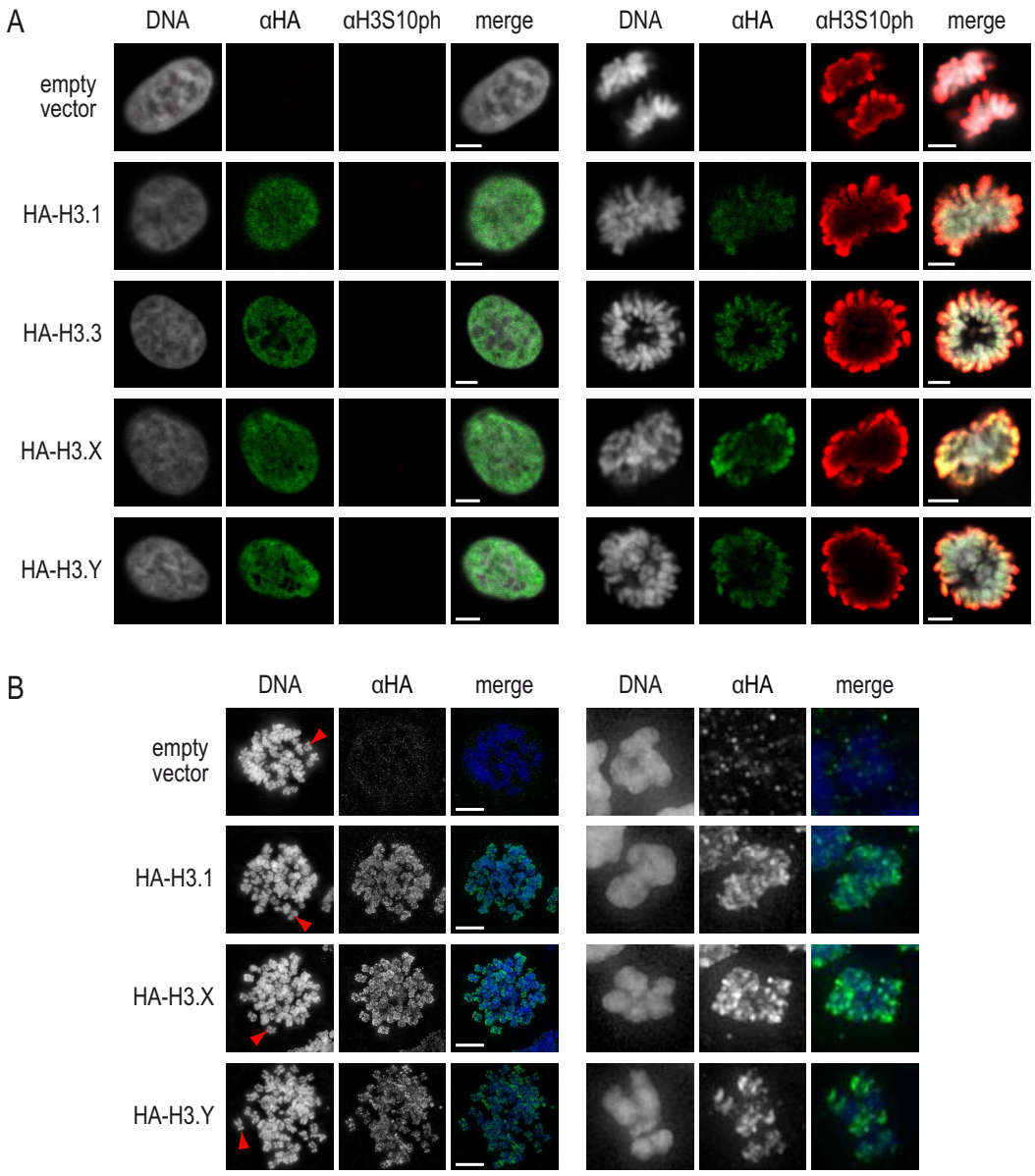

Figure 3.4. Sub-cellular localization of HA-tagged histone H3 variants.
(A) HA-tagged histone H3 variants localize exclusively to the nucleus in stably transfected HeLa cells as determined by confocal imaging of interphase cells (left). In mitotic cells, marked by αH3S10ph staining, HA-tagged histones are associated with condensed chromatin. Cells were co-stained with TO-PRO3 (DNA, gray, left), αHA (green, middle left) and αH3S10ph (red, middle right). Overlay is shown on the right (merge). Scale bar equals 5 µm. (B) Metaphase chromosome spreads of stably transfected HeLa cells show that all HA-tagged histone H3 variants are incorporated into chromatin. Depicted are projections of deconvolved widefield images of chromosomes co-stained with DAPI (DNA, blue, left) and αHA (green, middle). Overlay is shown on the right (merge). Blow-ups of single chromosomes, indicated by red arrowheads, are depcited on the right panel. Scale bar equals 10 µm.

mononucleosomes and immunoprecipitated these using αHA antibody. Silver staining of a 15 % SDS-gel with bound proteins showed successful precipitation of all four core histones (Fig. 3.6A, left). Western blotting of an identical gel, probed with αH3 and αH3.X/Y antibodies, revealed the presence of endogenous known H3 variant proteins in all samples except for the negative control (Fig. 3.6A, right), suggesting the presence of novel and known variants in the same nucleosome. 2100 Bioanalyzer analysis of bound DNA gave a single signal, corresponding in its size to mononucleosomal DNA (∼146 bp), thereby verifying digestion to mononucleosomes (Fig. 3.6B). Taken together, these data show that HA-H3.X and -H3.Y constitute core nucleosomal components and are, in contrast to H3.1 and H3.3 (Tagami et al., 2004), able to form heterotypic nucleosomes with known H3 variants.

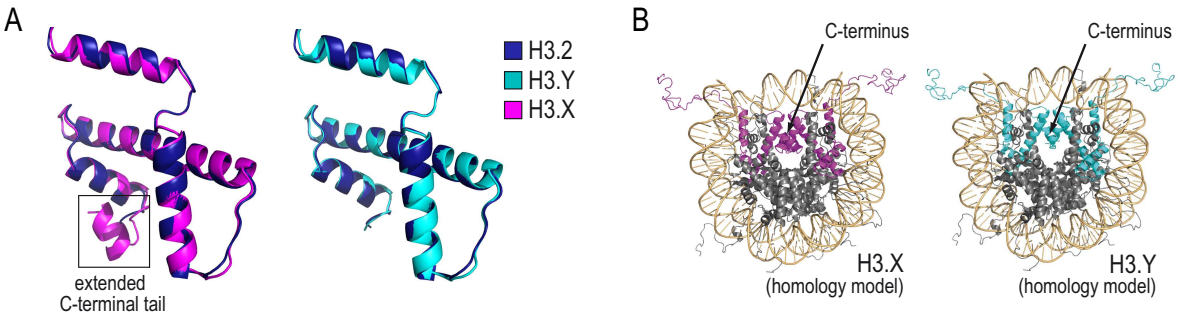

Figure 3.5. ***In silico*** **homology models of H3.X and H3.Y protein structure.**
(A) Overlays of H3.2 crystal structure (blue) with H3.X (purple, left) or H3.Y (cyan, right) *in silico* homology models. Predicted tertiary structures of both novel variants are almost identical to H3.2. Extended C-terminal tail of H3.X is proposed to fold into an additional α-helix (boxed area). (B) Both H3.2 molecules in the crystal structure of the nucleosome are replaced by H3.X (purple, left) or H3.Y (cyan, right) homology models. The additional α-helix of the H3.X protein is predicted to fold into the free space in the middle of the nucleosome, close to the acidic patch of H2A.

Next we wanted to analyze the *in vivo* stability of nucleosomes containing different H3 variants. These experiments were performed by our collaboration partner Lothar Schermelleh from the LMU Munich and his group. Novel and known H3 variants were cloned with an N-terminal GFP-tag under a constitutively active promoter and transiently transfected into HeLa Kyoto cells. These cells were chosen because of their slow cell motility. In a small area of the nucleus, the fluorescence signal was bleached, followed by a measurement of fluorescence recovery after photobleaching (FRAP) rates. All H3 variants show virtually no recovery of the fluorescence signal, even after 8 h, arguing for highly stable chromatin components. In contrast, GFP alone recovers within seconds (Fig. 3.7A,B). Quantification of long-term FRAP rates (Fig. 3.7B, bottom) indicates some minor differences between H3 variants, however, these differences are within the dynamic range of the method as illustrated by long-term FRAP curves including error bars (Fig. 3.7C).

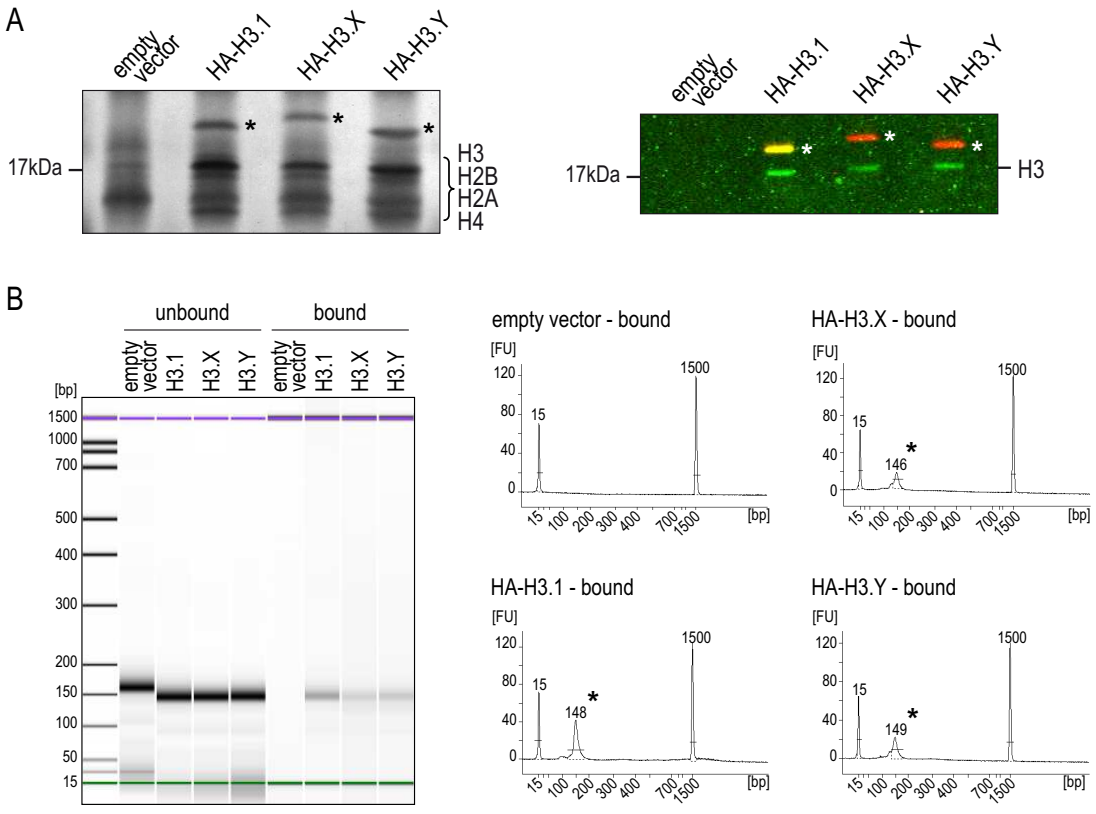

Figure 3.6. Composition of H3.X and H3.Y containing nucleosomes.
Chromatin of HeLa cells, constitutively expressing HA-tagged H3 variants, was digested to mononucleosomes and used for IP with αHA antibody coupled to magnetic beads. (A) Precipitated material was separated with 15% SDS-PAGE. Gels were either silver stained (left) or immunoblotted with subsequent Licor analysis (right) using αHA (red) and αH3 (green) antibodies. All HA-tagged variants (marked with asterisks) were part of a nucleosome as successful precipitation and presence of all core histones indicate. H3.X and H3.Y form heterotypic nucleosomes with other H3 variants, shown by H3 signal in Western blotting (right). (B) DNA of bound and unbound mononucleosomes was isolated and evaluated using the 2100 Bioanalyzer. Gel picture shows successful digestion and precipitation of DNA (left). Marker bands are depicted in purple and green. Size analysis of precipitated DNA verifies digestion to mononucleosomes. Asterisks indicate signal of bound DNA, numbers indicate DNA size in bp (right).

In conclusion, tagged novel variants localize to the nucleus in interphase and mitotic cells, are incorporated into chromatin and show very slow exchange mobility kinetics. Their behavior as well as their proposed tertiary structure is highly similar to the known H3 variants, the major difference being that HA-H3.X and -H3.Y are also able to form heterotypic nucleosomes.

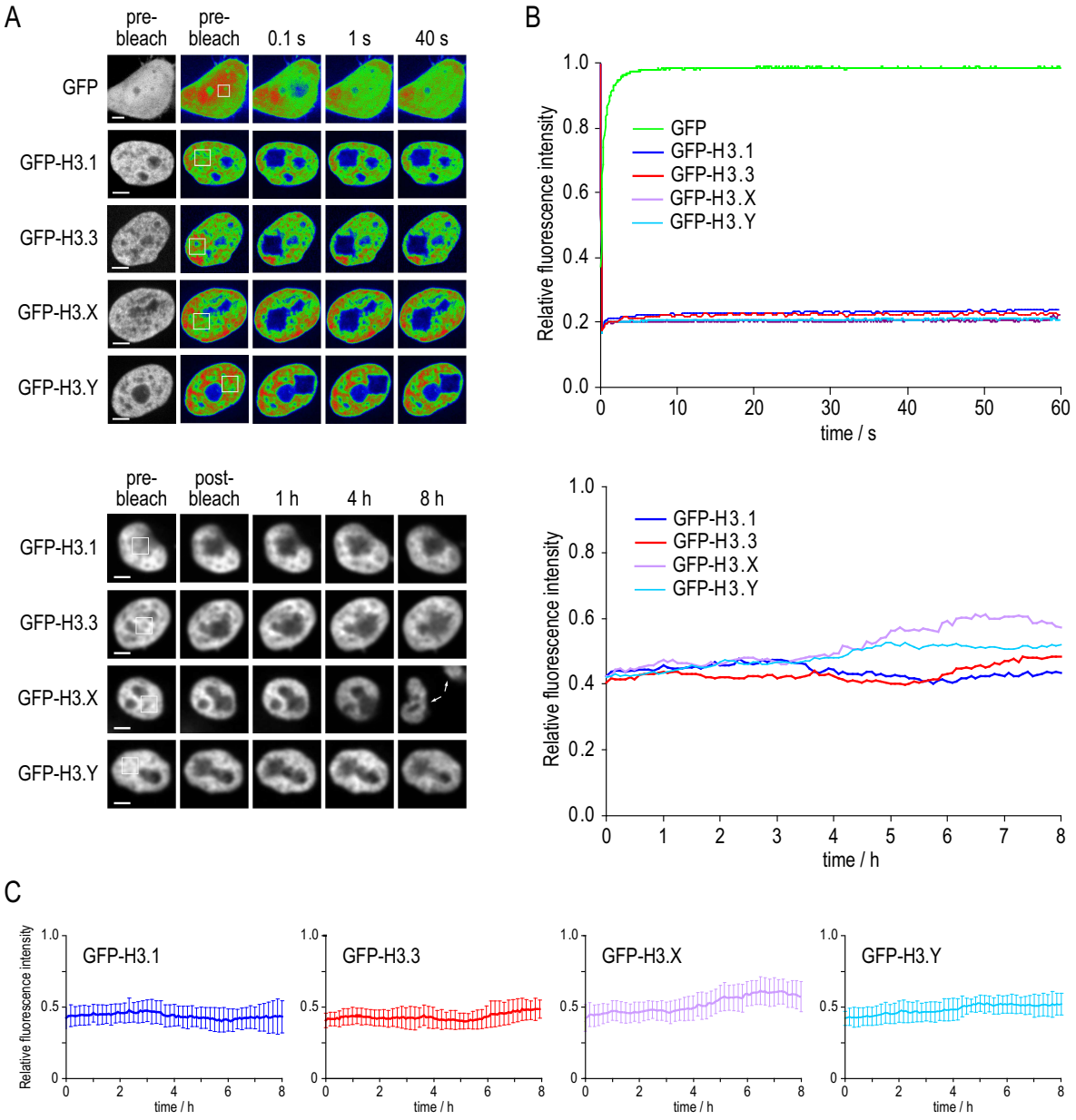

Figure 3.7. Exchange mobility behavior of GFP-tagged H3 variants.
HeLa Kyoto cells were transiently transfected with GFP-tagged H3 variants or GFP alone. GFP fluorescence was bleached in a small area of the nucleus and recovery of fluorescence signal was monitored over 1 min or 8 h by spinning disk microscopy. (A) Snapshots of one representative cell per construct at several time points before and after bleaching are depicted. Short-term FRAP analysis shows recovery of GFP signal within seconds (top), whereas GFP-tagged H3 variants do not show any recovery of the fluorescence signal over 8 h (bottom). Bleached area is indicated by a white box. Arrows indicate daughter cells after mitosis. Scale bar equals 5 µm. (B) Quantitatification of recovery rates after photobleaching. Mean curves of 10-20 cells are shown for short-term FRAP analysis (top). Error bars are omitted for clarity (standard deviation +/- 0.02). For long-term FRAP series (bottom), mean curves of 13-25 cells are plotted. (C) Depicted are mean curves of long-term FRAP experiments including error bars which represent the respective standard deviation: GFP-H3.1 (n=13), GFP-H3.3 (n=15), GFP-H3.X (n=18) and HFP-H3.Y (n=25). All GFP-tagged H3 variants show almost no recovery, indicating stable chromatin incorporation. Subtle differences are within the dynamic range of the measurement and not statistically significant.

3.4 Expression and sub-nuclear localization of endogenous H3.X/Y proteins

Having analyzed endogenous H3.X and H3.Y mRNA expression and characteristics of tagged novel H3 proteins, the next step was to examine endogenous H3.X and H3.Y protein expression. Therefore, we developed an H3.X/Y-specific monoclonal rat antibody together with our collaborator Elisabeth Kremmer from the Helmholtz-Center in Munich. The antibody is directed against amino acids (aa) 9 - 20 of H3.X and H3.Y (for peptide sequence see black line in Fig. 3.1). Antibody specificity was tested in various assays using HeLa cells stably expressing HA-tagged H3 variants. αH3.X/Y recognizes acid extracted HA-H3.X and -H3.Y proteins but none of the other histone variants in Western blot (Fig. 3.8A), IF microscopy (Fig. 3.8B) and FACS analysis (data not shown). Epitope-specificity was further determined by peptide competition experiments. αH3.X/Y antibody was incubated with the original peptide used for antibody generation or an unrelated H3.3 peptide prior to use for IF staining. αH3.X/Y specifically interacted with the H3.X/Y peptide, which prevented the binding of tagged H3.X

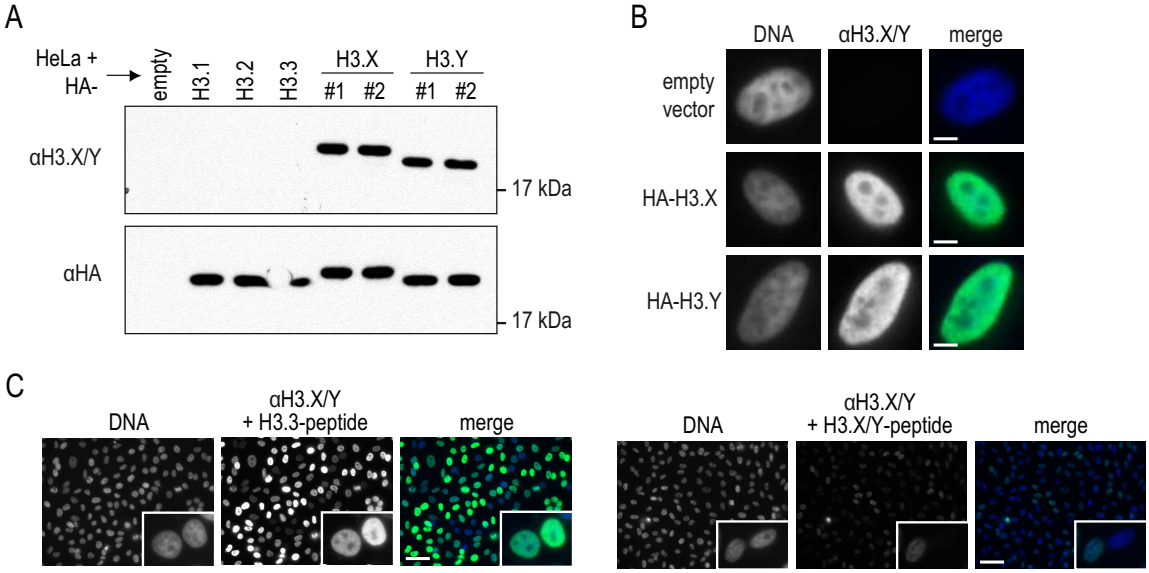

Figure 3.8. Evaluation of αH3.X/Y antibody specificity.
(A) Western blot analysis of acid extracted histones of HeLa cells, stably transfected with HA-tagged H3 variants. αH3.X/Y antibody recognizes specifically H3.X and H3.Y but none of the other H3 variants (top). Numbers indicate independently selected HeLa cell populations. Incubation with αHA antibody reveals presence and equal loading of all tagged variants (bottom). Note that all variants migrate slower than endogenous H3 (17 kDa) because of the HA-tag. H3.X migrates even more slowly because of its extra C-terminus. (B) IF microscopy images of HeLa cells stably transfected with empty vector, HA-H3.X or HA-H3.Y, co-stained with DAPI (DNA, blue, left) and αH3.X/Y (green, middle), shows nuclear localization of tagged H3.X and H3.Y protein. Merged pictures are depicted on the right, scale bar equals 5 µm. (C) Peptide competition assay to evaluate epitope-specificity of αH3.X/Y antibody. HeLa HA-H3.X cells were co-stained with DAPI (DNA, blue, left) and αH3.X/Y (green, middle) pre-incubated with an H3.3 (aa 22 - 41) peptide (top) or H3.X/Y (aa 9 - 20) peptide (bottom). HA-H3.X signal is lost in a H3.X/Y-sequence specific manner. Overlay is depicted on the right (merge). Insets show blow-ups of two representative cells. Scale bar equals 50 µm.

in the cell, leading to a loss of fluoresence signal. No binding of αH3.X/Y to the H3.3 peptide occured, thereby giving a strong signal for HA-H3.X (Fig. 3.8C).

With this highly specific tool, acid extracted histones from several human cell lines were analyzed for their content of endogenous H3.X/Y protein. Mouse NIH3T3 cells served as negative and HeLa HA-H3.X cells as positive control. Western blot analysis of these histones using αH3.X/Y antibody, revealed a faint band at 17 kDa for U2OS histones but not for

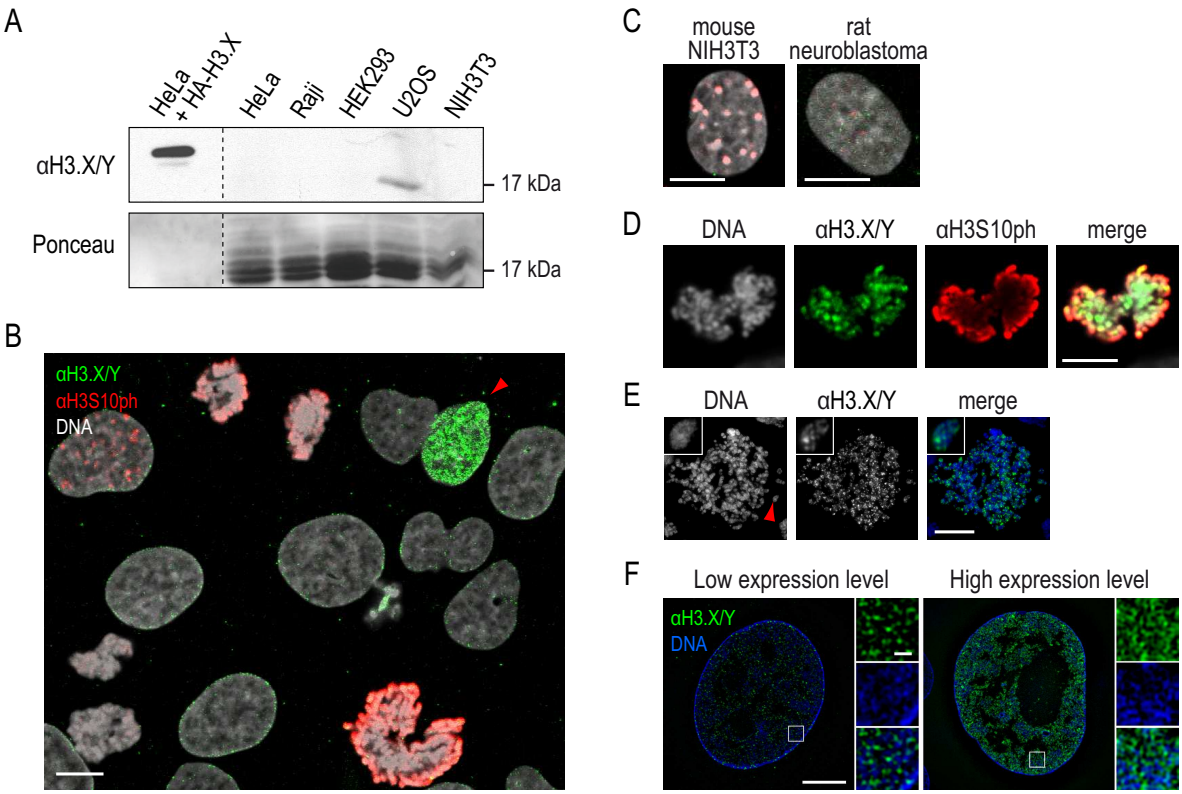

Figure 3.9. Endogenous H3.X/Y expression and sub-nuclear localization.
(A) Western blot analysis of acid extracted histones from different cell lines with αH3.X/Y antibody reveals a faint band for U2OS cells at 17 kDa but not for any other cell line (top). HeLa HA-H3.X cells were used as positive, mouse NIH3T3 cells as negative control. Membrane was stained with Ponceau S to check protein loading (bottom). Dotted lines indicate that intervening lanes have been spliced out. (B) Confocal imaging of U2OS cells co-stained with αH3.X/Y (green), H3S10ph (mitosis-specific, red) and TO-PRO3 (DNA, gray) shows a distinct pattern of H3.X/Y staining associated with the nuclear envelope in all inter- and prophase cells, as well as a general nuclear staining in very few cells (marked by a red arrowhead). Scale bar equals 10 µm. (C) Confocal imaging of mouse NIH3T3 and rat neuroblastoma cells co-stained with αH3.X/Y (green), H3S10ph (red) and TO-PRO3 (DNA, gray), used as negative control, shows no H3.X/Y staining. Scale bar equals 10 µm. (D) Confocal imaging of a mitotic U2OS cell co-stained with TO-PRO3 (DNA, gray, left), αH3.X/Y (green, middle left) and H3S10ph (red, middle right) shows chromatin association of H3.X/Y signal. Overlay is shown on the right, scale bar equals 10 µm. (E) Chromosome spreads of mitotically arrested U2OS cells show chromatin incorporation of H3.X/Y signal. Depicted is a projection of deconvolved widefield images of U2OS metaphase chromosome spreads co-stained with DAPI (DNA, blue, left) and αH3.X/Y (green, middle). Overlay is shown on the right, inset shows an enlargement of a single chromosome, indicated by a red arrowhead. Scale bar equals 10 µm. (F) Super-resolution 3D-SIM IF analysis of U2OS cells expressing low (left) or high (right) amounts of H3.X/Y co-stained with DAPI (blue) and αH3.X/Y (green). Scale bar equals 5 µm. Enlargements of boxed sections are depicted on the right with scale bar equaling 1 µm. H3.X/Y signal is mostly found outside of DAPI-dense regions. In (B)-(D) and (F) confocal mid-sections are shown.

histones of any other cell line (Fig. 3.9A). These data are consistent with previous findings, as the size of this band would be expected for H3.Y and U2OS cells express mostly H3.Y mRNA (see Fig. 3.3A). Moreover, in confocal images of U2OS cells stained with αH3.X/Y, a strong nuclear staining, co-localizing with DNA, was detected in some few cells but not in any other cell line (Fig. 3.9B, arrowhead). However, in all human cells, a dotted H3.X/Y staining associated with the nuclear envelope was visible (Fig. 3.9B and section 3.8). In contrast, mouse and rat cells, which were used as negative controls, do not display any H3.X/Y signal (Fig. 3.9C). In H3.X/Y expressing mitotic U2OS cells as well as in chromosome spreads of mitotically arrested H3.X/Y expressing U2OS cells, H3.X/Y signal is associated with condensed chromosomes, arguing for a stable chromatin incorporation of endogenous H3.X/Y protein (Fig. 3.9D,E). As seen for HA-tagged novel variants, H3.X/Y staining shows a distinct distribution along chromosome arms (Fig. 3.9E). To shed light on the sub-nuclear localization of endogenous H3.X/Y protein, our collaborator Lothar Schermelleh performed super-resolution imaging with 3-dimensional structured illumination microscopy (3D-SIM) analysis (Gustafsson et al., 2008; Schermelleh et al., 2008). This method provides the possibility to acquire images with a resolution below the diffraction limit of conventional optical microscopes and therefore allows to determine sub-nuclear localization of proteins more accurately (Fig. A.3, Appendix). In U2OS cells, co-stained with αH3.X/Y and DAPI, this technique finds the H3.X/Y signal primarily outside of DAPI-dense region, irrespective of H3.X/Y expression levels (Fig. 3.9F). This finding suggests an association of H3.X/Y with less condensed and more euchromatic areas.

In summary, these data show that endogenous H3.X and/or H3.Y protein is expressed in U2OS cells. It localizes to the nucleus, is incorporated into chromatin and seems to be associated with more euchromatic areas.

3.5 Induction of endogenous H3.X/Y expression in U2OS cells

3.5.1 Increase in H3.X/Y expressing U2OS cells through nutritional and proliferative stress

Previous analyses of U2OS cell samples have shown that only less than 0.1 % of cells show a general nuclear H3.X/Y staining in IF microscopy. In addition, this percentage as well as the amount of H3.X+Y mRNA, determined in qPCR measurements, varies considerably between biological replicates. Wondering what causes these fluctuations, some kind of stress stimulus was hypothesized to trigger H3.X/Y expression in U2OS cells. Together with Silke Mildner, a

diploma student in the Hake group, whom I supervised, I set out to test this hypothesis. The first set of stress conditions tested were UV irradition, causing DNA damage and at higher doses apoptosis, and proliferative stress or proliferative stress concomitant with starvation. UV treatment did not change the number of U2OS cells showing a general nuclear αH3.X/Y staining (Fig. 3.10) nor did hydroxyurea or etoposide, which induce DNA damage via other pathways than UV (data not shown). Interestingly, proliferative and nutritional stress together but not proliferative stress alone led to a 4-fold increase in the number of αH3.X/Y stained nuclei (Fig. 3.10).

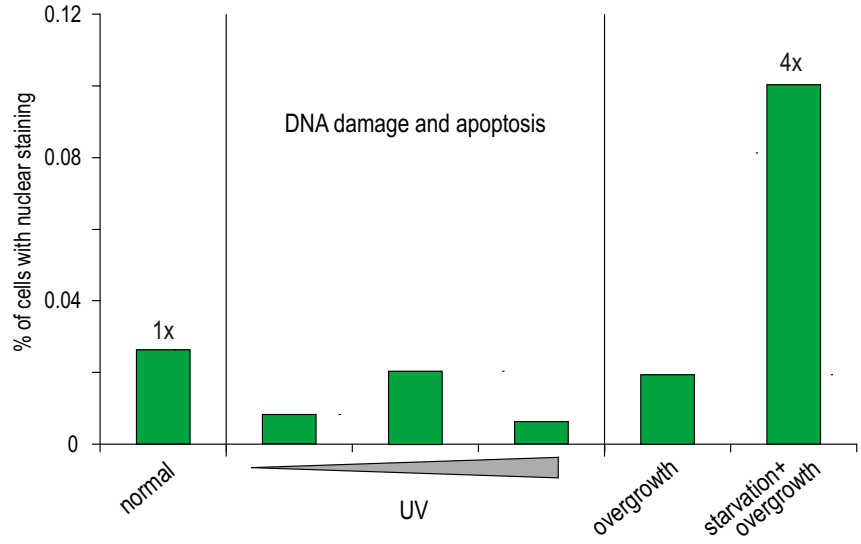

Figure 3.10. Test of different stress conditions as trigger for H3.X/Y expression in U2OS cells. U2OS cells were grown under different stress conditions for 8 days (normal, overgrowth or starvation and overgrowth) or treated with different doses of UV light to induce DNA damage and apoptosis (for details see section 2.3.1.2). Cells were co-stained with DAPI (DNA) and αH3.X/Y and percentage of cells showing a general nuclear staining was calculated and plotted (for details see section 2.3.4). Starvation and overgrowth but not overgrowth alone leads to an increase in the number of H3.X/Y expressing cells, whereas DNA damage and apoptosis does not show any effect.

Based on these findings, we next examined if starvation alone or only together with high cell density can lead to an increase in U2OS cells positive for αH3.X/Y staining. We cultivated U2OS cells for 8 days under different stress conditions (normal, starvation or starvation and overgrowth), calculated the percentage of cells with general nuclear αH3.X/Y staining from IF microscopy data, quantified H3.X/Y mRNA levels by qPCR and analyzed H3.X/Y protein levels by Western blotting using αH3.X/Y. With these experiments we could reproducibly show that starvation and overgrowth (SO) increases the number of cells with αH3.X/Y-positive nuclei by approximately 6-fold, whereas starvation (S) alone only leads to a 3-fold increase (Fig. 3.11A). H3.X+Y mRNA levels are likewise affected (Fig. 3.11B). In Western blot analysis of acid extracted histones, the 17 kDa band, only faintly visible in the lane with

histones from normally grown U2OS cells, appears much stronger after both stress treatments (Fig. 3.11C). Comparison with recombinant H3.X and H3.Y proteins loaded as size markers and positive controls, suggests that specifically H3.Y rather than H3.X protein levels are increased. This is in accordance with the mRNA data that show a stronger enrichment of H3.X+Y than H3.X amplicons, thereby arguing that these stress stimuli act particularly on H3.Y expression.

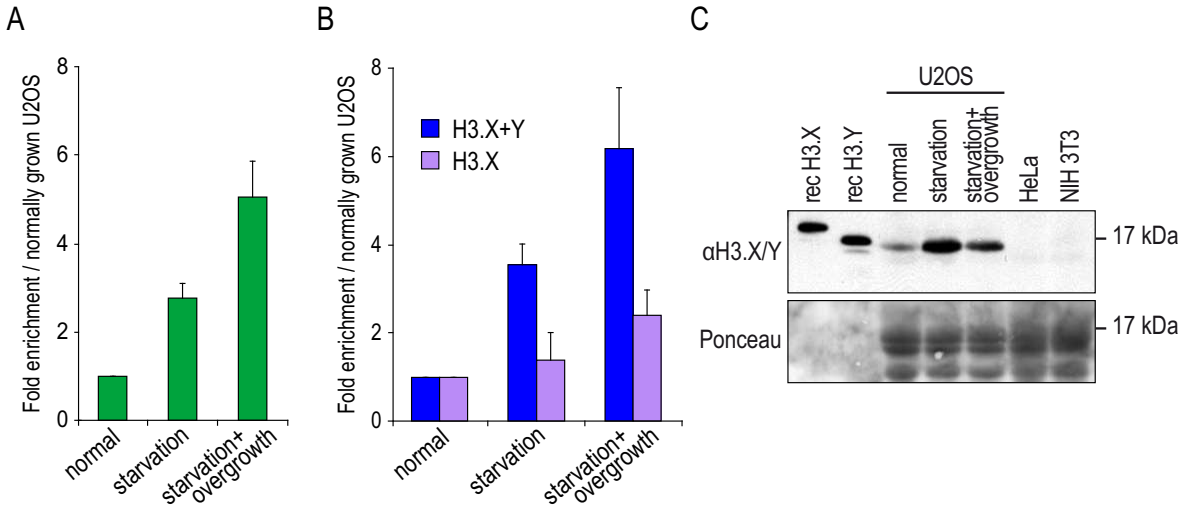

Figure 3.11. Increase of H3.X/Y expressing U2OS cells by nutritional and proliferative stress. U2OS cells were grown for 8 days under different stress conditions (normal, starvation or starvation and overgrowth) and subsequently analyzed for number of cells showing a general nuclear H3.X/Y staining, H3.X/Y mRNA and protein levels. (A) Cells were co-stained with DAPI (DNA) and αH3.X/Y and percentage of cells showing a general nuclear staining was calculated and plotted (for details see section 2.3.4). Starvation and overgrowth, and to a lesser extent starvation alone, increases number of cells with general nuclear H3.X/Y staining. Error bars represent SEM of three independent biological experiments. (B) H3.X/Y mRNA levels were quantified by qPCR using cDNA. H3.X+Y (blue) and H3.X (purple) levels are shown relative to HPRT1 and HMBS and normalized to normally grown U2OS cells. Nutritional and proliferative stress significantly increases H3.X+Y, but not H3.X levels. Error bars represent SEM of three independent biological experiments. (C) Acid extracted histones were analyzed for H3.X/Y protein levels by Western blotting using αH3.X/Y antibody (top). Recombinant H3.X and H3.Y proteins served as positive, acid extracted histones from HeLa and mouse NIH3T3 cells as negative controls. Ponceau S staining ensured equal protein loading (bottom). Starvation with and without overgrowth leads to an increase of a 17 kDa band in U2OS cells. One representative blot of three independent biological experiments is shown.

To further validate that indeed H3.Y expression is mostly affected by S and SO treatment, qPCR analysis with cDNA from one biological replicate of the above stress experiments (see Fig. 3.11) was performed, using several primer pairs targeting H3.X and H3.Y mRNA or specifically the one or the other. Amplicons were chosen to span the complete coding sequence of both variants (Fig. 3.12B). H3.X mRNA levels stay virtually constant upon S and SO treatment, whereas H3.Y-specific as well as some of the H3.X+Y-specific amplicons show a strong enrichment (Fig. 3.12A), confirming previous findings. Primer pair H3.X+Y #3 has previously been identified as the most sensitive of the H3.X+Y primer pairs. For data de-

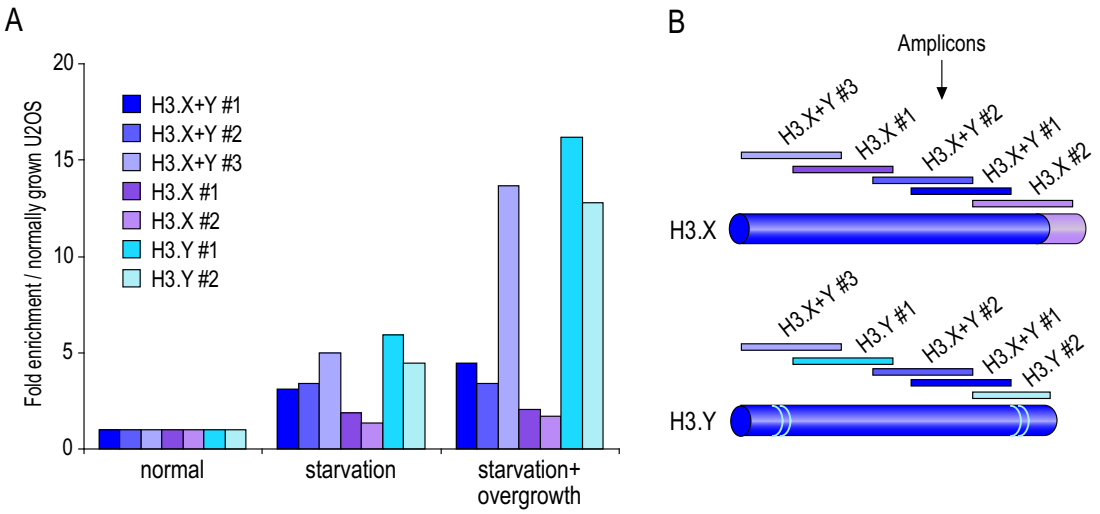

Figure 3.12. Evaluation of inducible endogenous H3.X and H3.Y expression.
(A) qPCR analysis of cDNA from U2OS cells grown under different stress conditions using different primer pairs for H3.X and H3.Y. The result of one of the three biological replicates depicted in Fig. 3.11 is shown. (B) Amplicons generated by three H3.X+Y-specific (shades of blue), two H3.X-specific (shades of purple) and two H3.Y-specific (shades of cyan) primer pairs span the complete coding regions ("primer-walk"). For primer sequences see Table A.1.

picted in Figs. 3.3A and 3.11B, primer pairs H3.X+Y #2 and H3.X #2 have been used.

To assess the question which factor(s) in the growth medium cause the observed effects, cells were also scored for αH3.X/Y-staining after serum-starvation, amino acid-depletion or growth under reduced oxygen levels, none of which had a reproducible effect on H3.X/Y expression (data not shown).

In summary, these data show a direct correlation between αH3.X/Y nuclear staining, H3.X/Y mRNA and protein levels, all being upregulated by starvation and overgrowth and to a lesser extent starvation alone. Furthermore, they suggest that particularly H3.Y expression is positively affected by these treatments.

3.5.2 Increase of endogenous H3.Y protein expression in U2OS cells after SO treatment

SO treatment increases the number of cells with αH3.X/Y nuclear staining, presumably caused by enhanced expression of H3.Y. To confirm this assumption, novel histone H3 variants were purified from U2OS cells and analyzed using mass spectrometry. Total histones were isolated from normally grown or SO treated U2OS cells and separated using reversed phase-high performance liquid chromatography (RP-HPLC) (Fig. 3.13A). Histone H3 variants elute in two peaks: peak I contains H3.2 and H3.3 whereas peak II contains only H3.1 protein (Fig. 3.13B) (Hake et al., 2006). Fractions 1 - 30, corresponding to histone H3 peaks,

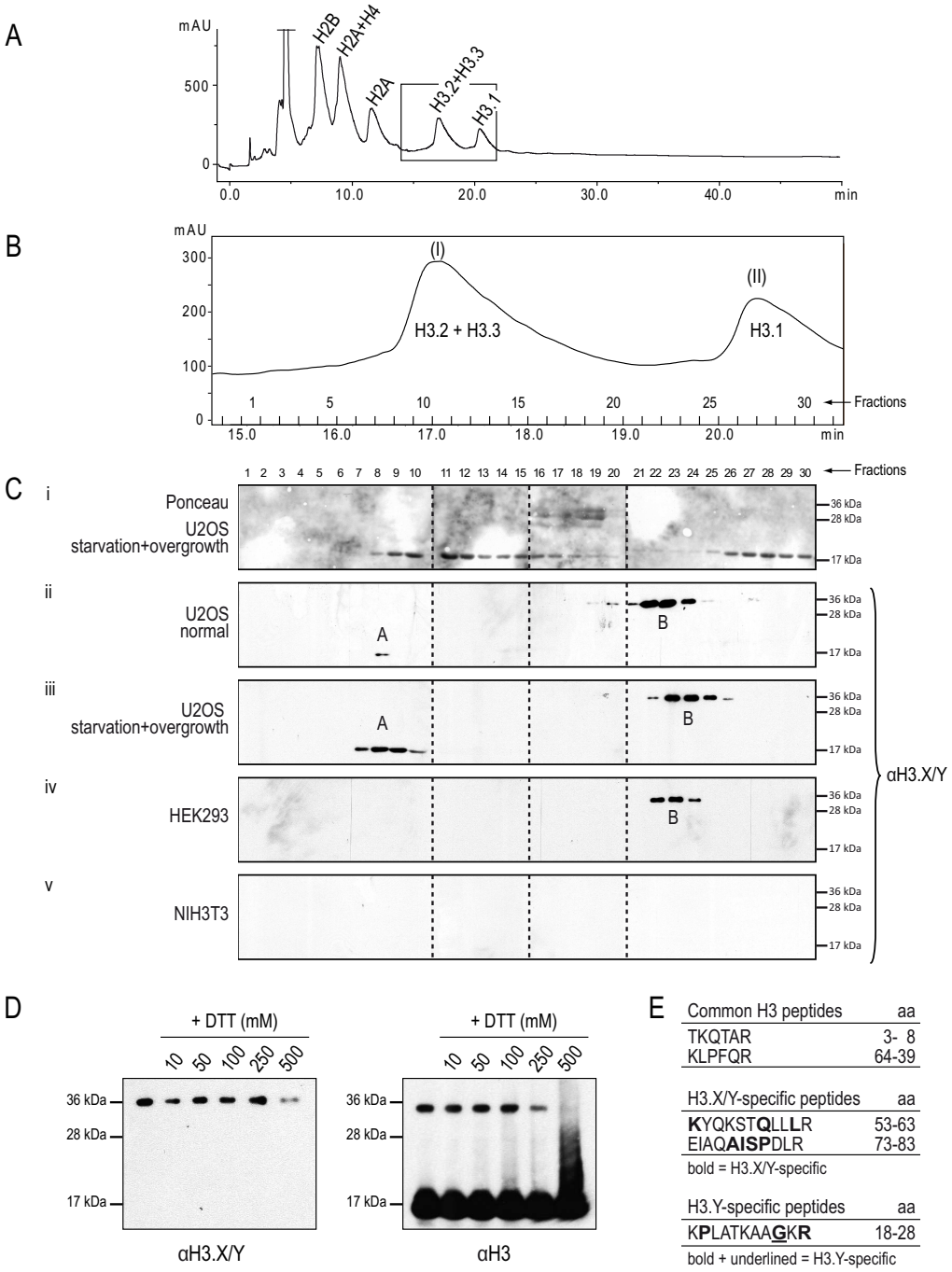

Figure 3.13. Purification and identification of endogenous H3.Y protein.
Acid extracted histones of normally grown and SO treated U2OS as well as HEK293 and mouse NIH3T3 cells were separated by RP-HPLC and fractions containing H3 variants were analyzed by Western blotting and mass spectrometry. (A) Typical histone RP-HPLC peak profile. Box indicates fractions used for analysis. (B) An enlargement of boxed section marked in (A) is shown. (C) Western blots with fractions 1-30 (marked in (B)) from different cell lines using αH3.X/Y antibody, show a weak band at 17 kDa in normally grown U2OS cells (A band, ii), which is strongly enhanced after SO treatment (A bands, iii) and not visible in any other cell line. Region B bands (∼35 kDa) are present in all human but not in mouse cells (ii-iv versus v). Ponceau S staining of U2OS SO membranes visualizes protein content in individual fractions (i). Dotted lines indicate that intervening lanes have been spliced out. (D) Fractions containing region B bands and fractions containing H3.1, H3.2 and H3.3 were treated with different amounts of DTT. Western blotting using αH3.X/Y for region B band fractions (left) and αH3 for H3 fractions (right) shows dissociation of H3 dimers but no effect on region B bands. (E) List of H3 and H3.X/Y peptides identified in combined region A fractions of normally grown and SO treated U2OS cells in LC-MS/MS analyses. Amino acids marked in bold are specific for H3.X and H3.Y, bold and underlined amino acid is H3.Y-specific. For MS/MS spectra see Fig. A.4.

were analyzed on Western blots probed with αH3.X/Y. Ponceau staining of membranes with histones from SO treated U2OS cells, shows amount of canonical H3 present in individual fractions (Fig. 3.13Ci). Proteins detected by αH3.X/Y elute right before peaks I and II (Fig. 3.13Cii,iii). As expected, a faint 17 kDa band, indicative of H3.Y, can be observed in normally grown U2OS cells and is strongly enhanced in SO treated cells (region A bands in Fig. 3.13Cii and iii). In addition, a 35 kDa protein, showing the same intensity under both growth conditions, is also detected by αH3.X/Y (region B bands in Fig. 3.13Cii and iii). For comparison, total histones from human HEK293 and mouse NIH3T3 cells were RP-HPLC-purified and corresponding fractions analyzed on Western blots. Both cell lines show no signal for region A bands, however, a strong region B band signal can be observed in HEK293 cells, proposing the corresponding protein to be present in all human but not in mouse cells (Fig. 3.13Civ,v). The size of the protein causing region B band signals is approximately twice the size of H3.X and H3.Y, giving rise to the idea that it might constitute a homo- or heterodimer of novel H3 variants. To test this hypothesis, region B band fractions and a mixture of peak I and II fractions were treated with increasing amounts of DTT to reduce disulfide bonds and thereby separate potential H3 dimers. Peak I and II fractions contain minimal amounts of H3 dimers, which can be separated using high DTT concentrations (Fig. 3.13D). No such effect on proteins in region B band fractions can be observed, arguing against a dimerization of novel H3 variants. Region A, as well as region B band fractions, were subjected to mass spectrometrical analysis using nano-ESI-LC-MS/MS. For proteins present in region B band fractions only one single peptide corresponding to H3.X/Y (aa 53 - 63) could be observed among several others, rendering the analysis of these fractions inconclusive. However, for proteins present in region A band fractions, two H3.X/Y-specific (aa 53 - 63 and aa 73 - 83), as well as one H3.Y-specific (aa 18 - 28) peptide, could be identified in addition to common H3 peptides in two biological replicates of SO treated and in normally grown U2OS cells (Fig. 3.13E and Fig. A.4A-C, Appendix). Interestingly, the H3.Y-specific peptide was also found to be acetylated on K18, K23 and K27 in some cases in both SO treated and normally grown U2OS cell samples (Fig. A.4D,E, Appendix). These PTMs are also present in canonical H3 variants, indicating that H3.Y was likely part of a nucleosome and present in chromatin fibers.

In summary, these data show that posttranslationally modified H3.Y is expressed in U2OS cells and that its levels are increased upon SO treatment.

3.6 Effects of H3.Y on gene expression

Previous experiments have shown that *H3.X* and *H3.Y* genes are expressed *in vivo* and that at least H3.Y constitutes a novel histone H3 variant. To examine the biological function(s) of H3.Y expression, RNA expression profiles of cells expressing enhanced or reduced levels of H3.Y have been generated. For both sets of experiments the hybridization was carried out by Dietmar Martin and Kerstin Maier of the Gene Center Affymetrix Microarray Platform (LMU Munich, Cramer Laboratory) and data analysis was performed by our collaborator Tobias Straub (LMU Munich, Becker Laboratory).

3.6.1 De-regulation of genes mainly implicated in growth control, survival or differentiation pathways in HeLa HA-H3.Y cells

The number of H3.Y expressing U2OS cells varies considerably between different samples. Therefore, the initial idea was to use HeLa cells constitutively expressing HA-tagged H3.Y and compare their RNA expression profile with that of empty vector transfected HeLa cells. Total RNA was isolated from two independently selected HeLa HA-H3.Y and HeLa empty vector cell populations, respectively, and hybridized to Affymetrix Human Gene 1.0 ST arrays. In HeLa HA-H3.Y cells, 119 genes were significantly up- and 73 significantly down-regulated (local false disvovery rate cutoff 0.2). The most upregulated gene was *H3.Y* (LOC391769), thereby verifying the sensitivity and accuracy of the assay. Gene ontology (GO) enrichment analysis revealed that affected genes are mainly implicated in growth control, survival or

A

GOBPID	Pvalue	Odds Ratio	Exp Count	Count	Size	Term
GO:0007165	0.000	3.171	18	38	2297	signal transduction
GO:0060389	0.000	41.146	0	4	17	pathway-restricted SMAD protein phosphorylation
GO:0007167	0.000	5.086	2	10	288	enzyme linked receptor protein signaling pathway
GO:0050789	0.000	2.405	38	55	4916	regulation of biological process
GO:0008285	0.000	4.982	2	8	230	negative regulation of cell proliferation
GO:0060021	0.001	20.828	0	3	22	palate development
GO:0007179	0.001	8.010	1	5	89	transforming growth factor beta receptor signaling pathway

B

GOBPID	Pvalue	Odds Ratio	Exp Count	Count	Size	Term
GO:0040008	0.000	8.673	1	6	204	regulation of growth
GO:0045661	0.000	87.256	0	2	8	regulation of myoblast differentiation
GO:0008361	0.000	8.898	1	5	162	regulation of cell size
GO:0045987	0.001	74.784	0	2	9	positive regulation of smooth muscle contraction
GO:0048741	0.001	19.122	0	3	45	skeletal muscle fiber development

Figure 3.14. GO enrichment analysis of de-regulated genes in HeLa HA-H3.Y cells.
List of GO terms resulting from an enrichment analysis of significantly up- (A) or down- (B) regulated genes in HeLa HA-H3.Y relative to HeLa empty vector cells as determined by microarray analysis. Size = total number of genes analyzed in this node (GO term), ExpCount = number of "responders" expected (entering the term by chance), Count = actual number of "responders" found in the node.

differentiation pathways (Fig. 3.14). Before analyzing the biological meaning of this result, several controls have been performed. As the array used is rather new, the first step was to validate the microarray results for a selection of genes. 9 of the strongest "responders" were chosen as well as the 7 most de-regulated genes in the listed GO groups. cDNA was synthesized from the same RNA used for microarray analysis, expression levels were quantified by qPCR relative to HPRT1 and HMBS and results were normalized to empty vector transfected HeLa cells. Comparison of microarray and qPCR data for these loci shows a general correlation of expression data (Fig. 3.15, left). However, depending on the localization of the primers and the uniformity of the data determined from individual probesets, the actual results differ to a certain extent. Another important question is the distinction

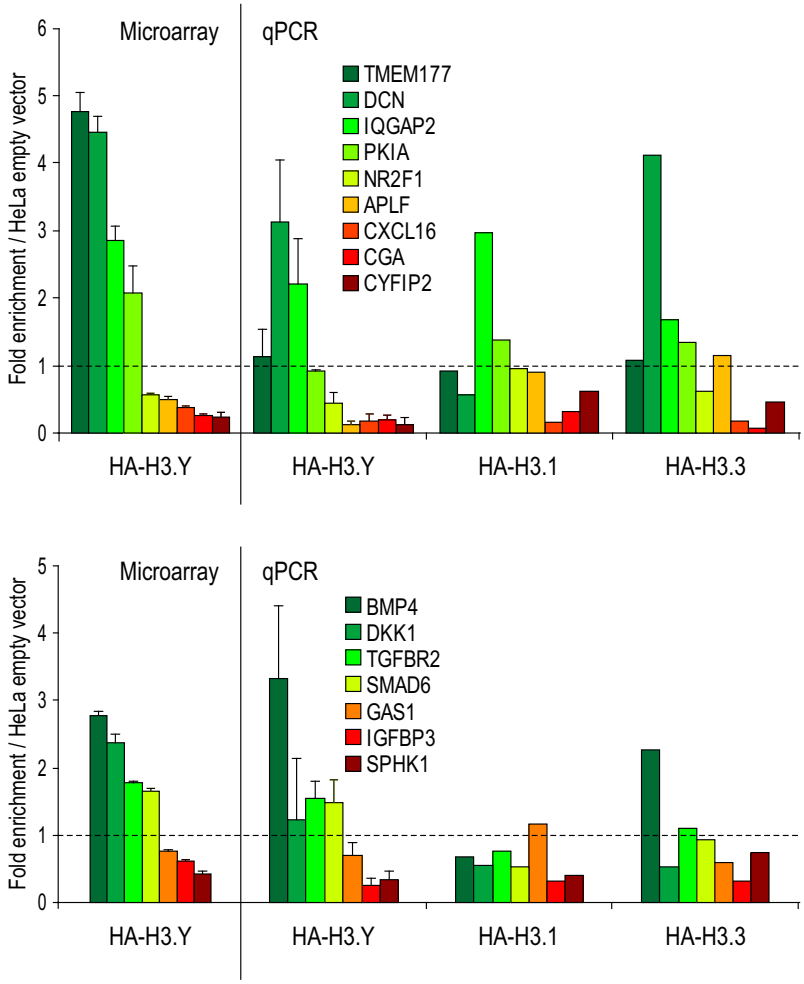

Figure 3.15. Gene expression levels in HeLa cells stably expressing HA-tagged H3 variants. Comparative qPCR analysis of cDNA from HeLa cells stably expressing HA-tagged H3.1, H3.3 or H3.Y with primer pairs for two subsets of genes, de-regulated in HeLa HA-H3.Y relative to HeLa empty vector cells. On the left, microarray data normalized to HeLa empty vector and on the right, qPCR results relative to HPRT1 and HMBS and normalized to HeLa empty vector are plotted. Error bars represent SEM of two independently selected HeLa cell populations. Subset 1 genes (top) were selected from the strongest "responders" in microarray analysis of HeLa HA-H3.Y compared to HeLa empty vector cells. Subset 2 genes (bottom) are significantly de-regulated in HeLa HA-H3.Y cells and part of GO groups listed in Fig. 3.14.

between H3.Y-specific effects and effects that result from the constitutive expression of any tagged H3 variant. Therefore, the same loci used for validation of the method, were analyzed for their expression levels in HeLa HA-H3.1 and -H3.3 cells using qPCR. Some of the genes strongly de-regulated in HeLa HA-H3.Y cells show almost no change in HeLa HA-H3.1 and -H3.3 cells (e.g. APLF), arguing for an H3.Y-specific effect, but several other genes, such as CXCL16 or IGFBP3, are de-regulated similarly in all three cell lines (Fig. 3.15, right). As these results make it impossible to deduce a general biological meaning from the expression data in HeLa HA-H3.Y cells without having the corresponding data for HeLa cells expressing other H3 variants, we decided to compare expression levels of individual de-regulated genes in HeLa HA-H3.Y with normally grown U2OS HA-H3.Y cells and U2OS and U2OS HA-H3.Y cells grown under SO conditions for 8 days. With this dataset, cell line dependent and general effects of HA-H3.Y can be distinguished from each other. Furthermore, effects of SO treatment can be compared to those caused by constitutive HA-H3.Y expression. Expression levels determined by qPCR are shown relative to HPRT1 and HMBS and normalized to U2OS empty vector cells, normally grown U2OS and U2OS HA-H3.Y cells, respectively. For HeLa HA-H3.Y, qPCR data shown in Fig. 3.15 (bottom) are depicted (Fig. 3.16). Comparison of expression levels in HeLa HA-H3.Y and U2OS HA-H3.Y cells, shows huge differences, arguing for a strong influence of the cellular background on HA-H3.Y function (Fig. 3.16, light brown vs. light blue bars). Dickkopf 1 (DKK1) for example, shows only mild up-regulation in HeLa

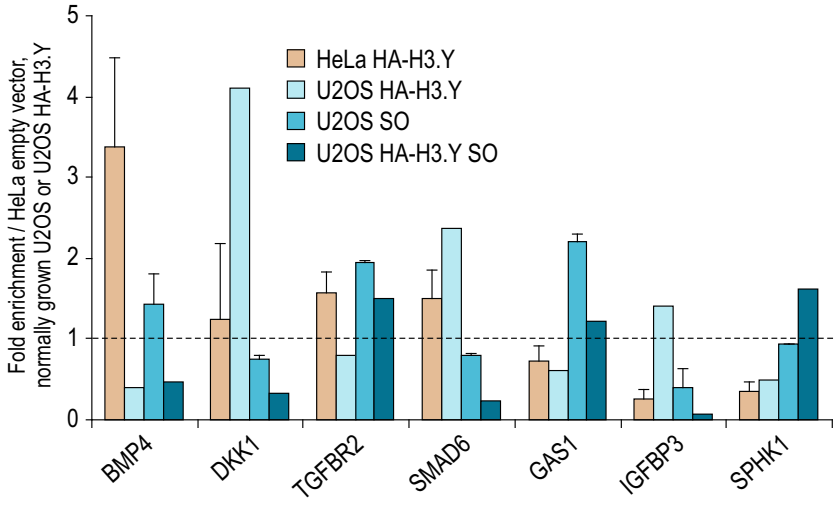

Figure 3.16. Influences of HA-H3.Y expression and SO treatment on gene expression. Comparative qPCR analysis of cDNA from HeLa HA-H3.Y, U2OS HA-H3.Y, U2OS SO and U2OS HA-H3.Y SO cells with primer pairs for subset 2 genes (see Fig. 3.15) shows cell line dependent effects of HA-H3.Y expression and no consistent synergistic effects of HA-H3.Y expression and SO treatment. Expression levels are calculated relative to HPRT1 and HMBS and shown as fold enrichment over HeLa empty vector, U2OS empty vector, normally grown U2OS and normally grown U2OS HA-H3.Y cells, respectively. Error bars represent SEM of two independently selected HeLa cell populations (HeLa HA-H3.Y) or two biological replicates (U2OS SO).

HA-H3.Y cells whereas levels are strongly increased in U2OS HA-H3.Y cells. As DKK1 is implicated in bone formation (Pinzone et al., 2009) and U2OS cells constitute bone derived cells, this difference is most likely caused by basic differences between HeLa and U2OS cells. In contrast to these extreme discrepancies, growth arrest specific protein 1 (GAS1) and the transforming growth factor β (TGFβ) -target sphingosine kinase (SPHK1) (Donati et al., 2009) show reduced levels in both cell lines, arguing for H3.Y-specific effects. Based on the finding that H3.Y expression is induced in U2OS cells after SO treatment, we hypothesized that HA-H3.Y expression and SO treatment have similar effects. However, this is not the case for any of the genes analyzed (Fig. 3.16, light vs. middle blue bars). The cause for this discrepancy is presumably that SO treatment affects the expression of many genes other than H3.Y. Analyzing the data with regard to synergistic effects of HA-H3.Y expression and SO treatment, the emerging picture is quite complex (Fig. 3.16, middle vs. dark blue bars). For several genes, such as SMAD6, an inhibitor of the TGFβ-cascade (Moustakas and Heldin, 2009) or insulin-like growth factor binding protein 3 (IGFBP3), which is known to stimulate TGFβ-signaling via the SMAD-pathway (Fanayan et al., 2000, 2002), SO treatment causes a reduction of gene expression, which is stronger when in addition HA-H3.Y is expressed, thereby showing a synergistic effect. For other genes, HA-H3.Y expression seems to do the contrary by attenuating the effect of SO treatment. Examples are GAS1 and TGFβ receptor 2 (TGFBR2) which activates the TGFβ-cascade (Moustakas and Heldin, 2009).
Taken together, these data show that H3.Y influences gene expression in a cell type specific manner. Since HeLa cells do not express endogenous H3.Y (see Fig. 3.3A), it is impossible to deduce the biological role of this novel variant from HeLa HA-H3.Y expression data.

3.6.2 Impairment of cell proliferation in U2OS cells after knockdown of H3.Y or H3.X+Y

To gain a deeper insight into the biological function(s) of H3.Y, U2OS cells with reduced endogenous H3.Y mRNA and protein levels after RNA interference (RNAi) -knockdown were used for global transcriptome analysis, a system closer to the *in vivo* situation than the constitutive expression of tagged protein. Due to the high sequence similarity of H3.X and H3.Y (see Fig. A.1, Appendix), only one small interfering RNA (siRNA) specifically targeting H3.X and one targeting H3.Y could be designed. In addition, one siRNA directed against both mRNAs (H3.X+Y) was used and control knockdowns were performed using luciferase targeting siRNA, a gene not present in human cells (for siRNA sequences see Table A.3). To test specificity of siRNAs, HeLa HA-H3.X and -H3.Y cells were transfected with siRNAs and co-stained with αHA and DAPI 4 days later. IF microscopy analysis shows that luciferase

control knockdown does not affect HA signals in both cell lines, whereas fluorescence signal is lost in both cases after transfection with H3.X+Y-siRNA (Fig. 3.17). H3.X-siRNA specifically reduces fluorescence signal in HA-H3.X but not in HA-H3.Y expressing HeLa cells, H3.Y-siRNA shows reversed specificity.

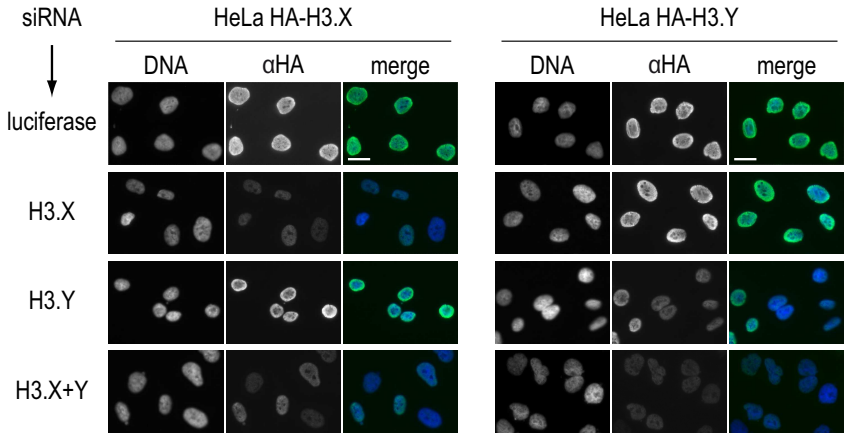

Figure 3.17. Evaluation of H3.X/Y siRNA specificity.
IF microscopy analysis of HeLa HA-H3.X (left) and -H3.Y (right) cells 4 days after siRNA transfection, shows specificity of H3.X-, H3.Y- and H3.X+Y-siRNAs. Cells were co-stained with DAPI (DNA, blue, left) and αHA (green, middle), overlay is shown on the right (merge). Scale bar equals 20 µm.

For global transcriptome analysis, two independent double siRNA-knockdowns of H3.Y, H3.X+Y and luciferase control in SO treated U2OS cells were performed. RNA was isolated and knockdown efficiency monitored by qPCR analysis (Fig. 3.18A). RNA was hybridized to Affymetrix Human Gene 1.0 ST arrays and expression levels in H3.Y and H3.X+Y relative to luciferase knockdown cells were determined. In H3.Y-siRNA knockdown cells, 293 genes were up- and 974 genes down-regulated, whereas cells treated with H3.X+Y-specific siRNAs showed 1106 up- and 1249 down-regulated genes (local false discovery rate cutoff 0.2). To eliminate H3.X-specific and off-target effects, genes de-regulated after both knockdowns were identified. Numbers of shared up- (73) and down-regulated (229) genes are depicted in Venn diagrams (Fig. 3.18B). GO enrichment analysis of overlapping genes revealed a long list of affected GO groups comprising, among others, cell cycle-controlling, chromatin organization, metabolic and signaling pathways (Fig. A.5, Appendix). To elucidate the connection between these groups, a simplified GO list was generated, containing major groups affected by the applied treatment. For shared up-regulated genes no such group could be identified, but down-regulated genes turned out to be mostly implicated in mitosis and DNA conformation changes (Fig. 3.18C). Since H3.Y seems to be implicated in mitosis and we previously noticed a reduction in cell number after H3.Y and H3.X+Y knock-down, U2OS cells were analyzed for their proliferation capacity after knockdown of H3.Y or H3.X+Y. Treatment

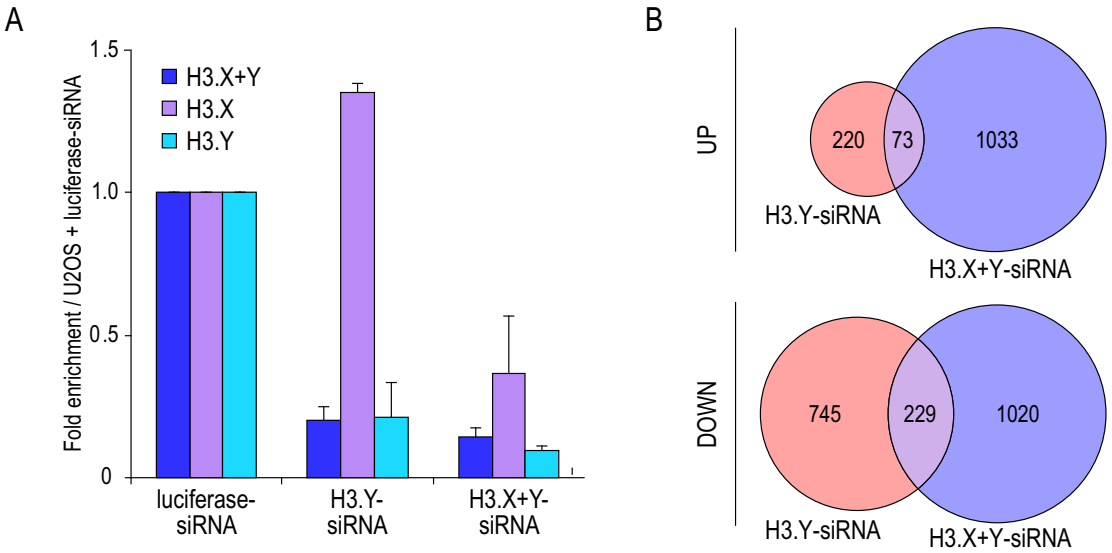

C

GO number	Node size	Sample match	Adjusted p-value	Term	Genes
0007067	250	20	2.939134e-08	Mitosis	CDC20, NUF2, ASPM, NSL1, KIF11, NCAPD3, NCAPD2, CDK2, NUP37, C14orf106, CDC6, CDC27, NDC80, BUB1, AURKA, NCAPG, MAD2L1, CCNA2, TTK, PBK
0071103	120	13	1.292158e-06	DNA conformation change	HIST2H2AC, NCAPD3, NCAPD2, MCM6, HIST1H2BK, NCAPG, HIST1H2BH, HIST1H2AH, HIST1H2BM, HIST1H2AB, HIST1H2BC, HIST1H2AK, MCM4

Figure 3.18. mRNA expression profiling of U2OS cells after H3.Y or H3.X+Y knockdown. Total RNA of SO treated U2OS cells transfected twice with siRNAs targeting luciferase, H3.Y or H3.X+Y, was used for global transcriptome analysis 4 days after first transfection. (A) qPCR analysis of H3.X and H3.Y levels in cDNA, transcribed from the same RNA used for microarray analysis, verifies efficient knockdown of H3.Y or H3.X+Y. Data is shown relative to HPRT1 and HMBS and normalized to luciferase-siRNA transfected cells. Error bars represent SEM of two independent biological experiments. (B) Venn diagrams show numbers of genes significantly up- (top) or down- (bottom) regulated after H3.Y (red) or H3.X+Y (blue) knockdown as identified by microarray analysis of two independent biological replicates when compared to luciferase control knockdown. Overlap represents number of genes that are de-regulated after both knockdowns (purple). (C) Simplified GO list of genes significantly down-regulated after both knockdowns. For a complete list see Fig. A.5. Node size = total number of genes analyzed in this node (GO term).

with H3.X-siRNA was also included to determine if novel H3 variants in general play a role in cell cycle control or if this is specific for H3.Y. Cells were transfected twice with siRNAs targeting luciferase (control), H3.X, H3.Y or H3.X+Y, seeded in E-plates one day after the second transfection and cell growth was monitored quantitatively over 96 h using a RTCA DP Analyzer. Growth curves clearly show that knockdown of both novel variants, but not the control knockdown, affects cell growth, although the influence of H3.Y seems to be stronger than that of H3.X (Fig. 3.19A, left). qPCR analysis of H3.X/Y levels 4 days after first transfection, shows knockdown efficiencies (Fig. 3.19A, right). Interestingly, single siRNA-knockdown of H3.X and H3.Y in HeLa cells, which do not express detectable amounts of H3.X/Y mRNA (see Fig. 3.3A), shows a similar growth phenotype for H3.Y, but hardly any effect of H3.X-siRNA knockdown (Fig. 3.19B). Cells were counted every day starting one day prior to transfection.

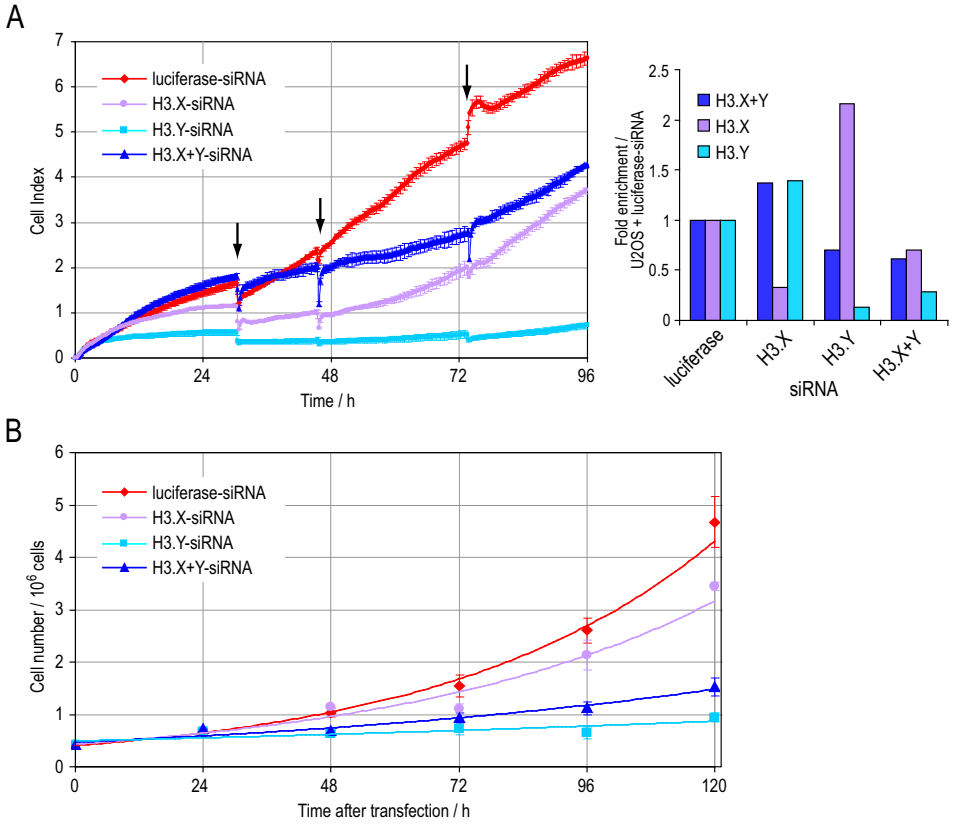

Figure 3.19. Influence of H3.X and/or H3.Y knockdown on proliferation capacity.
(A) U2OS cells were transfected twice with siRNAs targeting luciferase (control), H3.X, H3.Y and H3.X+Y and seeded in E-plates one day after the second transfection (t = 0 h). Cell growth was monitored over 4 days using the RTCA DP Analyzer. Error bars represent standard deviation of 4 (luciferase, H3.Y) or 2 (H3.X, H3.X+Y) technical replicates. Arrows indicate changes of growth medium. qPCR analysis of cDNA, synthesized from RNA extracted 4 days after first transfection, shows knockdown efficiency (right). H3.X/Y levels are depicted relative to HPRT1 and HMBS and normalized to luciferase control. (B) HeLa cells were transfected once with siRNAs targeting luciferase (control), H3.X, H3.Y and H3.X+Y. Cells were counted with the CASY Counter one day prior to transfection (t = 0 h) and for the following 5 days. Error bars represent standard deviation of 3 wells processed in parallel. In U2OS cells, knockdown of H3.X, H3.Y and H3.X+Y impair cell growth, whereas in HeLa cells only the knockdowns of H3.Y and H3.X+Y have this effect.

In summary, it could be shown that the depletion of H3.Y in U2OS cells has a strong effect on cell proliferation which is also reflected in the de-regulation of genes implicated in mitosis. Depletion of H3.X also has an impact on cell growth in U2OS but not in HeLa cells, whereas H3.Y-knockdown has a similar phenotype in both cell lines.

3.7 Expression of endogenous H3.X/Y protein in human brain

So far, expression of endogenous H3.Y protein has only been shown for U2OS cells. However, expression of H3.Y and partially also H3.X mRNA has been detected in different human tissues (see Fig. 3.3C), suggesting that also the corresponding protein(s) might be expressed in

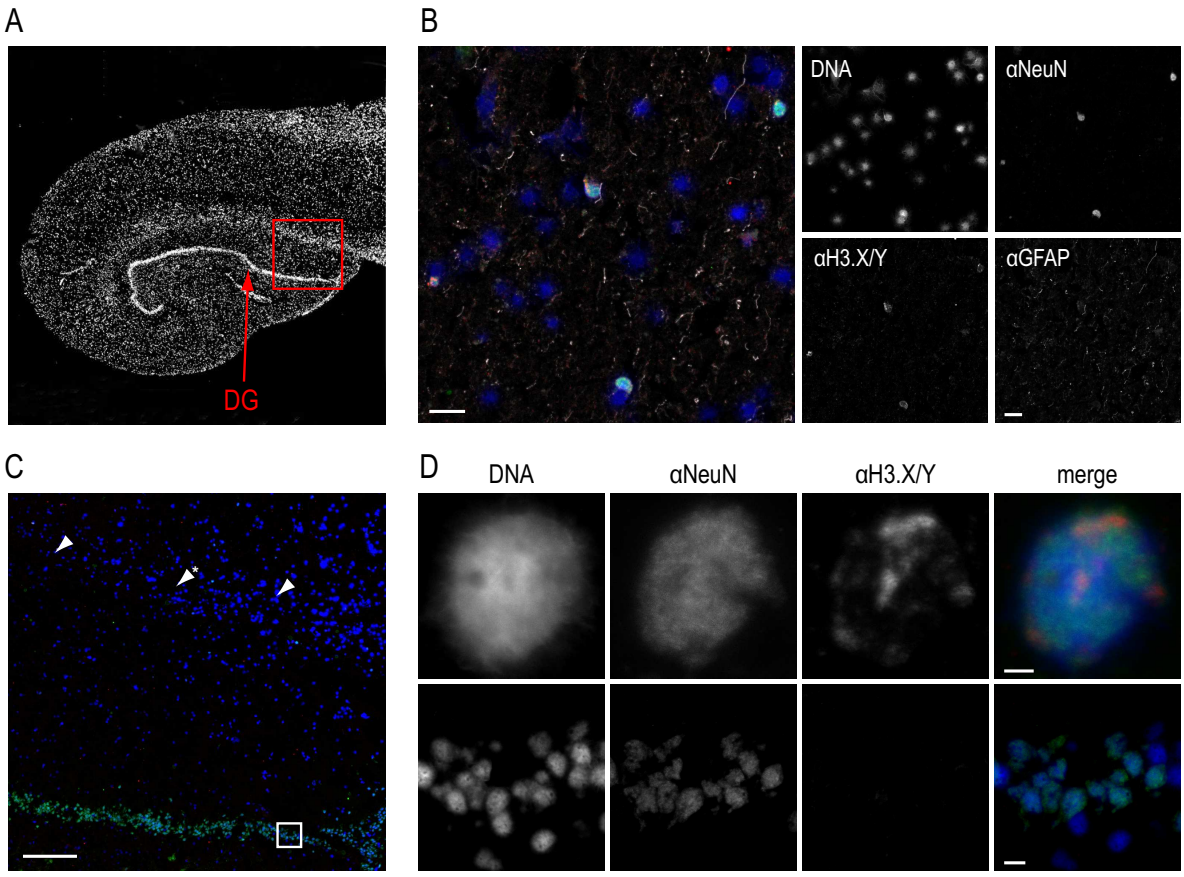

Figure 3.20. H3.X/Y expression in human brain.
Confocal imaging of commercially available human hippocampus sections, co-stained with αH3.X/Y (red), αNeuN (neuronal marker, green), αGFAP (astrocyte marker, white) and DAPI (DNA, blue), reveals H3.X/Y expression in a sub-population of neurons outside the dentate gyrus. (A) Overview picture of human hippocampus stained with DAPI (DNA). Individual 5x-pictures were merged using the photomerge function of Adobe Photoshop to create this view. The characteristic band of neurons (dentate gyrus = DG) is indicated with an arrow. (B) Area above DG with several H3.X/Y positive cells. Note that H3.X/Y overlaps with NeuN but not GFAP signal. Scale bar equals 20 µm. One representative staining out of three is shown. (C) Enlargement of boxed area indicated in (A). DG is visible at the bottom, arrowheads mark H3.X/Y positive neuronal cells. Scale bar equals 200 µm. One representative staining out of three is shown. (D) Higher resolution image of H3.X/Y positive cell, marked with an asterisk in (C), shows distinct sub-nuclear localization of H3.X/Y signal (top). Scale bar equals 2 µm. Enlargement of boxed section in (C) shows neurons in the DG without H3.X/Y staining (bottom). Scale bar equals 10 µm.

these tissues. Taking into account that many primate-specific genes are expressed in brain and reproductive organs (Tay et al., 2009) we chose to analyze commercially available sections of human hippocampus in IF to address the question of endogenous H3.X/Y protein expression in human tissues.

Sections were co-stained with αH3.X/Y, DAPI and in addition with αNeuN, marking neurons and αGFAP, staining astrocytes. Merged confocal images of DAPI-stained tissue with 5x-magnification shows organization of this brain area with the band of neuron nuclei indicating the dentate gyrus (DG) (Fig. 3.20A). Several nuclei stain positive with αH3.X/Y, all of them also showing a NeuN- but no GFAP-signal, identifying them as neurons (Fig. 3.20B). Higher

resolution images of boxed section marked in Fig. 3.20A finds some few αH3.X/Y stained cells, all localizing outside the DG (Fig. 3.20C, arrowheads). This finding is in accordance with our observation that only few U2OS cells show a general nuclear αH3.X/Y staining. Surprisingly, a close-up view of the H3.X/Y expressing cell indicated with an asterisk in Fig. 3.20C, shows a distinct sub-nuclear localization pattern of H3.X/Y protein, which is different to the staining in U2OS cells (Fig. 3.20D, top row). Neurons in the DG (boxed area in Fig. 3.20C) do not stain positive with αH3.X/Y (Fig. 3.20D, bottom row).
Concluding, H3.X and/or H3.Y protein is expressed in a subpopulation of neurons in the human hippocampus, highlighting the possibility that novel histone H3 variants might have cell-type specific functions. H3.X/Y protein(s) localizes solely to the nucleus and shows a distinct sub-nuclear localization pattern.

3.8 Epression of endogenous H3.X/Y protein in different primate species

H3.X and *H3.Y* constitute primate-specific genes. For humans, it could be shown that they encode for novel histone H3 variants and have an impact on the regulation of many genes implicated in cell cycle progression, but nothing is known about their expression and function in other primates. To address this question, primary fibroblasts from several primate species, each of them representing another branch of the phylogenetic tree of the primate lineage, were stained with αH3.X/Y and analyzed using confocal microscopy. Although none of the cells shows a general nuclear staining, as observed for some few cells in U2OS samples (see Fig. 3.9B), most of them do show the dotted H3.X/Y staining associated with the nuclear envelope (Fig. 3.21). Interestingly, the only cells that do not show this pattern, are derived from *Eulemur fulvus*, which is the most distantly related species to humans in this set, suggesting that *H3.X* and *H3.Y* have either evolved after the separation of the primate lineage in Haplorrhini and Strepsirrhini or the antibody binding site has been destroyed by mutations in this species. Since mouse and rat cells do not show this dotted αH3.X/Y staining (see Fig. 3.9C) and the αH3.X/Y antibody has been shown to be highly specific (see Fig. 3.8), it appears reasonable to think that this signal originates from some kind of H3.X/Y protein. Fueling this idea is the fact that the annotation of the *H3.X* locus has changed several times over the last years, predicting different splice forms (Fig. A.6, Appendix). However, multiple attempts to clone these alternative H3.X transcripts from human cDNA or quantify them in qPCR analysis have failed, making the expression of particularly these splice forms unlikely

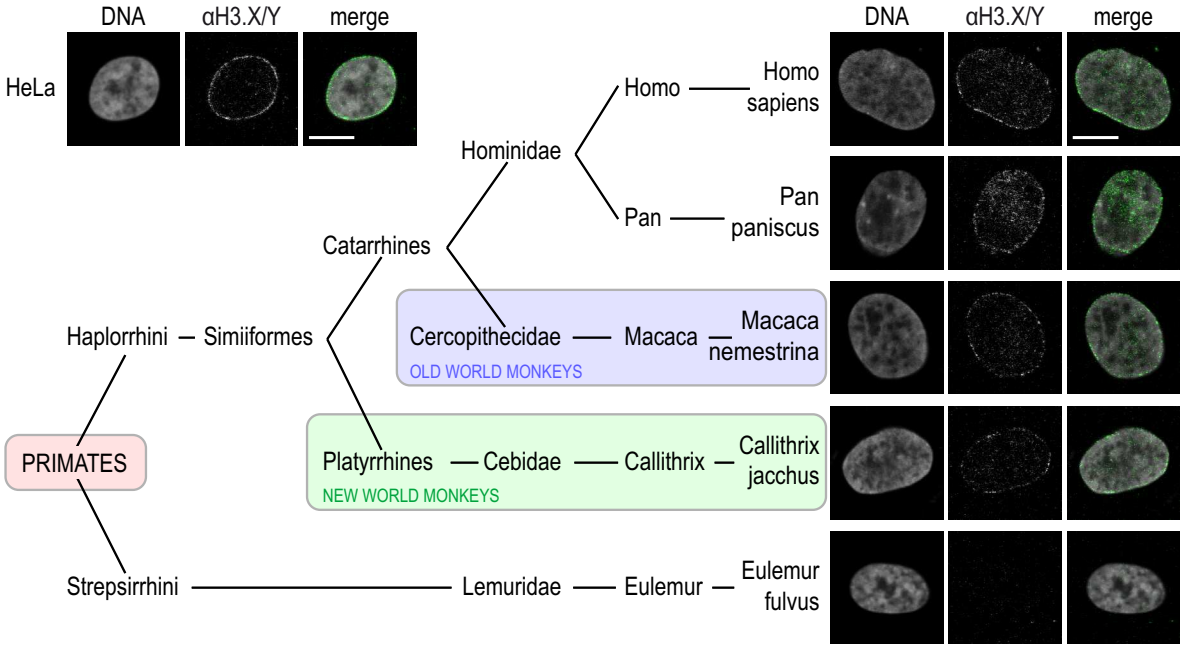

Figure 3.21. H3.X/Y expression in primates.
Confocal IF analysis of primary fibroblasts from different primates shows αH3.X/Y staining in all species analyzed, except for lemurs. The phylogenetic tree of the primate lineage illustrates evolutionary relationships. Cells were co-stained with TO-PRO3 (DNA, gray, left) and αH3.X/Y (green, middle). Overlay is shown on the right(merge). HeLa cells serve as positive control. Scale bar equals 10 µm.

(data not shown). Furthermore, also purification and subsequent mass spectrometrical identification of the protein causing this dotted staining has so far not been successful (data not shown).

In summary, αH3.X/Y antibody detects a protein associated with the nuclear envelope in several primate species. All attempts to confirm that this protein originates from the *H3.X* or *H3.Y* locus have failed so far. Future studies will have to reveal whether this staining is caused by another H3.X/Y protein species or is simply caused by a cross-reactivity of the antibody.

Taken together, it could be shown that H3.Y constitutes a novel histone H3 variant. H3.Y is expressed in human cells and specialized tissues, incorporated into chromatin, posttranslationally modified, and impacts the regulation of many genes implicated in cell cycle progression. The role of H3.X remains elusive and will have to be addressed in future experiments.

4 Discussion

4.1 *H3.X* and *H3.Y* are novel primate-specific histone genes

Searching the public database with the coding sequence of human histone *H3.1*, two novel histone H3 variant genes on human chromosome 5 have been identified, now termed *H3.X* and *H3.Y*. Consecutive database searches found *H3.X* and *H3.Y* genes also in the chimpanzee and the macaque genome but not in any other species. Although sequence data for other primates are not available yet, the absence of these genes in other mammals or even lower eukaryotes, suggests that they are primate-specific. Both genes are presumably dublications of one ancestral gene, as their sequences are highly similar (even in their 5' and 3' UTRs), with some differences in their putative promoter regions. Phylogenetic analysis of coding and 3' genomic sequences have revealed that *H3.X* and *H3.Y* are closer related to *H3.3* than to other H3 variant genes, proposing *H3.3* as the origin of *H3.X* and *H3.Y*, despite their lack of introns. The only primate-specific histone variant identified so far is H2BFWT, a protein only found in testis (Churikov et al., 2004). Interestingly, as observed for the *H2BFWT* locus, the genomic region syntenic to *H3.X* and *H3.Y* is much shorter in mouse and rat genomes, suggesting a common mechanism in the evolution of these variant genes.

4.2 Structure and behavior of H3.X and H3.Y proteins is similar to other H3 variants

Homology models of H3.X and H3.Y predict highly similar protein structures for novel and known H3. In the H3.X model, the extra C-terminus folds into an additional α-helix (Fig. 3.5) that is proposed to be in close proximity to one part of the H2A acidic patch (D90, E91, E92). H2A exposes a stretch of acidic amino acids on the surface of the nucleosome. This negatively charged patch is bound by the positively charged H4 tail of an adjacent nucleosome (Luger et al., 1997), thereby promoting folding into higher-order structures (Caterino and Hayes, 2007). Interaction of the H3.X C-terminus with H2A at these sites could stabilize the nucleo-

some and promote a more open chromatin structure by preventing the H4 tails of neighboring nucleosomes from binding. Future studies, using *in vitro* reconstituted chromatin, will address this question.

Despite the exchange of several functionally important residues, tagged H3.X and H3.Y behave almost identical to H3.1, H3.2 and H3.3. Matching their high structural similarity, all variants are stably incorporated into chromatin and show a solely nuclear localization (Figs. 3.4, 3.6 and 3.7). The only difference that has been observed in mononucleosome IPs was that H3.X and H3.Y primarily form heterotypic nucleosomes *in vivo* (Fig. 3.6), whereas H3.1 and H3.3 are only found in homotypic nucleosomes (Tagami et al., 2004). A similar behavior has been described for H2A variants H2A.Z (Viens et al., 2006) and macroH2A (Chakravarthy and Luger, 2006) which both assemble preferentially together with canonical H2A in nucleosomes.

4.3 H3.X and H3.Y mRNA, but only H3.Y protein is expressed in human cells

H3.X and H3.Y mRNA are both transcribed in the human osteosarcoma cell line U2OS (Fig. 3.3A). Some few U2OS cells (<0.1 %) show a general nuclear αH3.X/Y staining. This staining has been shown to be caused by H3.Y, thereby identifying H3.Y as novel primate-specific H3 variant. So far, it has been impossible to verify the presence of endogenous H3.X protein, neither for the currently nor for previously annotated transcripts. The expression of H3.X mRNA, but not H3.X protein in U2OS cells could mean that H3.X is a pseudogene without any function. Alternatively, H3.X could also be a regulatory ncRNA, maybe even regulating H3.Y expression (for details see section 4.6). In addition to these transformed cells, expression of H3.Y mRNA at low but significant levels has been detected in some human bone, breast, lung and ovary tumor tissues, as well as in testis and certain areas of the brain. Interestingly, H3.X mRNA could also be observed, albeit only in testis and brain (Fig. 3.3C). Consistent with these findings, H3.X/Y protein has been shown to be expressed in a subpopulation of neurons in the human hippocampus (Fig. 3.20), a brain region which mainly functions in the formation of long-term memories and the process of learning (Lagali et al., 2010). Many primate-specific genes are expressed in the brain, but they are not particularly enriched in this organ relative to all transcripts. In contrast, they are preferentially expressed in the reproductive system, where they may contribute to speciation (Tay et al., 2009). Taken together, *H3.Y*, and maybe *H3.X*, constitute the first primate-specific histone variants that are also expressed outside testis, likely confering specialized chromatin functions unique to

these higher vertebrates. Taking their tissue-specific expression patterns into account, it is tempting to speculate that H3.X and H3.Y might be involved in the process of speciation and, even more interestingly, in shaping higher brain functions.

4.4 A putative H3.X/Y protein is associated with nuclear pores

In all human cells and in cells of several closely related primate species, H3.X/Y protein staining can be observed at the nuclear envelope (Figs. 3.9B,F and 3.21). This staining co-localizes with nuclear pores as revealed by super-resolution IF analysis (Lothar Schermelleh, personal communication). Although it has so far not been possible to purify and analyze this H3.X/Y fraction in closer detail, the occurance of this staining in primates but not in rodents (Fig. 3.9B vs. C), together with the presence of an additional αH3.X/Y band in purified histones of human but not mouse cells (B bands in Fig. 3.13C i-iv vs. v), strongly argues for another H3.X/Y protein in primates. This protein has presumably a size of ∼35 kDa and associates with nuclear pores. It is most likely not a dimer of H3.X and/or H3.Y (Fig. 3.13D) or one of the previously annotated H3.X transcripts. Regarding the function of this unusually localized H3.X/Y fraction, one tantalizing hypothesis is that it tethers certain chromatin areas to nuclear pores. In yeast, it is well established that nuclear pores are implicated in the activation of associated genes. Moreover, nuclear pores also act as boundaries that prevent spreading of active or repressive chromatin marks. Several studies and the high level of conservation of some of the involved proteins suggest a similar situation in human cells (Köhler and Hurt, 2010). Taken together, this could mean that H3.X/Y proteins at the nuclear pore function as "insulator histones" that prevent spreading of PTMs, such as the methylation of H3K79, through the absence of the respective modifiable amino acid.

4.5 The number of H3.Y-expressing U2OS cells is increased by specific stress stimuli

H3.Y mRNA and protein is expressed in some few U2OS cells under normal growth conditions, but the number of cells expressing this novel H3 variant can be increased by nutritional starvation in combination with high cell density. Testing whether SO treatment can induce H3.Y expression also in other cell lines, it turned out that the ability to grow to such high cell densities is special for U2OS cells. A hint towards the cause for this resistance came from microarray analyses of HeLa HA-H3.Y cells, where *GAS1* was among the down-regulated genes

(Fig. 3.15). GAS1 blocks cell cycle progression in various cells (Sal et al., 1992, 1994) and is highly expressed under growth arrest conditions (Schneider et al., 1988). Its downregulation leads to a loss of contact inhibition and allows higher cell density (Evdokiou and Cowled, 1998). Surprisingly, normally grown U2OS cells have approximately 4-fold lower endogenous GAS1 mRNA levels than empty vector transfected HeLa cells, giving a possible explanation for the growth behavior of this cell line.
Although the number of cells expressing endogenous H3.Y is low, the individual cell expresses high levels (Fig. 3.9B). Compared to HeLa HA-H3.Y cells, the amount of endogenous H3.X+Y mRNA in these U2OS cells is more than 40-fold higher. This suggests that the induction of endogenous H3.Y expression is an all or nothing reaction, meaning that when the cell receives a certain signal or the threshold of an unknown factor is reached, H3.Y is expressed in massive amounts. The discrepancy in expression levels also explains the shortcoming of HeLa HA-H3.Y cells as a model system for H3.Y function, underlining the importance of identifying the main physiological trigger of H3.Y expression for future functional studies.

4.6 H3.Y influences gene expression and cell growth

To address the question of H3.Y's function, global transcriptome analyses have been performed, using U2OS cells depleted of H3.Y alone or in combination with H3.X. Some hundred genes were de-regulated after both RNAi knockdowns, implying an influence of H3.Y on gene expression. Whether this influence is direct or indirect will have to be investigated in future studies, generating binding profiles of H3.Y using ChIP-chip or ChIP-seq. Interestingly, more genes were down- rather than up-regulated, arguing for a role of H3.Y in the transcriptional activation of a subset of genes. In agreement with these results, H3.Y is primarily found in euchromatic regions (Fig. 3.9F). Most of the down-regulated genes are implicated in regulating the cell cycle and the structure of chromatin, matching the reported growth defect in U2OS cells with reduced levels of H3.Y (Fig. 3.19A). Surprisingly, although only less than 0.1 % of U2OS cells express H3.Y under normal growth conditions (Figs. 3.9B and 3.10), a strong and general growth defect is observed after H3.Y knockdown in these cells. It is therefore possible that all U2OS cells express H3.Y at a basal level (below the detection limit of our tools) that is crucial for the progression through the cell cycle. In line with this hypothesis, knockdown of H3.Y in HeLa cells, where no H3.Y mRNA has been detected (Fig. 3.3A), also strongly impairs cell growth (Fig. 3.19B). Recently, a similar phenotype has been reported for the linker histone variant H1.2. RNAi depletion of this variant leads to a de-regulation of ∼2 % of genes genome-wide, with most of them being down-regulated. Furthermore, the

lack of H1.2 causes a G1 arrest and expression changes in cell cycle-related genes (Sancho et al., 2008). This supports the idea of histone variants as important regulators of cell cycle progression and suggests that the stress-related appearance of H3.Y expressing U2OS cells might be caused by continued cell proliferation or the prevention of cell death.
Unlike the strong and cell line independent effect of H3.Y depletion on cell proliferation, the phenotypes of H3.X knockdown, alone or together with H3.Y, seem to depend on cellular background (Fig. 3.19). In U2OS cells, combined knockdown of H3.X and H3.Y has a milder effect on cell growth than H3.Y knockdown alone, whereas in HeLa cells the growth defect ist almost identical in both cases. Moreover, knockdown of H3.X has hardly any effect on HeLa cells, but U2OS cells are affected even more than after H3.X+Y depletion. Speculating, this could mean that H3.X and H3.Y are connected by some sort of regulatory feedback mechanism, which would also explain why H3.Y mRNA levels are reproducibly increased after knockdown of H3.X (Fig. 3.19A, right). HeLa cells might lack this regulation due to a lack of H3.X.
It will be interesting to see what future studies, investigating the regulatory network of H3.X and H3.Y, their role in cell proliferation, and in a subpopulation of neurons in the human hippocampus, will reveal about the endogenous function(s) of these novel H3 variants.

4.7 Outlook

4.7.1 Expression of endogenous H3.X and H3.Y

4.7.1.1 Trigger of H3.X and H3.Y expression in U2OS cells

In this work it could be shown that the number of U2OS cells expressing endogenous H3.Y (and H3.X) can be increased by nutritional and proliferative stress. However, all attempts to identify the actual component causing this effect under the described conditions, have failed so far. To get a better starting material for functional assays and to learn more about the expression of H3.X and H3.Y, potential candidates, such as signaling molecules or reactive oxygen species, will be tested for their ability to trigger H3.Y (and H3.X) expression.

4.7.1.2 H3.X and H3.Y promoter activity and regulation

A second approach to learn more about the endogenous expression of H3.X and H3.Y, possibly giving some indications about the nature of the factor triggering expression, is the analysis of the respective promoter sequences. Bioinformatic analysis of 1000 bp upstream of the ATG

using MatInspector (Genomatix Software GmbH) revealed a multitude of potential transcription factor binding sites, many of them also implicated in different types of cellular stress. To shed light on the regulation of endogenous H3.X and H3.Y expression, activity of these promoters and truncated versions of them will be assessed using a GFP-reporter system on an episomal vector. Promoter regions of interest will substitute the SV40 promoter of EBO-Sfi EGFP (SVG) thereby driving GFP expression when the promoter is active (Hake et al., 2003). To control for the presence of the promoter in the cell, an additional *DsRed2* gene (Clontech) with a separate promoter will be cloned into the vector. SVG will serve as positive and SVG without any promoter as negative control.

4.7.1.3 H3.X and H3.Y expression in human tissues

Given that *H3.X* and *H3.Y* genes are only present in primates, H3.X/Y proteins are expressed in a sub-population of neurons in the human hippocampus and the major function of this brain region is the formation of long-term memories and the process of learning (Lagali et al., 2010), it is tempting to speculate that these novel variants play an important role in the primate brain. In order to learn more about this interesting possibility, H3.X and H3.Y mRNA and protein expression will be analyzed by *in situ* hybridization and immunohistochemistry in samples of different human brain areas. Since our group is lacking the expertise to identify structures and cell types specific for certain brain regions and we also do not have access to human brain samples, a collaboration with a neurobiology group will have to be established for this part of the project. In addition to different brain regions, H3.X and H3.Y mRNA has also been detected in several normal and especially malignant human tissues. Therefore, their expression in human tumors and corresponding normal tissues will be investigated. It will be interesting to see, whether H3.X and/or H3.Y expression plays a role in the development of cancer in certain human organs.

4.7.1.4 H3.X and H3.Y expression during cell differentiation

Since novel histone variants show an effect on proliferation, it seems reasonable to think that they might also play a role in differentiation. However, because of their primate-specific appearance, it is not possible to use mouse embryonic stem (ES) cells for these assays and human ES cells are difficult to work with in Germany due to legal restrictions. An elegant way to circumvent these problems is the expression of Oct3/4, Sox2, c-Myc, and Klf4 in somatic cells, generating so-called induced pluripotent stem (iPS) cells. These cells behave like ES

cells, show all the specific features of ES cells and can differentiate into different lineages. First established for mouse embryonic or adult fibroblasts (Takahashi and Yamanaka, 2006; Wernig et al., 2007), this approach also works with human somatic cells (Takahashi et al., 2007; Yu et al., 2007). Using this fascinating tool, it will be possible to follow H3.X and H3.Y expression during differentiation of human cells.

4.7.2 *In vivo* function(s) of H3.X and H3.Y

4.7.2.1 Determination of H3.X/Y protein localization

A first step towards a deeper understanding of H3.X and H3.Y function is the high-resolution mapping of their localization on chromatin. To this end, DNA, isolated from bound material after αHA-IP of mononucleosomes from HeLa HA-H3.X and -H3.Y cells (see Fig. 3.6), will be subjected to high throughput sequencing, giving an initial idea about the genetic elements, H3.X/Y proteins are associated with. After having established a ChIP protocol working with αH3.X/Y antibody, the localization of endogenous H3.X/Y proteins in U2OS cells will be mapped using ChIP-chip.

4.7.2.2 Identification of H3.X and H3.Y chaperone(s)

Knowing where H3.X/Y proteins are localized leads to the question of how they are deposited. Judging from the sequence and what is known about mammalian H3 variant deposition, H3.X and H3.Y could be incorporated into chromatin by HIRA and/or Daxx (Tagami et al., 2004; Lewis et al., 2010). However, as this is pure speculation, it will be interesting to identify the chaperone(s) specific for H3.X and H3.Y protein. Following the procedure successfully used for identification of the H3.1- and H3.3-specific chaperones CAF-1 and HIRA, respectively (Tagami et al., 2004), both novel variants will be expressed with C-terminal FLAG- and HA- or GFP-tags in HeLa cells, tagged proteins will be pulled down from cytoplasmic and nuclear extracts together with associated (chaperone) complexes, which can subsequently be identified using mass spectrometry.

4.7.2.3 Replacement of *S. cerevisiae* H3 with H3.X and H3.Y

S. cerevisiae has two loci encoding for H3 and H4, each containing one *H3* (*HHT*) and one *H4* (*HHF*) gene. The genes at each locus are divergently transcribed and give rise to identical

proteins (Smith and Andrésson, 1983). We have access to strain WZY42, which has both endogenous loci disrupted and only one functional copy of the endogenous *HHT2-HHF2* locus on a plasmid also encoding the *URA3* marker gene (Weber et al., 2004). This strain allows the exchange of the *S. cerevisiae* H3 with different human H3 variants, to study their intrinsic properties. On plasmid pNOY439 (Keener et al., 1997), which carries the *HHT2-HHF2* locus with an N-terminal Myc-tag upstream of the *H3* gene and a *TRP* marker gene, the yeast *H3* gene has been replaced by human *H3.1*, *H3.3*, *H3.X* and *H3.Y* coding sequences, respectively. WZY42 will now be transformed with human H3 encoding plasmids and the plasmid encoding yeast H3 will be removed by selection on 5-fluorouracil (FOA) containing plates. A first attempt to generate these strains has failed, suggesting that yeast cells are severely affected by the exchange of endogenous H3 with human variants. This is particularly interesting as point mutations of most residues, even conserved and modifiable amino acids, do not impair viability (Nakanishi et al., 2008). It will also be interesting to see, if cells can cope better with human H3.3 than with the other variants, which would be expected as the yeast H3 constitutes an H3.3-like protein.

4.7.2.4 Effects of H3.X and H3.Y on cell cycle progression

Microarray analyses and growth curves of U2OS cells with reduced levels of H3.X, H3.Y or H3.X+Y point towards a role of H3.X and H3.Y in cell cycle progression. To determine where in this process novel H3 variants function, repeated and careful FACS analysis of the cell cycle profile in H3.X/Y knockdown cells will be necessary. As effects on the cell cycle profile are usually quite small and biological fluctuations rather pronounced, a well-founded statistical analysis will have to be deployed to make a statement about this issue. In addition, cell lines, expressing HA-H3.Y resistent to H3.Y- or H3.Y+Y-siRNAs, could be established to verify specificity of observed effects in rescue experiments.

4.7.3 *In vitro* characterization of H3.X and H3.Y

In parallel to the described experiments aiming to elucidate the function of H3.X and H3.Y *in vivo*, additional information can be acquired by characterizing the biochemical properties of these proteins. For this approach, both proteins have been cloned in vector pET21a(+) (Novagen) for recombinant expression in BL21-CodonPlus (DE3)-RIL (Stratagene) bacteria. Proteins will be expressed, purified and octamers of H3.X or H3.Y together with canonical H2A, H2B and H4 will be assembled. With these octamers, chromatin will be reconstituted

using a 25- or 12-mer of the 601 nucleosome positioning sequence (Lowary and Widom, 1998). This highly "variant pure" substrate can subsequently be used for various assays to determine the intrinsic stability, accessibility and behavior of H3.X- and H3.Y-containing chromatin fibers.

Abbreviations

α	Anti
aa	Amino acid
AOTF	Acousto Optic Tunable Filter
Bbd	Barr-body deficient
BMP4	Bone morphogenetic protein 4
BSA	Bovine serum albumin
CATD	Centromere targeting domain of CENP-A
CenH3	Centromere-specific histone H3
ChIP	Chromatin immunoprecipitation
DAPI	4',6-diamidino-2-phenylindole
DG	Dentate gyrus
DKK1	Dickkopf 1
DMEM	Dulbecco's Modified Eagle Medium
DMSO	Dimethylsulfoxide
Dnmt	DNA methyltransferase
3D-SIM	3-dimensional structured illumination microscopy
DSB	Double strand break
ELISA	Enzyme-linked immunosorbent assay
ES	Embryonic stem
FACS	Fluorescence-activated cell sorting
FCS	Fetal calf serum
FOA	5-fluorouracil
4HB	Four helix bundle
FRAP	Fluorescence recovery after photobleaching
GAS1	Growth arrest specific protein 1
GFAP	Glial fibrillary acidic protein
GO	Gene ontology
HEPES	2-(4-(2-Hydroxyethyl)- 1-piperazinyl)-ethansulfonsäure
HFD	Histone-fold domain
HIRIP3	HIRA interacting protein 3
HJURP	Holliday junction-recognizing protein
HRP	Horseradish peroxidase
IF	Immunofluorescence
IGFBP3	Insulin-like growth factor binding protein 1
IH	Immunohistochemistry
IP	Immunoprecipitation

iPS	Induced pluripotent stem
IPTG	Isopropyl β-D-1-Thiogalactopyranoside
lfdr	Local false discovery rate
MNase	Micrococcal nuclease
MS	Mass spectrometry
ND	Not determined
NeuN	Neuronal nuclei
ncRNAs	non-coding RNAs
no RevT	cDNA samples without reverse transcriptase
ON	Overnight
OVA	Ovalbumin
PAGE	Polyacrylamide gel electrophoresis
PBS	Phosphate buffered saline
P/S	Penicillin/Streptomycin
PTM	Posttranslational modification
qPCR	Quantitative PCR
RD	Replication dependent
RI	Replication independent
RITS	RNA-induced initiation of transcriptional gene silencing
RP-HPLC	Reversed phase-high performance liquid chromatography
RNAi	RNA interference
RT	Room temperature
S	Starvation
SDS	Sodium dodecyl sulfate
SEM	Standard error of the mean
siRNA	Short interfering RNA
SLBP	Stem loop binding protein
SO	Starvation and overgrowth
SPHK1	Sphingosine kinase 1
TBS	Tris buffered saline
TFA	Trifluoroacetic acid
TFBS	Transcription factor binding sites
TG	Throughout genome
TGFβ	Transforming growth factor β
TGFBR	TGFβ receptor
UTR	Untranslated region
WB	Western blot
Xi	Inactive X chromosome

Bibliography

Ahmad, K. and Henikoff, S. (2002), The histone variant H3.3 marks active chromatin by replication-independent nucleosome assembly. *Mol Cell* 9:1191–1200.

Andersen, J.S., Lam, Y.W., Leung, A.K.L., Ong, S.E., Lyon, C.E., Lamond, A.I. and Mann, M. (2005), Nucleolar proteome dynamics. *Nature* 433:77–83.

Bao, Y., Konesky, K., Park, Y.J., Rosu, S., Dyer, P.N., Rangasamy, D., Tremethick, D.J., Laybourn, P.J. and Luger, K. (2004), Nucleosomes containing the histone variant H2A.Bbd organize only 118 base pairs of DNA. *EMBO J* 23:3314–3324.

Becker, P.B. and Hörz, W. (2002), ATP-dependent nucleosome remodeling. *Annu Rev Biochem* 71:247–273.

Bernstein, E. and Allis, C.D. (2005), RNA meets chromatin. *Genes Dev* 19:1635–1655.

Bernstein, E. and Hake, S.B. (2006), The nucleosome: a little variation goes a long way. *Biochem Cell Biol* 84:505–517.

Bernstein, E., Muratore-Schroeder, T.L., Diaz, R.L., Chow, J.C., Changolkar, L.N., Shabanowitz, J., Heard, E., Pehrson, J.R., Hunt, D.F. and Allis, C.D. (2008), A phosphorylated subpopulation of the histone variant macroH2A1 is excluded from the inactive X chromosome and enriched during mitosis. *Proc Natl Acad Sci U S A* 105:1533–1538.

Black, B.E., Foltz, D.R., Chakravarthy, S., Luger, K., Woods, V.L. and Cleveland, D.W. (2004), Structural determinants for generating centromeric chromatin. *Nature* 430:578–582.

Black, B.E., Jansen, L.E.T., Maddox, P.S., Foltz, D.R., Desai, A.B., Shah, J.V. and Cleveland, D.W. (2007), Centromere identity maintained by nucleosomes assembled with histone H3 containing the CENP-A targeting domain. *Mol Cell* 25:309–322.

Blower, M.D., Sullivan, B.A. and Karpen, G.H. (2002), Conserved organization of centromeric chromatin in flies and humans. *Dev Cell* 2:319–330.

Bönisch, C., Nieratschker, S.M., Orfanos, N.K. and Hake, S.B. (2008), Chromatin proteomics and epigenetic regulatory circuits. *Expert Rev Proteomics* 5:105–119.

Boulard, M., Gautier, T., Mbele, G.O., Gerson, V., Hamiche, A., Angelov, D., Bouvet, P. and Dimitrov, S. (2006), The NH2 tail of the novel histone variant H2BFWT exhibits properties distinct from conventional H2B with respect to the assembly of mitotic chromosomes. *Mol Cell Biol* 26:1518–1526.

Burma, S., Chen, B.P., Murphy, M., Kurimasa, A. and Chen, D.J. (2001), ATM phosphorylates histone H2AX in response to DNA double-strand breaks. *J Biol Chem* 276:42462–42467.

Buschbeck, M., Uribesalgo, I., Wibowo, I., Rué, P., Martin, D., Gutierrez, A., Morey, L., Guigó, R., López-Schier, H. and Croce, L.D. (2009), The histone variant macroH2A is an epigenetic regulator of key developmental genes. *Nat Struct Mol Biol* 16:1074–1079.

Bustin, M., Catez, F. and Lim, J.H. (2005), The dynamics of histone H1 function in chromatin. *Mol Cell* 17:617–620.

Caterino, T.L. and Hayes, J.J. (2007), Chromatin structure depends on what's in the nucleosome's pocket. *Nat Struct Mol Biol* 14:1056–1058.

Chadwick, B.P. and Willard, H.F. (2001a), Histone H2A variants and the inactive X chromosome: identification of a second macroH2A variant. *Hum Mol Genet* 10:1101–1113.

Chadwick, B.P. and Willard, H.F. (2001b), A novel chromatin protein, distantly related to histone H2A, is largely excluded from the inactive X chromosome. *J Cell Biol* 152:375–384.

Chakravarthy, S. and Luger, K. (2006), The histone variant macro-H2A preferentially forms "hybrid nucleosomes". *J Biol Chem* 281:25522–25531.

Chang, L., Loranger, S.S., Mizzen, C., Ernst, S.G., Allis, C.D. and Annunziato, A.T. (1997), Histones in transit: cytosolic histone complexes and diacetylation of H4 during nucleosome assembly in human cells. *Biochemistry* 36:469–480.

Chen, H.T., Bhandoola, A., Difilippantonio, M.J., Zhu, J., Brown, M.J., Tai, X., Rogakou, E.P., Brotz, T.M., Bonner, W.M., Ried, T. and Nussenzweig, A. (2000), Response to RAG-mediated VDJ cleavage by NBS1 and gamma-H2AX. *Science* 290:1962–1965.

Cheng, Y., Miura, R.M. and Tian, B. (2006), Prediction of mRNA polyadenylation sites by support vector machine. *Bioinformatics* 22:2320–2325.

Cheung, W.L., Ajiro, K., Samejima, K., Kloc, M., Cheung, P., Mizzen, C.A., Beeser, A., Etkin, L.D., Chernoff, J., Earnshaw, W.C. and Allis, C.D. (2003), Apoptotic phosphorylation of histone H2B is mediated by mammalian sterile twenty kinase. *Cell* 113:507–517.

Churikov, D., Siino, J., Svetlova, M., Zhang, K., Gineitis, A., Bradbury, E.M. and Zalensky, A. (2004), Novel human testis-specific histone H2B encoded by the interrupted gene on the X chromosome. *Genomics* 84:745–756.

Clausell, J., Happel, N., Hale, T.K., Doenecke, D. and Beato, M. (2009), Histone H1 subtypes differentially modulate chromatin condensation without preventing ATP-dependent remodeling by SWI/SNF or NURF. *PLoS One* 4:e0007243.

Clayton, A.L. and Mahadevan, L.C. (2003), MAP kinase-mediated phosphoacetylation of histone H3 and inducible gene regulation. *FEBS Lett* 546:51–58.

Coon, J.J., Ueberheide, B., Syka, J.E.P., Dryhurst, D.D., Ausio, J., Shabanowitz, J. and Hunt, D.F. (2005), Protein identification using sequential ion/ion reactions and tandem mass spectrometry. *Proc Natl Acad Sci U S A* 102:9463–9468.

Cosgrove, M.S. (2007), Histone proteomics and the epigenetic regulation of nucleosome mobility. *Expert Rev Proteomics* 4:465–478.

Costanzi, C. and Pehrson, J.R. (1998), Histone macroH2A1 is concentrated in the inactive X chromosome of female mammals. *Nature* 393:599–601.

Costanzi, C. and Pehrson, J.R. (2001), MACROH2A2, a new member of the MARCOH2A core histone family. *J Biol Chem* 276:21776–21784.

Davey, C.A., Sargent, D.F., Luger, K., Maeder, A.W. and Richmond, T.J. (2002), Solvent mediated interactions in the structure of the nucleosome core particle at 1.9 a resolution. *J Mol Biol* 319:1097–1113.

de la Barre, A.E., Angelov, D., Molla, A. and Dimitrov, S. (2001), The N-terminus of histone H2B, but not that of histone H3 or its phosphorylation, is essential for chromosome condensation. *EMBO J* 20:6383–6393.

Donati, C., Cencetti, F., Palma, C.D., Rapizzi, E., Brunelli, S., Cossu, G., Clementi, E. and Bruni, P. (2009), TGFbeta protects mesoangioblasts from apoptosis via sphingosine kinase-1 regulation. *Cell Signal* 21:228–236.

Doyen, C.M., Montel, F., Gautier, T., Menoni, H., Claudet, C., Delacour-Larose, M., Angelov, D., Hamiche, A., Bednar, J., Faivre-Moskalenko, C., Bouvet, P. and Dimitrov, S. (2006), Dissection of the unusual structural and functional properties of the variant H2A.Bbd nucleosome. *EMBO J* 25:4234–4244.

Drané, P., Ouararhni, K., Depaux, A., Shuaib, M. and Hamiche, A. (2010), The death-associated protein DAXX is a novel histone chaperone involved in the replication-independent deposition of H3.3. *Genes Dev* 24:1253–1265.

Dryhurst, D., Ishibashi, T., Rose, K.L., Eirín-López, J.M., McDonald, D., Silva-Moreno, B., Veldhoen, N., Helbing, C.C., Hendzel, M.J., Shabanowitz, J., Hunt, D.F. and Ausió, J. (2009), Characterization of the histone H2A.Z-1 and H2A.Z-2 isoforms in vertebrates. *BMC Biol* 7:86.

Dunleavy, E.M., Roche, D., Tagami, H., Lacoste, N., Ray-Gallet, D., Nakamura, Y., Daigo, Y., Nakatani, Y. and Almouzni-Pettinotti, G. (2009), HJURP is a cell-cycle-dependent maintenance and deposition factor of CENP-A at centromeres. *Cell* 137:485–497.

Eckey, M., Hong, W., Papaioannou, M. and Baniahmad, A. (2007), The nucleosome assembly activity of NAP1 is enhanced by Alien. *Mol Cell Biol* 27:3557–3568.

Eirín-López, J.M., González-Tizón, A.M., Martínez, A. and Méndez, J. (2004), Birth-and-death evolution with strong purifying selection in the histone H1 multigene family and the origin of orphon H1 genes. *Mol Biol Evol* 21:1992–2003.

Eirín-López, J.M., Ishibashi, T. and Ausió, J. (2008), H2A.Bbd: a quickly evolving hypervariable mammalian histone that destabilizes nucleosomes in an acetylation-independent way. *FASEB J* 22:316–326.

Eitoku, M., Sato, L., Senda, T. and Horikoshi, M. (2008), Histone chaperones: 30 years from isolation to elucidation of the mechanisms of nucleosome assembly and disassembly. *Cell Mol Life Sci* 65:414–444.

Elsaesser, S.J., Goldberg, A.D. and Allis, C.D. (2010), New functions for an old variant: no substitute for histone H3.3. *Curr Opin Genet Dev* 20:110–117.

Espada, J. and Esteller, M. (2010), DNA methylation and the functional organization of the nuclear compartment. *Semin Cell Dev Biol* 21:238–246.

Evdokiou, A. and Cowled, P.A. (1998), Growth-regulatory activity of the growth arrest-specific gene, GAS1, in NIH3T3 fibroblasts. *Exp Cell Res* 240:359–367.

Faast, R., Thonglairoam, V., Schulz, T.C., Beall, J., Wells, J.R., Taylor, H., Matthaei, K., Rathjen, P.D., Tremethick, D.J. and Lyons, I. (2001), Histone variant H2A.Z is required for early mammalian development. *Curr Biol* 11:1183–1187.

Fan, Y., Sirotkin, A., Russell, R.G., Ayala, J. and Skoultchi, A.I. (2001), Individual somatic H1 subtypes are dispensable for mouse development even in mice lacking the H1(0) replacement subtype. *Mol Cell Biol* 21:7933–7943.

Fan, Y., Nikitina, T., Morin-Kensicki, E.M., Zhao, J., Magnuson, T.R., Woodcock, C.L. and Skoultchi, A.I. (2003), H1 linker histones are essential for mouse development and affect nucleosome spacing in vivo. *Mol Cell Biol* 23:4559–4572.

Fan, Y., Nikitina, T., Zhao, J., Fleury, T.J., Bhattacharyya, R., Bouhassira, E.E., Stein, A., Woodcock, C.L. and Skoultchi, A.I. (2005), Histone H1 depletion in mammals alters global chromatin structure but causes specific changes in gene regulation. *Cell* 123:1199–1212.

Fanayan, S., Firth, S.M., Butt, A.J. and Baxter, R.C. (2000), Growth inhibition by insulin-like growth factor-binding protein-3 in T47D breast cancer cells requires transforming growth factor-beta (TGF-beta) and the type II TGF-beta receptor. *J Biol Chem* 275:39146–39151.

Fanayan, S., Firth, S.M. and Baxter, R.C. (2002), Signaling through the Smad pathway by insulin-like growth factor-binding protein-3 in breast cancer cells. Relationship to transforming growth factor-beta 1 signaling. *J Biol Chem* 277:7255–7261.

Foltz, D.R., Jansen, L.E.T., Bailey, A.O., Yates, J.R., Bassett, E.A., Wood, S., Black, B.E. and Cleveland, D.W. (2009), Centromere-specific assembly of CENP-a nucleosomes is mediated by HJURP. *Cell* 137:472–484.

Fuchs, J., Demidov, D., Houben, A. and Schubert, I. (2006), Chromosomal histone modification patterns–from conservation to diversity. *Trends Plant Sci* 11:199–208.

Gabrilovich, D.I., Cheng, P., Fan, Y., Yu, B., Nikitina, E., Sirotkin, A., Shurin, M., Oyama, T., Adachi, Y., Nadaf, S., Carbone, D.P. and Skoultchi, A.I. (2002), H1(0) histone and differentiation of dendritic cells. A molecular target for tumor-derived factors. *J Leukoc Biol* 72:285–296.

Gamble, M.J. and Kraus, W.L. (2010), Multiple facets of the unique histone variant macroH2A: From genomics to cell biology. *Cell Cycle* 9.

Gamble, M.J., Frizzell, K.M., Yang, C., Krishnakumar, R. and Kraus, W.L. (2010), The histone variant macroH2A1 marks repressed autosomal chromatin, but protects a subset of its target genes from silencing. *Genes Dev* 24:21–32.

Garcia, B.A., Thomas, C.E., Kelleher, N.L. and Mizzen, C.A. (2008), Tissue-specific expression and post-translational modification of histone H3 variants. *J Proteome Res* 7:4225–4236.

Gautier, T., Abbott, D.W., Molla, A., Verdel, A., Ausio, J. and Dimitrov, S. (2004), Histone variant H2ABbd confers lower stability to the nucleosome. *EMBO Rep* 5:715–720.

Gerstein, M.B., Bruce, C., Rozowsky, J.S., Zheng, D., Du, J., Korbel, J.O., Emanuelsson, O., Zhang, Z.D., Weissman, S. and Snyder, M. (2007), What is a gene, post-ENCODE? History and updated definition. *Genome Res* 17:669–681.

Gineitis, A.A., Zalenskaya, I.A., Yau, P.M., Bradbury, E.M. and Zalensky, A.O. (2000), Human sperm telomere-binding complex involves histone H2B and secures telomere membrane attachment. *J Cell Biol* 151:1591–1598.

Goldberg, A.D., Allis, C.D. and Bernstein, E. (2007), Epigenetics: a landscape takes shape. *Cell* 128:635–638.

Goldberg, A.D., Banaszynski, L.A., Noh, K.M., Lewis, P.W., Elsaesser, S.J., Stadler, S., Dewell, S., Law, M., Guo, X., Li, X., Wen, D., Chapgier, A., DeKelver, R.C., Miller, J.C., Lee, Y.L., Boydston, E.A., Holmes, M.C., Gregory, P.D., Greally, J.M., Rafii, S., Yang, C., Scambler, P.J., Garrick, D., Gibbons, R.J., Higgs, D.R., Cristea, I.M., Urnov, F.D., Zheng, D. and Allis, C.D. (2010), Distinct factors control histone variant H3.3 localization at specific genomic regions. *Cell* 140:678–691.

González-Romero, R., Ausió, J., Méndez, J. and Eirín-López, J.M. (2008), Early evolution of histone genes: prevalence of an 'orphon' H1 lineage in protostomes and birth-and-death process in the H2A family. *J Mol Evol* 66:505–518.

González-Romero, R., Rivera-Casas, C., Ausió, J., Méndez, J. and Eirín-López, J.M. (2010), Birth-and-death long-term evolution promotes histone H2B Variant diversification in the male germinal cell line. *Mol Biol Evol* 27:1802–1812.

Govin, J., Escoffier, E., Rousseaux, S., Kuhn, L., Ferro, M., Thévenon, J., Catena, R., Davidson, I., Garin, J., Khochbin, S. and Caron, C. (2007), Pericentric heterochromatin reprogramming by new histone variants during mouse spermiogenesis. *J Cell Biol* 176:283–294.

Green, C.M. and Almouzni, G. (2003), Local action of the chromatin assembly factor CAF-1 at sites of nucleotide excision repair in vivo. *EMBO J* 22:5163–5174.

Guex, N. and Peitsch, M.C. (1997), SWISS-MODEL and the Swiss-PdbViewer: an environment for comparative protein modeling. *Electrophoresis* 18:2714–2723.

Gustafsson, M.G.L., Shao, L., Carlton, P.M., Wang, C.J.R., Golubovskaya, I.N., Cande, W.Z., Agard, D.A. and Sedat, J.W. (2008), Three-dimensional resolution doubling in wide-field fluorescence microscopy by structured illumination. *Biophys J* 94:4957–4970.

Gévry, N., Chan, H.M., Laflamme, L., Livingston, D.M. and Gaudreau, L. (2007), p21 transcription is regulated by differential localization of histone H2A.Z. *Genes Dev* 21:1869–1881.

Hake, S.B. and Allis, C.D. (2006), Histone H3 variants and their potential role in indexing mammalian genomes: the "H3 barcode hypothesis". *Proc Natl Acad Sci U S A* 103:6428–6435.

Hake, S.B., Tobin, H.M., Steimle, V. and Denzin, L.K. (2003), Comparison of the transcriptional regulation of classical and non-classical MHC class II genes. *Eur J Immunol* 33:2361–2371.

Hake, S.B., Garcia, B.A., Kauer, M., Baker, S.P., Shabanowitz, J., Hunt, D.F. and Allis, C.D. (2005), Serine 31 phosphorylation of histone variant H3.3 is specific to regions bordering centromeres in metaphase chromosomes. *Proc Natl Acad Sci U S A* 102:6344–6349.

Hake, S.B., Garcia, B.A., Duncan, E.M., Kauer, M., Dellaire, G., Shabanowitz, J., Bazett-Jones, D.P., Allis, C.D. and Hunt, D.F. (2006), Expression patterns and post-translational modifications associated with mammalian histone H3 variants. *J Biol Chem* 281:559–568.

Hanahan, D. (1985), Techniques for transformation of Escherichia coli. D.M. Glover, ed., DNA cloning; a practical approach, vol. 1, I.R.L. Press, Oxford, United Kingdom, 109–135.

Happel, N. and Doenecke, D. (2009), Histone H1 and its isoforms: contribution to chromatin structure and function. *Gene* 431:1–12.

Happel, N., Schulze, E. and Doenecke, D. (2005), Characterisation of human histone H1x. *Biol Chem* 386:541–551.

Hemmerich, P., Weidtkamp-Peters, S., Hoischen, C., Schmiedeberg, L., Erliandri, I. and Diekmann, S. (2008), Dynamics of inner kinetochore assembly and maintenance in living cells. *J Cell Biol* 180:1101–1114.

Hendzel, M.J., Wei, Y., Mancini, M.A., Hooser, A.V., Ranalli, T., Brinkley, B.R., Bazett-Jones, D.P. and Allis, C.D. (1997), Mitosis-specific phosphorylation of histone H3 initiates primarily within pericentromeric heterochromatin during G2 and spreads in an ordered fashion coincident with mitotic chromosome condensation. *Chromosoma* 106:348–360.

Heo, K., Kim, H., Choi, S.H., Choi, J., Kim, K., Gu, J., Lieber, M.R., Yang, A.S. and An, W. (2008), FACT-mediated exchange of histone variant H2AX regulated by phosphorylation of H2AX and ADP-ribosylation of Spt16. *Mol Cell* 30:86–97.

Howman, E.V., Fowler, K.J., Newson, A.J., Redward, S., MacDonald, A.C., Kalitsis, P. and Choo, K.H. (2000), Early disruption of centromeric chromatin organization in centromere protein A (Cenpa) null mice. *Proc Natl Acad Sci U S A* 97:1148–1153.

Huyen, Y., Zgheib, O., Ditullio, R.A., Gorgoulis, V.G., Zacharatos, P., Petty, T.J., Sheston, E.A., Mellert, H.S., Stavridi, E.S. and Halazonetis, T.D. (2004), Methylated lysine 79 of histone H3 targets 53BP1 to DNA double-strand breaks. *Nature* 432:406–411.

Im, H., Park, C., Feng, Q., Johnson, K.D., Kiekhaefer, C.M., Choi, K., Zhang, Y. and Bresnick, E.H. (2003), Dynamic regulation of histone H3 methylated at lysine 79 within a tissue-specific chromatin domain. *J Biol Chem* 278:18346–18352.

Ishibashi, T., Li, A., Eirín-López, J.M., Zhao, M., Missiaen, K., Abbott, D.W., Meistrich, M., Hendzel, M.J. and Ausió, J. (2010), H2A.Bbd: an X-chromosome-encoded histone involved in mammalian spermiogenesis. *Nucleic Acids Res* 38:1780–1789.

Ishimi, Y., Hirosumi, J., Sato, W., Sugasawa, K., Yokota, S., Hanaoka, F. and Yamada, M. (1984), Purification and initial characterization of a protein which facilitates assembly of nucleosome-like structure from mammalian cells. *Eur J Biochem* 142:431–439.

Ishimi, Y., Kojima, M., Yamada, M. and Hanaoka, F. (1987), Binding mode of nucleosome-assembly protein (AP-I) and histones. *Eur J Biochem* 162:19–24.

Ismail, I.H. and Hendzel, M.J. (2008), The gamma-H2A.X: is it just a surrogate marker of double-strand breaks or much more? *Environ Mol Mutagen* 49:73–82.

Ito, T., Bulger, M., Kobayashi, R. and Kadonaga, J.T. (1996), Drosophila NAP-1 is a core histone chaperone that functions in ATP-facilitated assembly of regularly spaced nucleosomal arrays. *Mol Cell Biol* 16:3112–3124.

Izzo, A., Kamieniarz, K. and Schneider, R. (2008), The histone H1 family: specific members, specific functions? *Biol Chem* 389:333–343.

Jansen, L.E.T., Black, B.E., Foltz, D.R. and Cleveland, D.W. (2007), Propagation of centromeric chromatin requires exit from mitosis. *J Cell Biol* 176:795–805.

Keener, J., Dodd, J.A., Lalo, D. and Nomura, M. (1997), Histones H3 and H4 are components of upstream activation factor required for the high-level transcription of yeast rDNA by RNA polymerase I. *Proc Natl Acad Sci U S A* 94:13458–13462.

Köhler, A. and Hurt, E. (2010), Gene regulation by nucleoporins and links to cancer. *Mol Cell* 38:6–15.

Köhler, G. and Milstein, C. (1975), Continuous cultures of fused cells secreting antibody of predefined specificity. *Nature* 256:495–497.

Kimmins, S. and Sassone-Corsi, P. (2005), Chromatin remodelling and epigenetic features of germ cells. *Nature* 434:583–589.

Koning, L.D., Corpet, A., Haber, J.E. and Almouzni, G. (2007), Histone chaperones: an escort network regulating histone traffic. *Nat Struct Mol Biol* 14:997–1007.

Konishi, A., Shimizu, S., Hirota, J., Takao, T., Fan, Y., Matsuoka, Y., Zhang, L., Yoneda, Y., Fujii, Y., Skoultchi, A.I. and Tsujimoto, Y. (2003), Involvement of Histone H1.2 in Apoptosis Induced by DNA Double-Strand Breaks. *Cell* 114:673 – 688.

Korber, P. and Hörz, W. (2004), SWRred not shaken; mixing the histones. *Cell* 117:5–7.

Kozak, M. (1991), An analysis of vertebrate mRNA sequences: intimations of translational control. *J Cell Biol* 115:887–903.

Krude, T. (1995), Chromatin assembly factor 1 (CAF-1) colocalizes with replication foci in HeLa cell nuclei. *Exp Cell Res* 220:304–311.

Lagali, P., Corcoran, C. and Picketts, D. (2010), Hippocampus development and function: role of epigenetic factors and implications for cognitive disease. *Clinical Genetics* :no–no.

Lee, J., Park, H.S., Kim, H.H., Yun, Y.J., Lee, D.R. and Lee, S. (2009), Functional polymorphism in H2BFWT-5'UTR is associated with susceptibility to male infertility. *J Cell Mol Med* 13:1942–1951.

Lewis, P.W., Elsaesser, S.J., Noh, K.M., Stadler, S.C. and Allis, C.D. (2010), Daxx is an H3.3-specific histone chaperone and cooperates with ATRX in replication-independent chromatin assembly at telomeres. *Proc Natl Acad Sci U S A* .

Li, A., Maffey, A.H., Abbott, W.D., e Silva, N.C., Prunell, A., Siino, J., Churikov, D., Zalensky, A.O. and Ausió, J. (2005), Characterization of nucleosomes consisting of the human testis/sperm-specific histone H2B variant (hTSH2B). *Biochemistry* 44:2529–2535.

Lorain, S., Quivy, J.P., Monier-Gavelle, F., Scamps, C., Lécluse, Y., Almouzni, G. and Lipinski, M. (1998), Core histones and HIRIP3, a novel histone-binding protein, directly interact with WD repeat protein HIRA. *Mol Cell Biol* 18:5546–5556.

Lowary, P.T. and Widom, J. (1998), New DNA sequence rules for high affinity binding to histone octamer and sequence-directed nucleosome positioning. *J Mol Biol* 276:19–42.

Loyola, A. and Almouzni, G. (2004), Histone chaperones, a supporting role in the limelight. *Biochim Biophys Acta* 1677:3–11.

Luger, K., Mäder, A.W., Richmond, R.K., Sargent, D.F. and Richmond, T.J. (1997), Crystal structure of the nucleosome core particle at 2.8 A resolution. *Nature* 389:251–260.

Luk, E., Vu, N.D., Patteson, K., Mizuguchi, G., Wu, W.H., Ranjan, A., Backus, J., Sen, S., Lewis, M., Bai, Y. and Wu, C. (2007), Chz1, a nuclear chaperone for histone H2AZ. *Mol Cell* 25:357–368.

Mahadevaiah, S.K., Turner, J.M., Baudat, F., Rogakou, E.P., de Boer, P., Blanco-Rodríguez, J., Jasin, M., Keeney, S., Bonner, W.M. and Burgoyne, P.S. (2001), Recombinational DNA double-strand breaks in mice precede synapsis. *Nat Genet* 27:271–276.

Maier, V.K., Chioda, M. and Becker, P.B. (2008), ATP-dependent chromatosome remodeling. *Biol Chem* 389:345–352.

Marzluff, W.F., Wagner, E.J. and Duronio, R.J. (2008), Metabolism and regulation of canonical histone mRNAs: life without a poly(A) tail. *Nat Rev Genet* 9:843–854.

Matsuda, R., Hori, T., Kitamura, H., Takeuchi, K., Fukagawa, T. and Harata, M. (2010), Identification and characterization of the two isoforms of the vertebrate H2A.Z histone variant. *Nucleic Acids Res* 38:4263–4273.

Mazurkiewicz, J., Kepert, J.F. and Rippe, K. (2006), On the mechanism of nucleosome assembly by histone chaperone NAP1. *J Biol Chem* 281:16462–16472.

McBryant, S.J., Park, Y.J., Abernathy, S.M., Laybourn, P.J., Nyborg, J.K. and Luger, K. (2003), Preferential binding of the histone (H3-H4)2 tetramer by NAP1 is mediated by the amino-terminal histone tails. *J Biol Chem* 278:44574–44583.

Meergans, T., Albig, W. and Doenecke, D. (1997), Varied expression patterns of human H1 histone genes in different cell lines. *DNA Cell Biol* 16:1041–1049.

Mehta, G.D., Agarwal, M.P. and Ghosh, S.K. (2010), Centromere identity: a challenge to be faced. *Mol Genet Genomics* 284:75–94.

Montel, F., Fontaine, E., St-Jean, P., Castelnovo, M. and Faivre-Moskalenko, C. (2007), Atomic force microscopy imaging of SWI/SNF action: mapping the nucleosome remodeling and sliding. *Biophys J* 93:566–578.

Moustakas, A. and Heldin, C.H. (2009), The regulation of TGFbeta signal transduction. *Development* 136:3699–3714.

Nakagawa, S., Niimura, Y., Gojobori, T., Tanaka, H. and ichiro Miura, K. (2008), Diversity of preferred nucleotide sequences around the translation initiation codon in eukaryote genomes. *Nucleic Acids Res* 36:861–871.

Nakanishi, S., Sanderson, B.W., Delventhal, K.M., Bradford, W.D., Staehling-Hampton, K. and Shilatifard, A. (2008), A comprehensive library of histone mutants identifies nucleosomal residues required for H3K4 methylation. *Nat Struct Mol Biol* 15:881–888.

Nei, M. and Rooney, A.P. (2005), Concerted and birth-and-death evolution of multigene families. *Annu Rev Genet* 39:121–152.

Nunez, E., Fu, X.D. and Rosenfeld, M.G. (2009), Nuclear organization in the 3D space of the nucleus - cause or consequence? *Curr Opin Genet Dev* 19:424–436.

Palmer, D.K., O'Day, K., Wener, M.H., Andrews, B.S. and Margolis, R.L. (1987), A 17-kD centromere protein (CENP-A) copurifies with nucleosome core particles and with histones. *J Cell Biol* 104:805–815.

Pehrson, J.R. and Fried, V.A. (1992), MacroH2A, a core histone containing a large nonhistone region. *Science* 257:1398–1400.

Pehrson, J.R., Costanzi, C. and Dharia, C. (1997), Developmental and tissue expression patterns of histone macroH2A1 subtypes. *J Cell Biochem* 65:107–113.

Petersen, S., Casellas, R., Reina-San-Martin, B., Chen, H.T., Difilippantonio, M.J., Wilson, P.C., Hanitsch, L., Celeste, A., Muramatsu, M., Pilch, D.R., Redon, C., Ried, T., Bonner, W.M., Honjo, T., Nussenzweig, M.C. and Nussenzweig, A. (2001), AID is required to initiate Nbs1/gamma-H2AX focus formation and mutations at sites of class switching. *Nature* 414:660–665.

Pinzone, J.J., Hall, B.M., Thudi, N.K., Vonau, M., Qiang, Y.W., Rosol, T.J. and Shaughnessy, J.D. (2009), The role of Dickkopf-1 in bone development, homeostasis, and disease. *Blood* 113:517–525.

Piontkivska, H., Rooney, A.P. and Nei, M. (2002), Purifying selection and birth-and-death evolution in the histone H4 gene family. *Mol Biol Evol* 19:689–697.

Polo, S.E., Roche, D. and Almouzni, G. (2006), New histone incorporation marks sites of UV repair in human cells. *Cell* 127:481–493.

Probst, A.V., Dunleavy, E. and Almouzni, G. (2009), Epigenetic inheritance during the cell cycle. *Nat Rev Mol Cell Biol* 10:192–206.

Qiu, J. (2006), Epigenetics: unfinished symphony. *Nature* 441:143–145.

Rasmussen, T.P., Huang, T., Mastrangelo, M.A., Loring, J., Panning, B. and Jaenisch, R. (1999), Messenger RNAs encoding mouse histone macroH2A1 isoforms are expressed at similar levels in male and female cells and result from alternative splicing. *Nucleic Acids Res* 27:3685–3689.

Rinn, J.L., Kertesz, M., Wang, J.K., Squazzo, S.L., Xu, X., Brugmann, S.A., Goodnough, L.H., Helms, J.A., Farnham, P.J., Segal, E. and Chang, H.Y. (2007), Functional demarcation of active and silent chromatin domains in human HOX loci by noncoding RNAs. *Cell* 129:1311–1323.

Rogakou, E.P., Pilch, D.R., Orr, A.H., Ivanova, V.S. and Bonner, W.M. (1998), DNA double-stranded breaks induce histone H2AX phosphorylation on serine 139. *J Biol Chem* 273:5858–5868.

Rogakou, E.P., Boon, C., Redon, C. and Bonner, W.M. (1999), Megabase chromatin domains involved in DNA double-strand breaks in vivo. *J Cell Biol* 146:905–916.

Rogakou, E.P., Nieves-Neira, W., Boon, C., Pommier, Y. and Bonner, W.M. (2000), Initiation of DNA fragmentation during apoptosis induces phosphorylation of H2AX histone at serine 139. *J Biol Chem* 275:9390–9395.

Rooney, A.P., Piontkivska, H. and Nei, M. (2002), Molecular evolution of the nontandemly repeated genes of the histone 3 multigene family. *Mol Biol Evol* 19:68–75.

Rozen, S. and Skaletsky, H. (2000), Primer3 on the WWW for general users and for biologist programmers. *Methods Mol Biol* 132:365–386.

Ruhl, D.D., Jin, J., Cai, Y., Swanson, S., Florens, L., Washburn, M.P., Conaway, R.C., Conaway, J.W. and Chrivia, J.C. (2006), Purification of a human SRCAP complex that remodels chromatin by incorporating the histone variant H2A.Z into nucleosomes. *Biochemistry* 45:5671–5677.

Saha, A., Wittmeyer, J. and Cairns, B.R. (2006), Chromatin remodelling: the industrial revolution of DNA around histones. *Nat Rev Mol Cell Biol* 7:437–447.

Sal, G.D., Ruaro, M.E., Philipson, L. and Schneider, C. (1992), The growth arrest-specific gene, gas1, is involved in growth suppression. *Cell* 70:595–607.

Sal, G.D., Collavin, L., Ruaro, M.E., Edomi, P., Saccone, S., Valle, G.D. and Schneider, C. (1994), Structure, function, and chromosome mapping of the growth-suppressing human homologue of the murine gas1 gene. *Proc Natl Acad Sci U S A* 91:1848–1852.

Sancho, M., Diani, E., Beato, M. and Jordan, A. (2008), Depletion of Human Histone H1 Variants Uncovers Specific Roles in Gene Expression and Cell Growth. *PLoS Genet* 4:e1000227.

Santenard, A., Ziegler-Birling, C., Koch, M., Tora, L., Bannister, A.J. and Torres-Padilla, M.E. (2010), Heterochromatin formation in the mouse embryo requires critical residues of the histone variant H3.3. *Nat Cell Biol* .

Sawatsubashi, S., Murata, T., Lim, J., Fujiki, R., Ito, S., Suzuki, E., Tanabe, M., Zhao, Y., Kimura, S., Fujiyama, S., Ueda, T., Umetsu, D., Ito, T., ichi Takeyama, K. and Kato, S. (2010), A histone chaperone, DEK, transcriptionally coactivates a nuclear receptor. *Genes Dev* 24:159–170.

Schermelleh, L., Carlton, P.M., Haase, S., Shao, L., Winoto, L., Kner, P., Burke, B., Cardoso, M.C., Agard, D.A., Gustafsson, M.G.L., Leonhardt, H. and Sedat, J.W. (2008), Subdiffraction multicolor imaging of the nuclear periphery with 3D structured illumination microscopy. *Science* 320:1332–1336.

Schneider, C., King, R.M. and Philipson, L. (1988), Genes specifically expressed at growth arrest of mammalian cells. *Cell* 54:787–793.

Schneider, R. and Grosschedl, R. (2007), Dynamics and interplay of nuclear architecture, genome organization, and gene expression. *Genes Dev* 21:3027–3043.

Sekulic, N., Bassett, E.A., Rogers, D.J. and Black, B.E. (2010), The structure of (CENP-A-H4)(2) reveals physical features that mark centromeres. *Nature* .

Shechter, D., Dormann, H.L., Allis, C.D. and Hake, S.B. (2007), Extraction, purification and analysis of histones. *Nat Protoc* 2:1445–1457.

Shibahara, K. and Stillman, B. (1999), Replication-dependent marking of DNA by PCNA facilitates CAF-1-coupled inheritance of chromatin. *Cell* 96:575–585.

Simpson, R.T. (1978), Structure of the chromatosome, a chromatin particle containing 160 base pairs of DNA and all the histones. *Biochemistry* 17:5524–5531.

Singleton, S., Mudrak, O., Morshedi, M., Oehninger, S., Zalenskaya, I. and Zalensky, A. (2007), Characterisation of a human sperm cell subpopulation marked by the presence of the TSH2B histone. *Reprod Fertil Dev* 19:392–397.

Sirotkin, A.M., Edelmann, W., Cheng, G., Klein-Szanto, A., Kucherlapati, R. and Skoultchi, A.I. (1995), Mice develop normally without the H1(0) linker histone. *Proc Natl Acad Sci U S A* 92:6434–6438.

Smith, M.M. and Andrésson, O.S. (1983), DNA sequences of yeast H3 and H4 histone genes from two non-allelic gene sets encode identical H3 and H4 proteins. *J Mol Biol* 169:663–690.

Staynov, D.Z. (2008), The controversial 30 nm chromatin fibre. *Bioessays* 30:1003–1009.

Stiff, T., O'Driscoll, M., Rief, N., Iwabuchi, K., Löbrich, M. and Jeggo, P.A. (2004), ATM and DNA-PK function redundantly to phosphorylate H2AX after exposure to ionizing radiation. *Cancer Res* 64:2390–2396.

Strahl, B.D. and Allis, C.D. (2000), The language of covalent histone modifications. *Nature* 403:41–45.

Sullivan, K.F. (2001), A solid foundation: functional specialization of centromeric chromatin. *Curr Opin Genet Dev* 11:182–188.

Tabaska, J.E. and Zhang, M.Q. (1999), Detection of polyadenylation signals in human DNA sequences. *Gene* 231:77–86.

Tachiwana, H., Osakabe, A., Kimura, H. and Kurumizaka, H. (2008), Nucleosome formation with the testis-specific histone H3 variant, H3t, by human nucleosome assembly proteins in vitro. *Nucleic Acids Res* 36:2208–2218.

Tachiwana, H., Kagawa, W., Osakabe, A., Kawaguchi, K., Shiga, T., Hayashi-Takanaka, Y., Kimura, H. and Kurumizaka, H. (2010), Structural basis of instability of the nucleosome containing a testis-specific histone variant, human H3T. *Proc Natl Acad Sci U S A* 107:10454–10459.

Tagami, H., Ray-Gallet, D., Almouzni, G. and Nakatani, Y. (2004), Histone H3.1 and H3.3 complexes mediate nucleosome assembly pathways dependent or independent of DNA synthesis. *Cell* 116:51–61.

Takahashi, K. and Yamanaka, S. (2006), Induction of pluripotent stem cells from mouse embryonic and adult fibroblast cultures by defined factors. *Cell* 126:663–676.

Takahashi, K., Tanabe, K., Ohnuki, M., Narita, M., Ichisaka, T., Tomoda, K. and Yamanaka, S. (2007), Induction of pluripotent stem cells from adult human fibroblasts by defined factors. *Cell* 131:861–872.

Talbert, P.B. and Henikoff, S. (2010), Histone variants–ancient wrap artists of the epigenome. *Nat Rev Mol Cell Biol* 11:264–275.

Tay, S.K., Blythe, J. and Lipovich, L. (2009), Global discovery of primate-specific genes in the human genome. *Proc Natl Acad Sci U S A* 106:12019–12024.

Th'ng, J.P.H., Sung, R., Ye, M. and Hendzel, M.J. (2005), H1 family histones in the nucleus. Control of binding and localization by the C-terminal domain. *J Biol Chem* 280:27809–27814.

Trostle-Weige, P.K., Meistrich, M.L., Brock, W.A. and Nishioka, K. (1984), Isolation and characterization of TH3, a germ cell-specific variant of histone 3 in rat testis. *J Biol Chem* 259:8769–8776.

Turner, B.M. (2000), Histone acetylation and an epigenetic code. *Bioessays* 22:836–845.

van Holde, K.E. (1988), Chromatin. Springer, New York.

van Roijen, H.J., Ooms, M.P., Spaargaren, M.C., Baarends, W.M., Weber, R.F., Grootegoed, J.A. and Vreeburg, J.T. (1998), Immunoexpression of testis-specific histone 2B in human spermatozoa and testis tissue. *Hum Reprod* 13:1559–1566.

Viens, A., Mechold, U., Brouillard, F., Gilbert, C., Leclerc, P. and Ogryzko, V. (2006), Analysis of human histone H2AZ deposition in vivo argues against its direct role in epigenetic templating mechanisms. *Mol Cell Biol* 26:5325–5335.

Waddington, C.H. (1942), The epigenotype. Endeavour, 1, 18–20.

Weber, S.A., Gerton, J.L., Polancic, J.E., DeRisi, J.L., Koshland, D. and Megee, P.C. (2004), The kinetochore is an enhancer of pericentric cohesin binding. *PLoS Biol* 2:E260.

Wei, Y., Yu, L., Bowen, J., Gorovsky, M.A. and Allis, C.D. (1999), Phosphorylation of histone H3 is required for proper chromosome condensation and segregation. *Cell* 97:99–109.

Wernig, M., Meissner, A., Foreman, R., Brambrink, T., Ku, M., Hochedlinger, K., Bernstein, B.E. and Jaenisch, R. (2007), In vitro reprogramming of fibroblasts into a pluripotent ES-cell-like state. *Nature* 448:318–324.

Witt, O., Albig, W. and Doenecke, D. (1996), Testis-specific expression of a novel human H3 histone gene. *Exp Cell Res* 229:301–306.

Wong, L.H., Ren, H., Williams, E., McGhie, J., Ahn, S., Sim, M., Tam, A., Earle, E., Anderson, M.A., Mann, J. and Choo, K.H.A. (2009), Histone H3.3 incorporation provides a unique and functionally essential telomeric chromatin in embryonic stem cells. *Genome Res* 19:404–414.

Wong, L.H., McGhie, J.D., Sim, M., Anderson, M.A., Ahn, S., Hannan, R.D., George, A.J., Morgan, K.A., Mann, J.R. and Choo, K.H.A. (2010), ATRX interacts with H3.3 in maintaining telomere structural integrity in pluripotent embryonic stem cells. *Genome Res* 20:351–360.

Woodcock, C.L. and Ghosh, R.P. (2010), Chromatin higher-order structure and dynamics. *Cold Spring Harb Perspect Biol* 2:a000596.

Wysocka, J., Reilly, P.T. and Herr, W. (2001), Loss of HCF-1-chromatin association precedes temperature-induced growth arrest of tsBN67 cells. *Mol Cell Biol* 21:3820–3829.

Yan, C. and Boyd, D.D. (2006), Histone H3 acetylation and H3 K4 methylation define distinct chromatin regions permissive for transgene expression. *Mol Cell Biol* 26:6357–6371.

Yu, J., Vodyanik, M.A., Smuga-Otto, K., Antosiewicz-Bourget, J., Frane, J.L., Tian, S., Nie, J., Jonsdottir, G.A., Ruotti, V., Stewart, R., Slukvin, I.I. and Thomson, J.A. (2007), Induced pluripotent stem cell lines derived from human somatic cells. *Science* 318:1917–1920.

Zalensky, A.O., Siino, J.S., Gineitis, A.A., Zalenskaya, I.A., Tomilin, N.V., Yau, P. and Bradbury, E.M. (2002), Human testis/sperm-specific histone H2B (hTSH2B). Molecular cloning and characterization. *J Biol Chem* 277:43474–43480.

Zhang, Y. (2008), I-TASSER server for protein 3D structure prediction. *BMC Bioinformatics* 9:40.

Zlatanova, J. and Thakar, A. (2008), H2A.Z: view from the top. *Structure* 16:166–179.

Appendix

Table A.1. Oligonucleotides for qPCR

Name	Sequence	Description
GAPDH FWD	5' CTGCACCACCAACTGCTTAG	monitoring cDNA
GAPDH REV	5' CTTCACCACCTTCTTGATGTC	synthesis
HPRT1 FWD	5' AAGGGTGTTTATTCCTCATGGA	directed against
HPRT1 REV	5' AATCCAGCAGGTCAGCAAAG	reference genes with
HMBS FWD	5' AGTGTGGTGGCAACATTGAA	stable expression
HMBS REV	5' GCATGTTCAAGCTCCTTGGT	levels
CENP-A FWD	5' TCACTCGTGGTGTGGACTTC	anneal to histone H3
CENP-A REV	5' GCACATCCTTTGGGAAGAGA	variant CENP-A
H3.X+Y #1 FWD	5' GGACCTGCGCTTCCAGAG	
H3.X+Y #1 REV	5' CATGTCTCGGGGCATAATTG	
H3.X+Y #2 FWD	5' GTCCACGCAGCTGCTCCT	hybridize with H3.X
H3.X+Y #2 REV	5' GGCACACAGGTTGGTGTCTT	and H3.Y mRNA
H3.X+Y #3 FWD	5' AAGCAGACCGCCCGCAAAG	
H3.X+Y #3 REV	5' TTCTGATTTCCCGCAGCGCC	
H3.X #1 FWD	5' ACCAAAGCCGCCAGAAAA	
H3.X #1 REV	5' GAGCAGCTGCGTGGACTT	hybridize specifically
H3.X #2 FWD	5' GAAGACACCAACCTGTGTGC	with H3.X mRNA
H3.X #2 REV	5' AGTGCAAGGTTTCCCAGGAG	
H3.Y #1 FWD	5' CCACCAAAGCAGCCGGAAA	
H3.Y #1 REV	5' GCTGCGTGGACTTCTGGTACT	hybridize specifically
H3.Y #2 FWD	5' GCCTACCTGGTGCAGCTCTT	with H3.Y mRNA
H3.Y #2 REV	5' TTAAGGACCCTCTCTGCGGAGG	
H3.X-1 + H3.X-2 FWD	5' GCCATGGCTGGAATGACC	
H3.X-1 + H3.X-2 REV	5' GGCCTTGTGCTCTCTCCTCT	
H3.X-2 FWD	5' GAGTCAGAGGCACCCATTG	target different
H3.X-2 REV	5' CACATGTCCAGAGCCTCTTCT	hypothetical
H3.X long #1 FWD	5' GCAGGGCTTTACTGAGACCA	H3.X-transcripts
H3.X long #1 REV	5' CAACCCAACCCCACACTTAC	
H3.X long #2 FWD	5' AGCTGGTAAGTGTGGGGTTG	
H3.X long #2 REV	5' CGTCAGAAAACAAGGGCAGT	
TMEM177 FWD	5' CGTGGTCCAATGGCTCTAC	
TMEM177 REV	5' GAAGGTGAAGGTGGTGAAGG	
DCN FWD	5' GGACCGTTTCAACAGAGAGG	
DCN REV	5' GACCACTCGAAGATGGCATT	
IQGAP2 FWD	5' CAAGATGGTCGTCAGCTTCA	
IQGAP2 REV	5' CACCCAAGCCTTGTACACCT	target genes which
PKIA FWD	5' GGGAGAAGCAGCAAAATCTG	show a significant
PKIA REV	5' GCAGCACAGCCATTTTCTTT	change in expression
CYFIP2 FWD	5' CATCGGCTGCTCTGTAAGC	levels after stable
CYFIP2 REV	5' TTCAGTTCCCAGAAGACATGC	expression of
CGA FWD	5' CAGAATGCACGCTACAGGAA	HA-H3.Y
CGA REV	5' AGCAAGTGGACTCTGAGGTGA	
CXCL16 FWD	5' ATGCTTACTCGGGGATTGTG	
CXCL16 REV	5' CAAGGTGGACAGGAGCATCT	
APLF FWD	5' GGGCGACTCACTTCAGGAT	
APLF REV	5' CATGCAGGATGTCCTCTTGA	

Oligonucleotides for qPCR (continued)

Name	Sequence	Description
NR2F1 FWD	5' TACGTGAGGAGCCAGTACCC	target genes which show a significant change in expression levels after stable expression of HA-H3.Y
NR2F1 REV	5' CCTACCAAACGGACGAAGAA	
BMP4 FWD	5' GACTTCGAGGCGACACTTCT	
BMP4 REV	5' GCTGTGGATCTGCTCTTCCT	
TGFBR2 FWD	5' GACTGAGTGCTGGGACCAC	
TGFBR2 REV	5' GGAGCCGTCTTCAGGAATCT	
SMAD6 FWD	5' TCCCTACTCTCGGCTGTCTC	
SMAD6 REV	5' GAGAATTCACCCGGAGCA	
DKK1 FWD	5' CATCAGACTGTGCCTCAGGA	
DKK1 REV	5' CCACAGTAACAACGCTGGAA	
IGFBP3 FWD	5' GGTGTCTGATCCCAAGTTCC	
IGFBP3 REV	5' CGGAGGAGAAGTTCTGGGTA	
GAS1 FWD	5' TGAGCCGCTACCTGACCTAC	
GAS1 REV	5' ACACGCAGTCGTTGAGCA	
SPHK1 FWD	5' TGAGCAGGTCACCAATGAAG	
SPHK1 REV	5' GGCTGAGCACAGAGAAGAGG	

Table A.2. Oligonucleotides for cloning

Name	Sequence	Description
H3.X+Y EcoRI FWD	5' GGAATTCAGGCAATCGCTGCG CGCACCAAGCAGACCGC	cloning of H3.X and H3.Y cDNA into pIRES HA Neo
H3.X BamHI REV	5' CGGGATCCCTAGAGTGCAAGG TTTCCCA	
H3.Y BamHI REV	5' CGGGATCCTTAAGGACCCTCT CTGCGGAG	
H3.X+Y HindIII FWD	5' GAGGATAAGCTTCAGCGCGCA CCAAGCAG	cloning of H3.X and H3.Y cDNA into pEGFP-C1
H3.X SacII REV	5' GATAATCCGCGGCTAGAGTGC AAGGTTTCCC	
H3.Y SacII REV	5' GATAATCCGCGGTTAAGGACC CTCTCTGCGG	
H3.X+Y NdeI FWD	5' GGAATTCCATATGATGGCGCG CACCAAGCAGAC	cloning of H3.X and H3.Y cDNA into pET-21a(+)
H3.X XhoI REV	5' CCGCTCGAGCTAGAGTGCAAG GTTTCCCAG	
H3.Y XhoI REV	5' CCGCTCGAGTTAAGGACCCTC TCTGCGGAG	
H3.1+2 HindIII FWD	5' GAGGATAAGCTTCAGCGCGTA CTAAGCAGACGG	cloning of H3.1, H3.2 and H3.3 cDNA into pEGFP-C1
H3.1+2 SacII REV	5' GATAATCCGCGGTCACGCCCT CTCCCCAC	
H3.3 HindIII FWD	5' GAGGATAAGCTTCAGCCCGAA CCAAGCAGACTG	
H3.3 SacII REV	5' GATAATCCGCGGTTAAGCTCT CTCTCCCCG	
H3.X+Y siRNA mut FWD	5' GGCACCCTGGCGCTGAGAGAG ATTCGGAAGTACCAGAAGTCC	site-directed mutagenesis of siRNA-target sequences in H3.Y
H3.X+Y siRNA mut REV	5' GGACTTCTGGTACTTCCGAAT CTCTCTCAGCGCCAGGGTGCC	
H3.Y siRNA mut FWD	5' CTGGCCCGCCGCCTCAGACGC GAAGGACCTTAAGGATCCACTAG	
H3.Y siRNA mut REV	5' CTAGTGGATCCTTAAGGTCCT TCGCGTCTGAGGCGGCGGGCCAG	

Table A.3. Oligonucleotides for RNAi

Name	Sequence	Description
luciferase sense luciferase antisense	5' CUUACGCUGAGUACUUCGAdTdT 5' UCGAAGUACUCAGCGUAAGdTdT	control siRNA
H3.X sense H3.X antisense	5' CACCAAAGCCGCCAGAAAAdTdT 5' UUUUCUGGCGGCUUUGGUGdTdT	siRNA targets specifically H3.X
H3.Y sense H3.Y antisense	5' CCGCAGAGAGGGUCCUUAAdTdT 5' UUAAGGACCCUCUCUGCGGdTdT	siRNA targets specifically H3.Y
H3.X+Y sense H3.X+Y antisense	5' GCGGGAAAUCAGAAAGUACdTdT 5' GUACUUUCUGAUUUCCCGCdTdT	siRNA targets H3.X and H3.Y

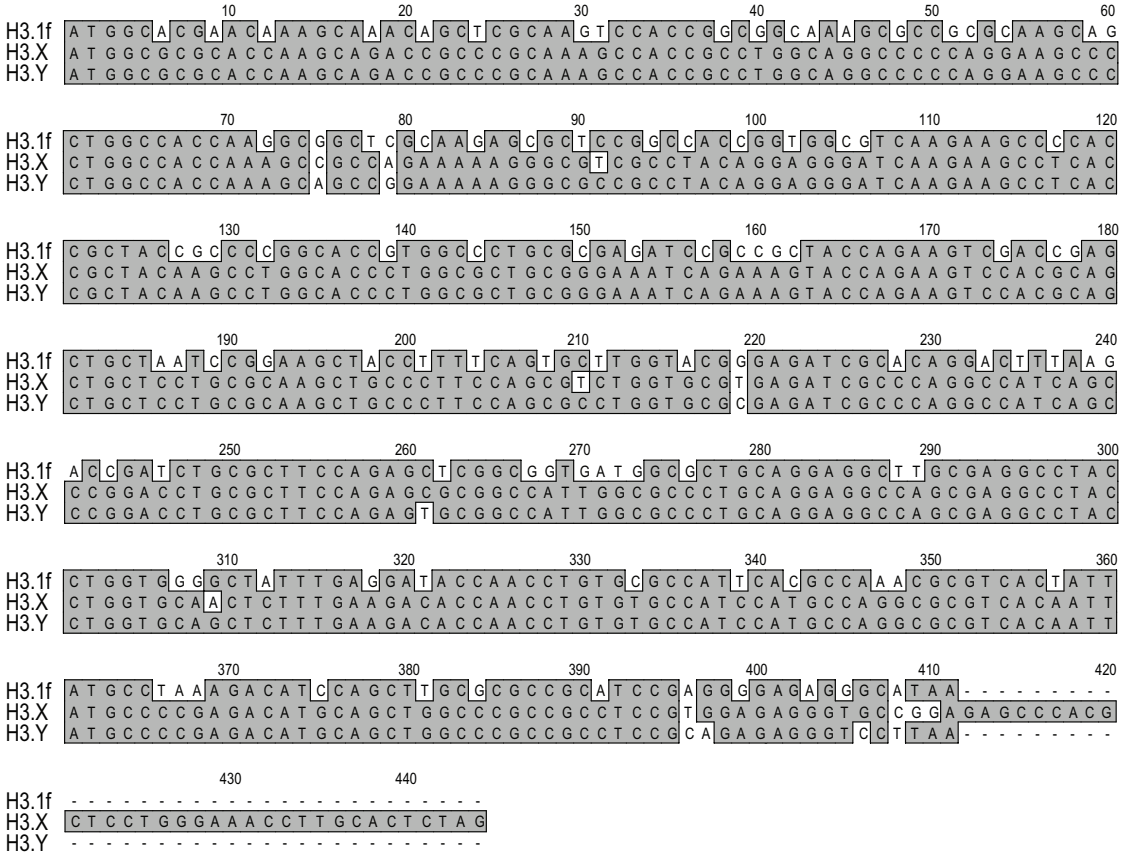

Figure A.1. Nucleotide sequence alignment of human *H3.X* and *H3.Y* with *H3.1*.
Alignment of coding nucleotide sequences of human *H3.1f* (NM_003533), *H3.X* (LOC340096) and *H3.Y* (LOC391769) genes. Identical nucleotides are highlighted in dark gray and changes are set apart on a white background.

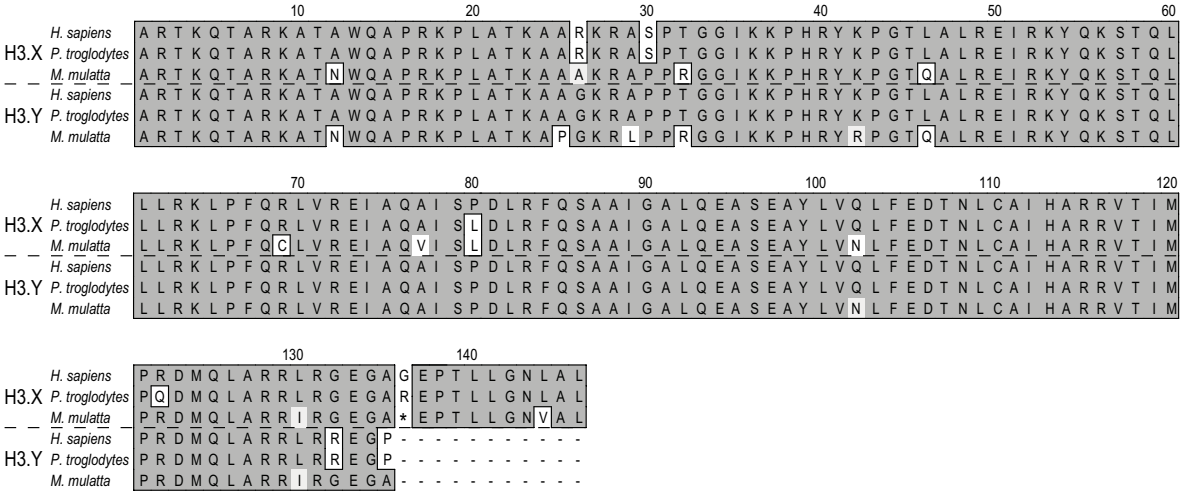

Figure A.2. Amino acid sequence alignment of H3.X and H3.Y from different primate species. Alignment of human (*H. sapiens*), chimpanzee (*P. troglodytes*) and macaque (*M. mulatta*) H3.X and H3.Y protein sequences. Sequence similarity is encoded by background color: identical aa = dark gray, similar aa = light gray, different aa = white. Note that the macaque H3.X ends, like H3.Y, after aa 135 (asterisk indicates stop codon) but following amino acids would code for the extra C-terminus of H3.X.

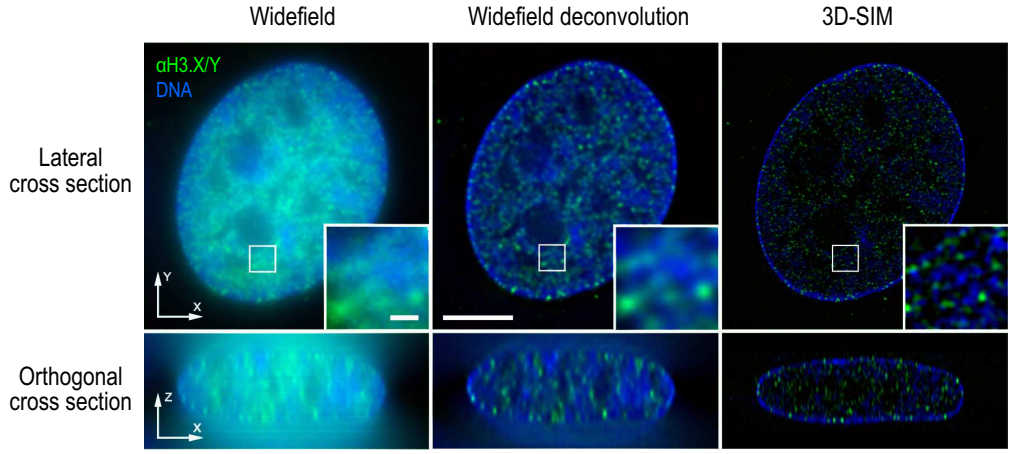

Figure A.3. Comparison of different microscopy techniques.
Lateral (top) and orthogonal (bottom) sections of U2OS cells, co-stained with αH3.X/Y (green) and DAPI (DNA, blue), are depicted. Images were acquired using a widefield (left) or an OMX DeltaVision (right) microscope. A deconvolved version of the left image is shown in the middle. Scale bar equals 5 µm. Insets show enlargements of boxed areas with scale bar equaling 0.5 µm. With 3D-SIM resolution, but not with that of conventional microscopy, localization of H3.X/Y protein outside of DAPI-dense regions is visible.

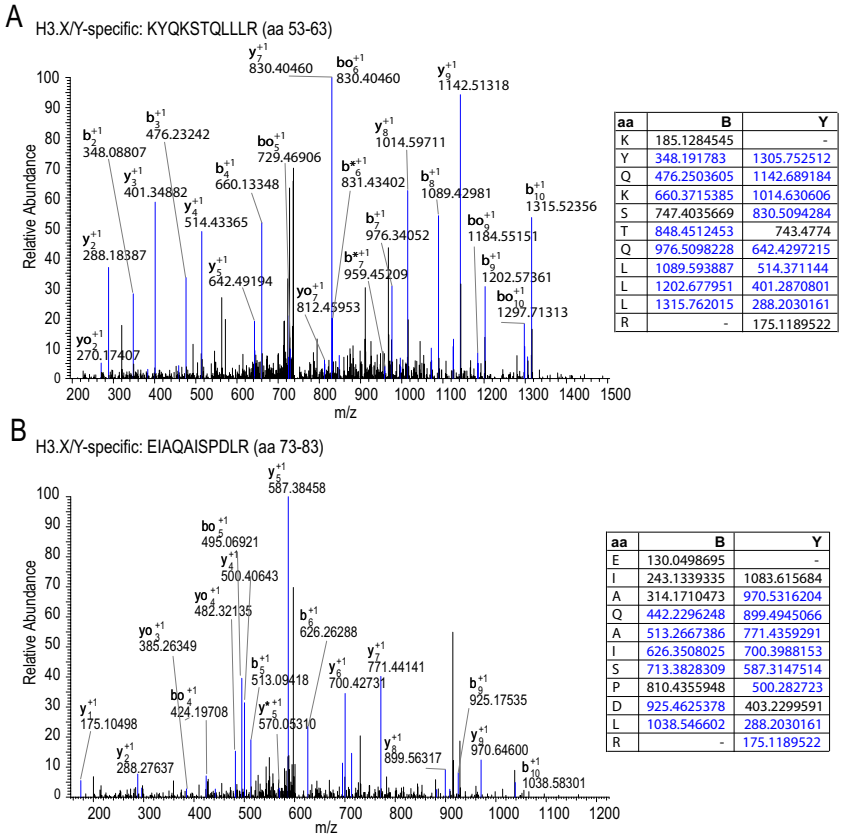

aa	B	Y
K	185.1284545	-
Y	348.191783	1305.752512
Q	476.2503605	1142.689184
K	660.3715385	1014.630606
S	747.4035669	830.5094284
T	848.4512453	743.4774
Q	976.5098228	642.4297215
L	1089.593887	514.371144
L	1202.677951	401.2870801
L	1315.762015	288.2030161
R	-	175.1189522

aa	B	Y
E	130.0498695	-
I	243.1339335	1083.615684
A	314.1710473	970.5316204
Q	442.2296248	899.4945066
A	513.2667386	771.4359291
I	626.3508025	700.3988153
S	713.3828309	587.3147514
P	810.4355948	500.282723
D	925.4625378	403.2299591
L	1038.546602	288.2030161
R	-	175.1189522

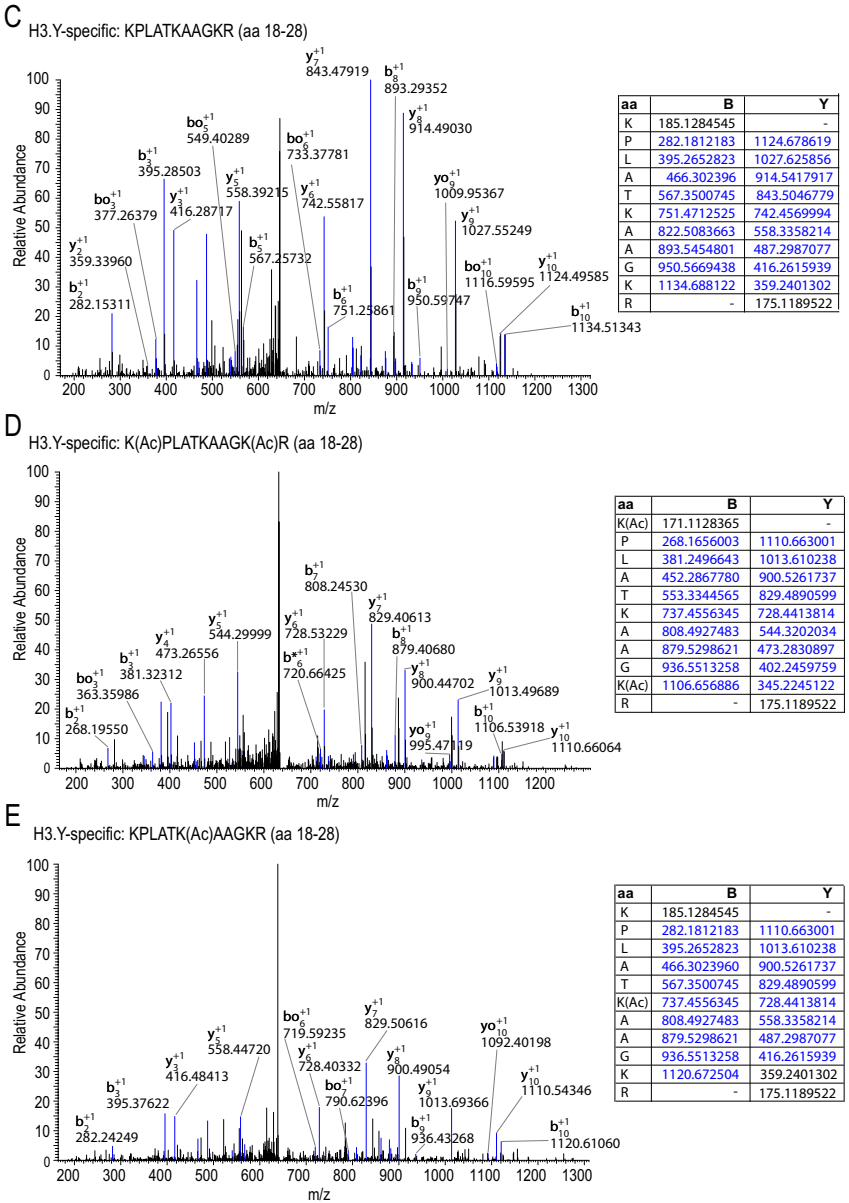

aa	B	Y
K	185.1284545	-
P	282.1812183	1124.678619
L	395.2652823	1027.625856
A	466.302396	914.5417917
T	567.3500745	843.5046779
K	751.4712525	742.4569994
A	822.5083663	558.3358214
A	893.5454801	487.2987077
G	950.5669438	416.2615939
K	1134.688122	359.2401302
R	-	175.1189522

aa	B	Y
K(Ac)	171.1128365	-
P	268.1656003	1110.663001
L	381.2496643	1013.610238
A	452.2867780	900.5261737
T	553.3344565	829.4890599
K	737.4556345	728.4413814
A	808.4927483	544.3202034
A	879.5298621	473.2830897
G	936.5513258	402.2459759
K(Ac)	1106.656886	345.2245122
R	-	175.1189522

aa	B	Y
K	185.1284545	-
P	282.1812183	1110.663001
L	395.2652823	1013.610238
A	466.3023960	900.5261737
T	567.3500745	829.4890599
K(Ac)	737.4556345	728.4413814
A	808.4927483	558.3358214
A	879.5298621	487.2987077
G	936.5513258	416.2615939
K	1120.672504	359.2401302
R	-	175.1189522

Figure A.4. MS/MS spectra of H3.X/Y- and H3.Y-specific peptides. NanoLC-ESIMS/MS analysis of propionylated and trypsin-digested proteins in RP-HPLC fractions corresponding to region A bands from U2OS SO experiment 1 (see Fig. 3.13Ciii). Depicted are MS/MS spectra of doubly charged precursor ions of peptides specific for H3.X and H3.Y ((A) m/z = 745.44, (B) m/z = 606.83) and unmodified or acetylated H3.Y-specific peptide ((C) m/z = 654.90, (D) m/z = 640.88 and (E) m/z = 647.90). Boxes on the right show specific b and y ions after fragmentation.

A

GOBPID	Pvalue	Odds Ratio	Exp Count	Count	Size	Term
GO:0032274	0.000	166.667	0	2	5	gonadotropin secretion
GO:0042523	0.000	166.667	0	2	5	positive regulation of tyrosine phosphorylation of Stat5 protein
GO:0046884	0.000	166.667	0	2	5	follicle-stimulating hormone secretion
GO:0042522	0.000	99.983	0	2	7	regulation of tyrosine phosphorylation of Stat5 protein
GO:0042506	0.000	83.312	0	2	8	tyrosine phosphorylation of Stat5 protein
GO:0060986	0.001	62.473	0	2	10	endocrine hormone secretion

B

GOBPID	Pvalue	Odds Ratio	Exp Count	Count	Size	Term
GO:0000280	0.000	6.951	3	20	248	nuclear division
GO:0007067	0.000	6.951	3	20	248	mitosis
GO:0048285	0.000	6.710	4	20	256	organelle fission
GO:0000087	0.000	6.653	4	20	258	M phase of mitotic cell cycle
GO:0051301	0.000	5.937	4	22	318	cell division
GO:0000279	0.000	5.515	5	22	340	M phase
GO:0022403	0.000	4.767	6	24	428	cell cycle phase
GO:0007049	0.000	3.538	12	35	864	cell cycle
GO:0000278	0.000	4.671	6	24	436	mitotic cell cycle
GO:0071103	0.000	9.106	2	13	122	DNA conformation change
GO:0022402	0.000	4.019	8	27	571	cell cycle process
GO:0006323	0.000	9.123	1	11	102	DNA packaging
GO:0007059	0.000	10.287	1	10	83	chromosome segregation
GO:0006261	0.000	11.797	1	9	66	DNA-dependent DNA replication
GO:0065004	0.000	9.327	1	9	81	protein-DNA complex assembly
GO:0000075	0.000	8.952	1	9	84	cell cycle checkpoint
GO:0006334	0.000	9.422	1	8	71	nucleosome assembly
GO:0051276	0.000	3.453	7	20	470	chromosome organization
GO:0006260	0.000	4.924	3	13	213	DNA replication
GO:0031497	0.000	8.856	1	8	75	chromatin assembly
GO:0009066	0.000	21.496	0	5	22	aspartate family amino acid metabolic process
GO:0034728	0.000	8.475	1	8	78	nucleosome organization
GO:0006270	0.000	20.300	0	5	23	DNA replication initiation
GO:0009067	0.000	29.070	0	4	14	aspartate family amino acid biosynthetic process
GO:0051726	0.000	3.772	4	14	295	regulation of cell cycle
GO:0006259	0.000	2.988	7	19	508	DNA metabolic process
GO:0000070	0.000	12.588	0	5	34	mitotic sister chromatid segregation
GO:0006996	0.000	2.203	18	35	1311	organelle organization
GO:0000819	0.000	12.168	0	5	35	sister chromatid segregation
GO:0051318	0.000	19.372	0	4	19	G1 phase
GO:0009086	0.000	43.353	0	3	8	methionine biosynthetic process
GO:0006333	0.000	5.579	2	8	114	chromatin assembly or disassembly
GO:0006082	0.000	2.841	7	18	502	organic acid metabolic process
GO:0007091	0.000	16.139	0	4	22	mitotic metaphase/anaphase transition
GO:0007093	0.000	10.425	1	5	40	mitotic cell cycle checkpoint
GO:0007094	0.000	30.961	0	3	10	mitotic cell cycle spindle assembly checkpoint
GO:0045841	0.000	30.961	0	3	10	negative regulation of mitotic metaphase/anaphase transition
GO:0008652	0.000	9.599	1	5	43	cellular amino acid biosynthetic process
GO:0031570	0.000	9.118	1	5	45	DNA integrity checkpoint
GO:0007076	0.000	27.089	0	3	11	mitotic chromosome condensation
GO:0071174	0.000	27.089	0	3	11	mitotic cell cycle spindle checkpoint
GO:0009309	0.000	6.867	1	6	70	amine biosynthetic process
GO:0044283	0.000	3.415	4	12	275	small molecule biosynthetic process
GO:0016043	0.001	1.813	33	51	2371	cellular component organization
GO:0006555	0.001	24.077	0	3	12	methionine metabolic process
GO:0071173	0.001	24.077	0	3	12	spindle assembly checkpoint
GO:0019752	0.001	2.682	7	17	498	carboxylic acid metabolic process
GO:0043436	0.001	2.682	7	17	498	oxoacid metabolic process
GO:0010948	0.001	12.098	0	4	28	negative regulation of cell cycle process
GO:0007346	0.001	4.575	2	8	137	regulation of mitotic cell cycle
GO:0031577	0.001	21.667	0	3	13	spindle checkpoint
GO:0045839	0.001	21.667	0	3	13	negative regulation of mitosis
GO:0051784	0.001	21.667	0	3	13	negative regulation of nuclear division
GO:0042180	0.001	2.614	7	17	510	cellular ketone metabolic process
GO:0000097	0.001	19.696	0	3	14	sulfur amino acid biosynthetic process

Figure A.5. GO groups significantly affected by H3.Y and H3.X+Y knockdown in U2OS cells. Comprehensive list of GO groups comprising genes that are significantly up- (A) or down- (B) regulated after siRNA knockdown of H3.Y and H3.X+Y in U2OS cells compared to luciferase control knockdown. For number of overlapping genes see Venn diagrams in Fig. 3.18B. Size = total number of genes analyzed in this node (GO term), ExpCount = number of "responders" expected (entering the term by chance), Count = actual number of "responders" found in the node.

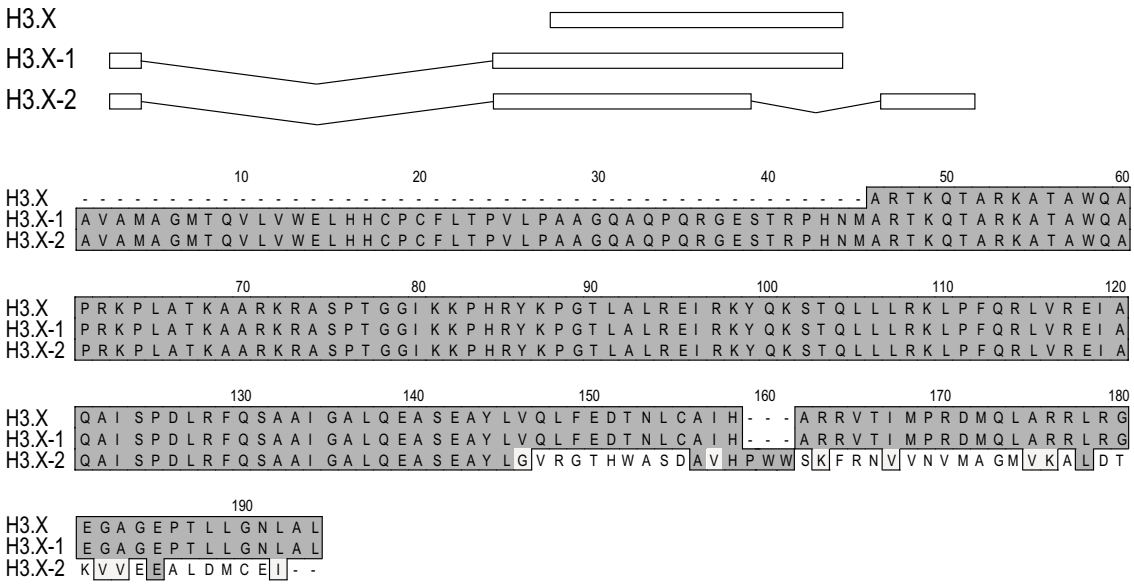
H3.X
H3.X-1
H3.X-2
10 20 30 40 50 60
H3.X - - -

List of Figures

1.1 Crystal structure of the nucleosome 5
1.2 Chromatin - composition and compaction 6
1.3 Epigenetic regulation 8
1.4 Protein sequences of human core histone variants 13

3.1 Amino acid sequence alignment of human histone H3 variants 45
3.2 Phylogenetic tree of H3.X and H3.Y from different species 46
3.3 H3.X/Y mRNA levels in different cell lines and human tissues 47
3.4 Sub-cellular localization of HA-tagged histone H3 variants 49
3.5 *In silico* homology models of H3.X and H3.Y protein structure 50
3.6 Composition of H3.X and H3.Y containing nucleosomes 51
3.7 Exchange mobility behavior of GFP-tagged H3 variants 52
3.8 Evaluation of αH3.X/Y antibody specificity 53
3.9 Endogenous H3.X/Y expression and sub-nuclear localization 54
3.10 Test of different stress conditions as trigger for H3.X/Y expression in U2OS cells 56
3.11 Increase of H3.X/Y expressing U2OS cells by nutritional and proliferative stress 57
3.12 Evaluation of inducible endogenous H3.X and H3.Y expression 58
3.13 Purification and identification of endogenous H3.Y protein 59
3.14 GO enrichment analysis of de-regulated genes in HeLa HA-H3.Y cells 61
3.15 Gene expression levels in HeLa cells stably expressing HA-tagged H3 variants 62
3.16 Influences of HA-H3.Y expression and SO treatment on gene expression . . . 63
3.17 Evaluation of H3.X/Y siRNA specificity 65
3.18 mRNA expression profiling of U2OS cells after H3.Y or H3.X+Y knockdown 66
3.19 Influence of H3.X and/or H3.Y knockdown on proliferation capacity 67
3.20 H3.X/Y expression in human brain 68
3.21 H3.X/Y expression in primates 70

A.1 Nucleotide sequence alignment of human *H3.X* and *H3.Y* with *H3.1f* III
A.2 Amino acid sequence alignment of H3.X and H3.Y from different primate species IV
A.3 Comparison of different microscopy techniques IV
A.4 MS/MS spectra of H3.X/Y- and H3.Y-specific peptides V
A.5 GO groups significantly affected by H3.Y and H3.X+Y knockdown in U2OS cells VI
A.6 Alternative H3.X transcripts VII

List of Tables

1.1 Human core histone variants 12

2.8 Mammalian cell lines 28
2.9 Stably transfected mammalian cell lines 28

A.1 Oligonucleotides for qPCR I

A.2 Oligonucleotides for cloning II

A.3 Oligonucleotides for RNAi III

Curriculum vitae

Sonja M. Wiedemann

Birth name:	Nieratschker
Date of birth:	March 1st 1983
Place of birth:	München

Education

10/2007 - present **PhD thesis at the Ludwig-Maximilians-University of Munich, Adolf-Butenandt-Institute, Prof. Peter Becker, Group of Dr. Sandra Hake**
Member of the International Max Planck Research School for Molecular and Cellular Life Sciences
Project: Identification and characterization of two novel primate-specific histone H3 variants, H3.X and H3.Y

01/2006 - 05/2006 **Internship at the University of Michigan, Ann Arbor, MI, USA, Department of Molecular, Cellular & Developmental Biology, Laboratory of Dr. Ursula Jakob**
Project: Oxidative stress and its implication for aging in the model organism *Caenorhabditis elegans*

10/2002 - 08/2007 **Studies in biochemistry at the University of Regensburg**
Diploma thesis: Glycosylation defects and apoptosis in *Saccharomyces cerevisiae* - Identification of RPR1 and Lhp1 as new components
Scholarships: German National Merit Foundation (Studienstiftung des deutschen Volkes), Bavarian Scholarship Programme for highly talented students (Bayerische Begabtenförderung)

09/1993 - 06/2002 **Secondary school: Schyren-Gymnasium Pfaffenhofen a.d. Ilm**
Abitur

Publications

Wiedemann S.M., Mildner S.N., Bönisch C., Israel L., Maiser A., Matheisl S., Straub T., Merk R., Leonhardt H., Kremmer E., Schermelleh L., and Hake S.B. 2010. Identification and characterization of two novel primate-specific histone H3 variants, H3.X and H3.Y. *J Cell Biol*, 190(5): 777-791

Bönisch C.*, **Nieratschker S.M.***, Orfanos N.K. and Hake S.B. 2008. Chromatin proteomics and epigenetic regulatory circuits. *Expert Rev. Proteomics*, 5(1): 105-119 (* equal contribution)

Bönisch C., **Wiedemann S.M.**, Bielmeier C., Dambacher S., Israel L., Mehlhorn C., Schneider K., Merk R., Kremmer E., Schermelleh L. and Hake S.B. 2010. Identification and characterization of a novel splice-form of the human histone variant H2A.Z. (in preparation)